THE EFFECT OF HIGH AUSTENITIZATION TEMPERATURES ON THE MECHANICAL PROPERTIES AND MICROSTRUCTURE OF AISI 5140 STEEL

by

Osman Nurettin UÇ

B.S. in M.E., Boğaziçi Universiy, 1984

Submitted to the Institute for Graduate Studies in Science and Engineering in partial fulfillment of the requirements for the degree of

Master of Science

in

Mechanical Engineering

Boğaziçi University

1986

THE EFFECT OF HIGH AUSTENITIZATION TEMPERATURES ON THE MECHANICAL PROPERTIES AND MICROSTRUCTURE OF AISI 5140 STEEL

APPROVED BY

Doç. Dr. Sabri ALTINTAŞ (Thesis supervisor) S. Altıntaş

Doç. Dr. Gülay AŞKAR Ç. Aşkar

Prof. Dr. Kâşif ONARAN K. Onaran

Prof. Dr. Akın TEZEL Akın Tezel

DATE OF APPROVAL :

ACKNOWLEDGEMENTS

I would like to express my sincere gratitude to my thesis supervisor Doç. Dr. Sabri ALTINTAŞ for his guidance during this study.

I want to acknowledge "ASİL ÇELİK San. ve Tic. A.Ş." for providing the required steel. I am particularly grateful to Mr. Ergun ONUR, head of Metallurgy Department, for his invaluable permission to use all the available facilities of the company for both machining and testing. I also wish to express my sincere appreciation to Mr. Mehmet ÇİLİNGİR for many helpful discussions and suggestions during the course of the study.

I am also indebted to Mr. Önder YÜKSEL and Mr. İlhan TAŞKIRAN for their appreciable permission to make the heat treatments in "PANKURT San. A.Ş.".

My grateful appreciation goes also to Dr. Nazım BOZKURT from ITU for his help in microscopic study, Dr. Mehmet DEMİRKOL from TUBITAK for his help in fracture toughness testing and fractography, Doç, Dr. Tayfur ÖZTÜRK for his appreciable permission to make scanning electron microscope study in METU, and İbrahim ZEYBEK from "Paşabahçe Cam San. A.Ş." for his helps to use the machining facilities of the institution.

I would like to express my sincere thanks to Doç. Dr. Gülay AŞKAR, Prof. Dr. Kâşif ONARAN and Prof. Dr. Akın TEZEL for serving on my thesis committee. I also owe a debt of gratitude to them for their suggestions and corrections.

Finally, I should like to mention the help of my friends, Mustafa BÜYÜKABACI and Enes YILDIZ during the evaluation and documentation phases.

THE EFFECT OF HIGH AUSTENITIZATION TEMPERATURES ON THE MECHANICAL PROPERTIES AND MICROSTRUCTURE OF AISI 5140 STEEL

ABSTRACT

In this study, the effect of high austenitization temperatures to improve the mechanical properties of AISI 5140 steel was investigated.

Firstly, a general understanding of iron-carbon system, transformation of austenite under both equilibrium and non-equilibrium conditions were given, and the concept of hardenability was introduced. Secondly, hardening and tempering of low alloy steels were viewed and then the studies on high temperature austenitization were summarized.

In the experimental work, the test specimens were austenitized at either 845°C, 1000°C, 1100°C or 1200°C. The resulting martensitic structures were tempered at either 200°C or 570°C. Double austenitization -consisted of 1200°C austenitization followed by oil quenching; after the oil quenching, tempering at 200°C, and then reaustenitizing at 845°C- was also employed. Then, the mechanical properties were measured with hardness testing, tensile testing, Charpy impact testing, plane strain fracture toughness testing and Jominy end-quench testing. The resulting microstructures after different hardening treatments were studied by optical microscope. The fracture surfaces were examined using scanning electron microscope (SEM).

Hardenability increased with increasing austenitization temperature. Plane strain fracture toughness and Charpy impact energy measurements of lightly tempered structures exhibited an approximate of 80 per cent increase for specimens austenitized at 1200°C compared to those conventionally austenitized at 845°C. The yield and ultimate tensile strengths were unaffected by the austenitization temperature.

Finally, the increase in hardenability has been associated with increased grain sizes; and the prevention of the formation of certain microstructural features, especially ferrite and upper bainite with high austenitization temperatures have been related to the increase in toughness.

YÜKSEK OSTENİTLEME SICAKLIKLARININ AISI 5140 ÇELİĞİNİN MEKANİK ÖZELLİKLERİ VE MİKROYAPISI ÜZERİNDEKİ ETKİSİ

ÖZET

Bu çalışmada, AISI 5140 çeliğinin mekanik özelliklerinin iyileştirilmesinde yüksek ostenitleme sıcaklıklarının etkisi incelenmiştir.

İlk olarak, demir-karbon sistemi, ostenitin gerek denge ve gerekse denge-dışı şartlardaki dönüşümü hakkında genel bilgi verilmiş ve sertleşebilirlik kavramından bahsedilmiştir. İkinci olarak, düşük alaşımlı çeliklerin sertleştirilmesi ve menevişlenmesi konusu gözden geçirilmiş ve yüksek sıcaklıklarda ostenitleme ile ilgili olarak yapılan çalışmalar özetlenmiştir.

Deneysel çalışmada, deney numuneleri 845°C, 1000°C, 1100°C veya 1200°C de ostenitlenmiştir. Elde edilen martensitic yapılar 200°C veya 570°C de menevişlenmiştir. 1200°C de ostenitlemeyi müteakip yağda soğutma, daha sonra 200°C de menevişleme, bilahare 845°C de tekrar ostenitlemeden oluşan "çift ostenitleme" de uygulanmıştır. Daha sonra, mekanik özellikler sertlik testi, çekme testi, darbe-çentik testi, düzlemsel genleme kırılma tokluğu (K_{1c}) testi ve Jominy sertleşebilirlik testi ile ölçülmüştür. Çeşitli sertleştirme işlemleri sonucu oluşan mikroyapılar optik mikroskopla, kırılma yüzeyleri ise elektron mikroskobu (SEM) ile incelenmiştir.

Sertleşebilirlik artan ostenitleme sıcaklıklarıyla artmıştır. 1200°C de ostenitlenen ve düşük sıcaklıklarda

menevişlenen malzemelerin yüzeysel genleme kırılma tokluğu (K_{1c}) ve darbe-çentik enerjileri konvansiyonel 845°C ostenitlemesine nisbetle yaklaşık yüzde 80 artış göstermişlerdir. Akma ve çekme mukavemetleri ostenitleme sıcaklığından etkilenmemiştir.

Son olarak, sertleşebilirliğin artması büyümüş tane yapısına bağlanmış ve ferrit ve üst beynit gibi mikroyapısal elemanların oluşumunun yüksek ostenitleme sıcaklıkları sonucu önlenmiş olması da, toklukta artışa sebep olarak gösterilmiştir.

TABLE OF CONTENTS

LIST OF FIGURES

LIST OF TABLES

LIST OF SYMBOLS

A_c	-	Critical temperature on heating.
A_r	-	Critical temperature on cooling.
A_1	-	Eutectoid transformation temperature.
A_3	-	The temperature at which the separation of ferrite from austenite on cooling or the completion of solution of ferrite in austenite on heating begins.
E	-	Young's modulus.
K_A	-	Apparent fracture toughness, a mean of estimating the fracture toughness without recourse of fatigue cracking.
K_{1c}	-	Plane strain fracture toughness.
K_{1d}	-	Dynamic fracture toughness.
M_f	-	Martensite finish temperature.
M_s	-	Martensite start temperature.
ρ	-	Crack root radius.
ρ_o	-	Effective or critical root radius.
σ_f	-	Critical fracture stress.
σ_{yy}^{max}	-	Maximum tensile stress.
σ_y	-	Yield strength.
σ_u	-	Ultimate tensile strength.
ε_f	-	Critical fracture strain.

I. INTRODUCTION

A contructural steel, quenched from the austenitizing temperature and subsequently tempered in the range 500-700°C, obtains useful mechanical properties, e.g., a high ratio of yield strength to ultimate tensile strength, high elongation, reduction of area and toughness. This heat treatment which resulted in a tough structure with tempering in the range of 500-700°C is called "tough hardening".

These low alloy structural steels are generally not used at yield strengths above 1400 MPa (200,000 psi) -resulted from tempering at low temperatures, because of their poor fracture toughness at such high strength levels.

Commercial low alloy steels are conventionally austenitized at the lower end of the austenite range (typically 840-870°C) to produce fine prior austenite grain sizes, quenched fast enough to produce martensite and tempered, insuring good strength at relatively low or moderate fracture toughness.

In 1970's, however, there has been considerable interest in employing much higher austenitization temperatures (up to 1200°C) to increase the fracture toughness of such steels without loss in strength. Unfortunately, although increases in fracture toughness by over a factor of two have been reported following such high temperature austenitizing treatment, this marked improvement in plane strain fracture toughness is often not parallel with a corresponding increase in Charpy V-notch impact energy. In fact, a decrease in Charpy impact energy has been observed concurrent with the increase in K_{1c} for Fe-Cr-C steels, En 25, 4340 and 300M steel, in both as-quenched

and quenched and tempered conditions [1-6]*. Increasing Charpy impact values accompanied the increase in K_{1c} have also been reported for 4130 and 4140 steels [7-9].

The explanation for such effects has been suggested that superior toughness obtained after high austenitizing temperatures may result from:

(a) Retardation of the grain boundary nucleation af a second phase [7-9],

(b) Solution of carbides at high temperatures [3,8-12],

(c) Formation of thicker films of retained austenite around martensite laths [6,8,14-16],

(d) Elimination of twinned martensite plates [2,12-14,16-18],

(a) Thermodynamic suppression of embrittling elements from segregation to grain boundaries [9,17,19-21].

In the present study, the effect of high austenitizing temperatures on mechanical properties of AISI 5140 steel will be investigated and the results will be linked to the changes in the microstructure.

(*) Parenthetical references placed superior to the line of the text refer to the bibliography.

II. FUNDAMENTAL CONSIDERATIONS

Steel which is primarily alloy of iron and carbon is the most important engineering and constructural material; it accounts for approximately 80 per cent of all metal produced [22]. Steel has attained this degrees of prominence because it combines strength, ease of fabricating into many shapes, and a wide range of properties along with low cost.

While some steels are relatively soft and ductile and can be readily formed into various shapes, such as automobile fenders and body parts, others can be hardened sufficiently to serve as tools for cutting steel into desired shapes. Still others can be made to possess strength plus toughness, for use as automobile axles or as propeller shafts for ocean-going vessels. A prosaic example of an extremely hard steel is the common razor blade. From these examples it becomes apparent that the word "steel" is an all-inclusive term which has many sub-classifications; in fact, there are several thousand different steels, when judged on the basis of the many compositions produced commercially.

Our ability to produce steels for a wide variety of uses, ranging from relatively soft strip steel to hard tool steel, depends in many instances upon suitable heat treatments of a given steel during or after forming.

Before considering the heat treatment of steel, it will be helpful to explain just what steel is and to briefly consider the internal structure of steel.

2.1. The Iron-Carbon Equilibrium Diagram

The iron-carbon equilibrium diagram furnishes a map showing the ranges of composition and temperatures within which the various phases are stable and the boundaries at which phase changes occur. Although heat treatment is largely concerned with a controlled departure from equilibrium, this diagram represents the limiting conditions and is basic to an understanding of heat treating principles.

Pure iron exists in three main allotropic forms; α -iron (ferrite) and δ -iron, which are body-centered cubic, and γ -iron (austenite) which is face-centered cubic. The maximum solubility of carbon in alpha-iron is 0.025 per cent and occurs at 723°C. At room temperature, ferrite can dissolve only 0.008 per cent carbon. Austenite is the term applied to the solid solution of carbon in free iron. Most heat-treating operations, such as annealing, normalizing and heating for hardening, begin with heating the steel into the austenitic range to dissolve the carbide in the iron. The maximum solubility of carbon in austenite is 2.11 per cent.

In iron-carbon alloys, carbon in excess of solubility limit forms a second phase called iron-carbide or cementite. This phase is rather hard and brittle and contains 6.67 per cent carbon which corresponds to the composition of Fe_3C. Thus, the iron-carbon diagram does not show the phase relationships between iron and carbon, but rather between iron and cementite.

It will be noted in Figure 1, the critical temperatures A_1, A_3 and A_{cm} are arrests in heating or cooling and have been symbolized with the letter A, from the French word "arret" meaning arrest or delay point. A_c is the abbreviation for the critical point on a heating curve and A_r for the arrest point on cooling curve. (The subscript c is from the French word "chauffage", meaning heating; and r is from "refroidissement", meaning cooling.)

Although, in principle, the transformations A_c and A_r result from the same temperature of equilibrium,

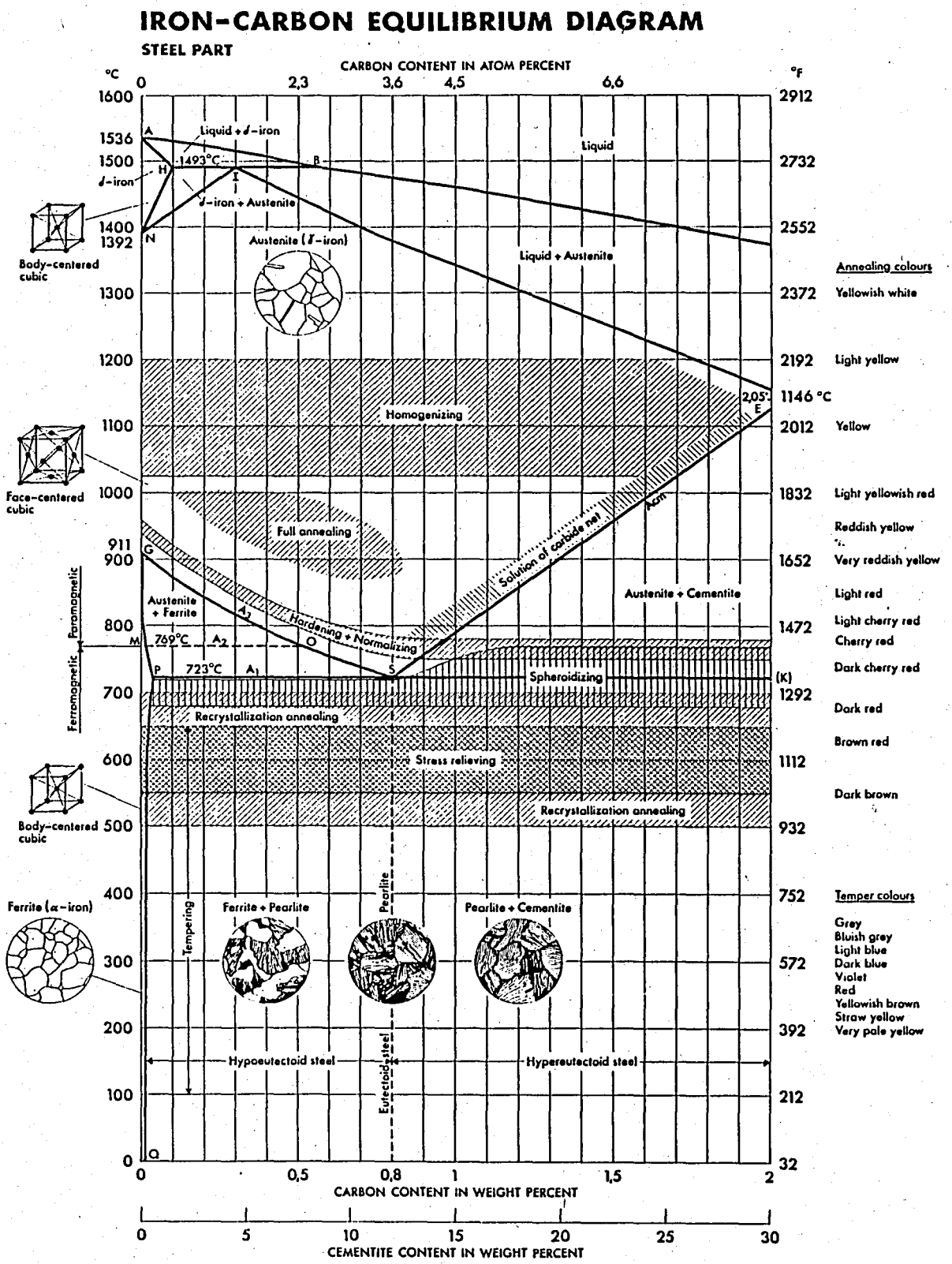

Figure 1. The iron-carbon equilibrium diagram [23].

in practice, the A_r temperatures are lower than the corresponding A_c temperatures, falling as the cooling is more rapid, even with very slow heating or cooling, these temperatures do not coincide, and therefore, the subscript "e" for equilibrium is used in the designation of the critical temperatures in the equilibrium diagram.

2.2. Transformation of Austenite under Equilibrium Cooling

2.2.1. Eutectoid Steel

A plain carbon steel containing 0.77 per cent carbon becomes a solid solution at any temperature in the austenite temperature range, between 723 °C and 1370 °C. All the carbon is dissolved in the austenite. When this solid solution is slowly cooled, the homogeneous solid solution transforms into two distinct new solid phases. The new phases are ferrite and cementite, formed simultaneously in a characteristic lamellar structure, which is known as pearlite. This structure is illustrated in Figure 2. It is generally similar in its characteristics to an eutectic structure, but since it is formed from a solid solution rather than from a liquid phase, it is known as "eutectoid structure". When pearlite is heated slowly, it completely changes to austenite at this temperature or slightly above.

Figure 2. Pearlite in an eutectoid steel (0.77 % carbon, etched by 4 % nital, 1000x) [24].

2.2.2. Hypoeutectoid Steels

Carbon steels containing less than 0.77 per cent carbon are known as hypoeutectoid steels. The iron-carbon diagram shows that the equilibrium constituents are ferrite and pearlite, the relative amount of each depending upon the carbon content. The diagram shows that the solubility of carbon in ferrite increases until 723 °C. At this temperature, ferrite contains about 0.025 per cent carbon. The first phase change on heating (if the steel contains above 0.025 per cent carbon) occurs at 723 °C. On heating just above this temperature, the pearlite all changes to austenite. Some proeutectoid ferrite, however, remains unchanged. As the temperature rises further above A_1, the austenite dissolves more and more of the surrounding proeutectoid ferrite, becoming lower and lower in carbon, until the A_3 temperature, the last of the proeutectoid ferrite has been absorbed into the austenite having the same average carbon content as the steel.

On slow cooling, the reverse changes occur. The austenite first rejects ferrite (generally at grain boundaries) on cooling below A_3 and becomes progressively richer in carbon, until just above the A_1 temperature, it is substantially of eutectoid composition. On cooling below A_1, this eutectoid austenite changes to pearlite so that the final product after cooling below A_1 is a mixture of ferrite and pearlite, the relative proportions of each constituent depending upon the carbon content.

2.2.3. Hypereutectoid Steels

Steels containing from 0.77 per cent to about 2.0 per cent carbon are termed hypereutectoid steels. The behavior of hypereutectoid steels is similar to that of hypoeutectoid steels except that the excess constituent is cementite rather than ferrite, so that on heating above A_1, the austenite generally dissolves the excess cementite until at the A_{cm} temperature all of the proeutectoid cementite has

been dissolved and austenite of the same carbon content as the steel is formed. Similarly, on cooling below A_3, cementite precipitates and carbon content of the austenite approaches the austenite composition. On cooling below A_1, this eutectoid austenite changes to pearlite, and the room temperature constituent is, therefore, pearlite and proeutectoid cementite.

2.3. Transformation of Austenite under Non-Equilibrium Cooling

Thus far, we have been concerned with equilibrium conditions. Under equilibrium conditions, that is, with very slow cooling, it has been shown that austenite transforms to pearlite when it is cooled below the A_1 critical temperature, and at a temperature only a little below the A_{e1} temperature. When more rapidly cooled, however, this transformation is depressed and does not occur until a lower temperature is reached. The faster the cooling rate, the lower is the temperature at which transformation occurs [24-26]. Furthermore, the nature of the ferrite-carbide aggregate formed when the austenite transforms varies markedly with the temperature of transformation and the properties are found to vary correspondingly. Thus, heat treatment is seen to involve a controlled supercooling of austenite, and in order to take full advantage of the wide range of structures and properties which this permits, a knowledge of the transformation behavior of austenite and the properties of the resulting aggregates is essential.

2.4. Isothermal Transformation Diagrams (IT diagrams)

The iron-carbon diagram serves only as equilibrium diagram, it tells us what structures are ultimately arrived at, provided sufficient time is afforded. The iron-carbon diagram itself, tells us nothing about the time required for the reaction to take place. The transformation behavior

of austenite can best be studied by isothermal transformation diagram of the type shown in Figure 3.

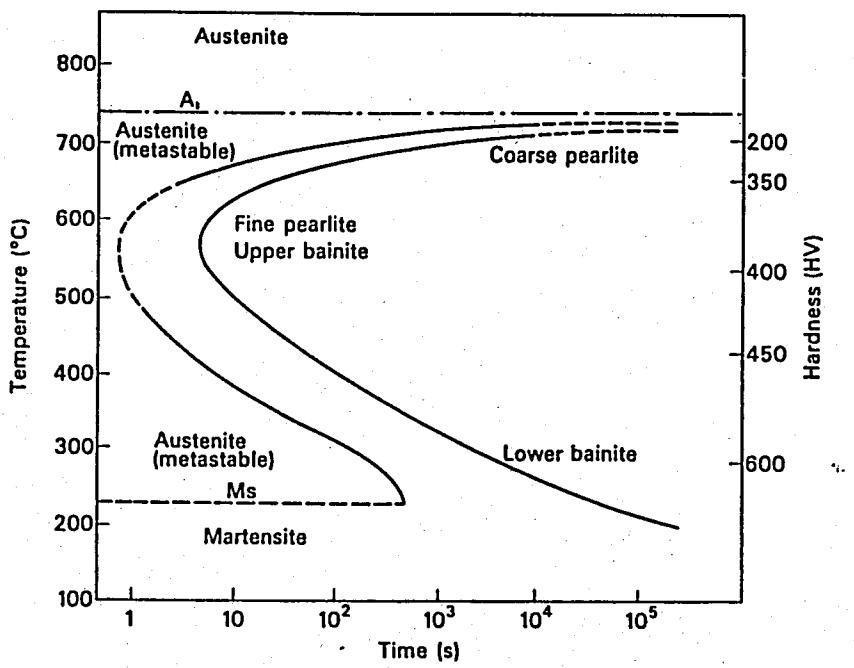

Figure 3. Typical isothermal transformation diagram for 0. 8 per cent carbon eutectoid steel [26].

The isothermal transformation diagram (IT diagram) shows that the austenite transformation occurs slowly, both at high temperatures and at low temperatures. It is slow at higher temperatures because there is not enough supercooling to readily nucleate the new ferrite and carbide from the previous austenite. The austenite decomposition is slow at lower temperatures because diffusion rates are slow and therefore carbon seperation from the ferrite into carbide is small.

With slow cooling, austenite decomposes into pearlite. The pearlite which is obtained by very slow cooling (or the transformation is allowed to occur around 700°C) is coarse. As the cooling rate below A_1, in this case 723°C, is increased (or the transformation is allowed to occur at a lower temperature around 550°C), the structure as a whole becomes refined and particularly the structure of pearlite itself. At slightly lower temperature, around

450°C, the austenite transforms to bainite, which is also intimate mixture of ferrite and iron-carbide, but with a morphology and mode of formation different from those of pearlite.

If we study the products on isoterms taken at progressively lower temperatures in Figure 3, we see that the structure becomes finer and hardness increases. In the pearlitic transformation region, as the transformation temperature decreases, the lamellae become more closely spaced. The hardness is seen to increase as the lamellar spacing becomes smaller. For bainitic structures, again, the hardness increases as the transformation temperature decreases, though the bainite formed at the highest possible temperature is often softer than pearlite formed at a still higher temperature [24].

2.5. Continuous Cooling Diagrams (CCT diagrams)

Isothermal transformation diagram tells what structure is formed at each reaction temperature, if the cooling is interrupted so that the reaction goes to completion at that temperature. The information is equally useful for interpreting behaviors when the cooling proceeds directly without interruption. The final microstructure after continuous cooling will obviously depend upon the times spent at the various transformation temperature ranges through which the piece is cooled. The transformation behavior on continuous cooling, thus represents an integration of these times.

The continuous cooling diagram lies below and to the right of the corresponding isothermal diagram. That is, transformation on continuous cooling will start at a lower temperature and after a longer time than the intersection of the cooling curve and the isothermal diagram would predict, and this displacement is a function of the cooling rate, being larger as the cooling rate increases.

The isothermal transformation (IT) and continuous cooling diagrams (CCT) for AISI 5140 steel are shown in Figures 4 and 5.

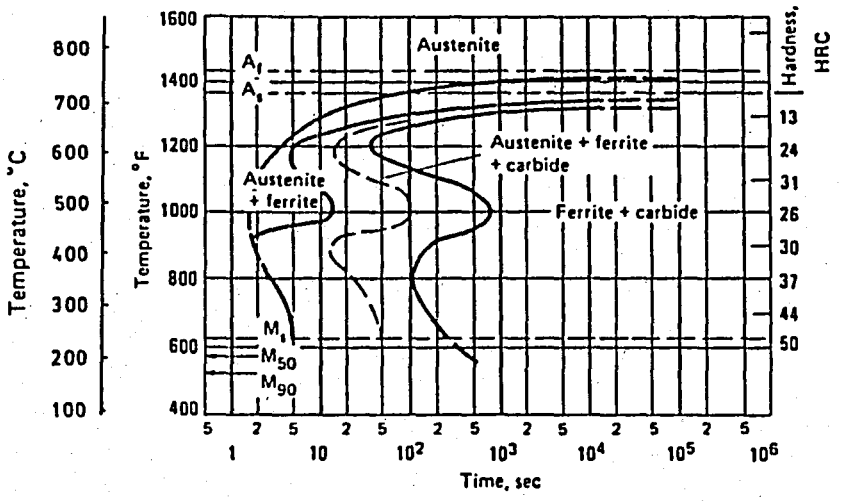

Figure 4. The IT diagram for AISI 5140 steel (22).

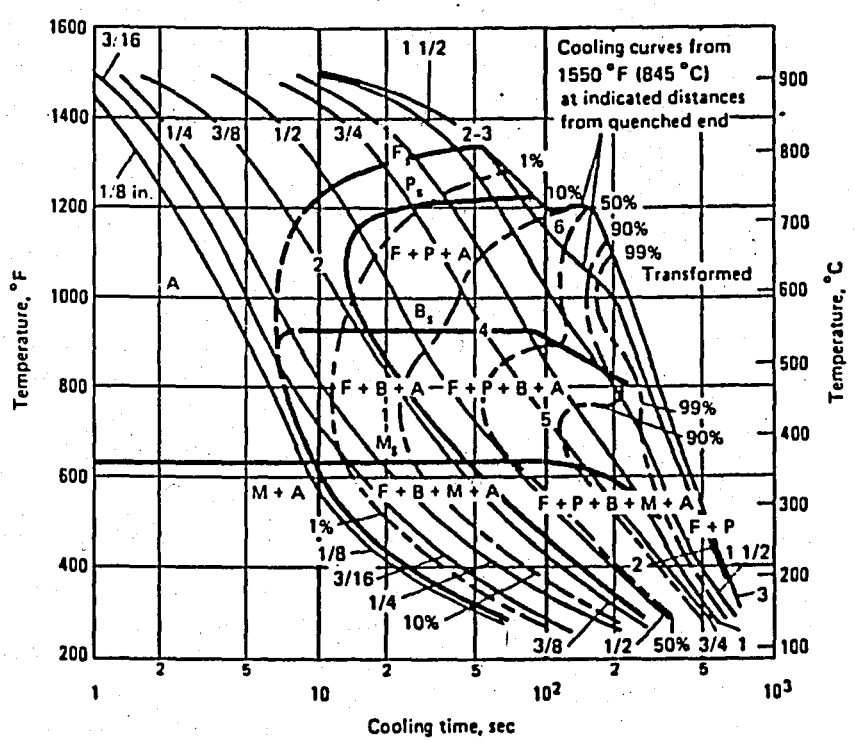

Figure 5. The CCT diagram for AISI 5140 steel (22).

2.6. Bainite

The structure of steel formed during isothermal holding between the nose of the curve and M_s temperature was studied by Bain [25], and the transformation product, subsequently named in his honour, bainite. Bainite formed at higher temperatures is rather like fine pearlite in its properties and appearance. Lower bainite, formed at lower temperatures, becomes more like martensite [25].

Figure 6 (a) Upper bainite 4800x [27].

Figure 6 (b) Lower bainite 2400x [27].

The morphological difference between upper and lower bainite is demonstrated in Figure 6, which also helps to illustrate the difference in properties. In both structures, the ferrite morphology is acicular and the main difference is in the location of the iron-carbide that is precipitated during transformation. In upper bainite, the iron-carbide particles are elongated and directed along the boundaries of ferrite regions. In lower bainite, the iron-carbide particles are much shorter and oriented across the ferrite regions. This clear difference in morphology helps us to explain the very great difference in toughness between the two types of bainite. Upper bainite is very brittle because of the ease of fracture along cementite layers between the ferrite crystals. Lower bainite is much

tough because there is no such easy fracture path provided by the cementite [27].

Bainites are stronger than ferrite/pearlite structures of the same composition, because of finer grain size, the dispersion-hardening effect of the cementite particles and higher residual carbon in solution, internal stresses due to transformation and relatively high dislocation density [27]. However, the notch toughness of martensitic structure decreases regularly with increasing amount of bainite. It would appear that although bainitic structures have high strength, they lack toughness due to their high dislocation density [24].

2.7. Martensite

If the steel is very rapidly cooled (fast enough to avoid cutting the nose of the IT curve) no ferrite or pearlite at all are formed. This is not an unreasonable event to rationalize; the decomposition of austenite to ferrite and cementite is controlled by diffusion processes of carbon and iron atoms. Thus, a small but finite amount of time is required if the transformation to ferrite and pearlite is to occur, and when cooling rate is extremely rapid, this time is not available, but face-centered cubic iron must transform to body-centered cubic iron. This is a transformation that cannot be avoided in plain carbon steels. Consequently, the carbon originally in the austenite, is now trapped in a ferritic structure which (because of the low natural solubility of ferrite for carbon) becomes very badly distorted. It is, in fact, no longer a true body-centered cubic phase. The extreme distortion imposed by the carbon atoms is said to account for the substantially higher hardness of this product. The material produced by quenching a steel at such a rate that the formation of ferrite and cementite is avoided is known as martensite. When the carbon content is very low, transformation to martensite requires phenomenologically high cooling rates, even when the cooling rate is extremely fast, ferrite is

formed instead of martensite [27]. One would expect that steels of higher carbon content, being more distorted, would produce martensite of greater hardness [27], and this is in fact so, as Figure 7 illustrates.

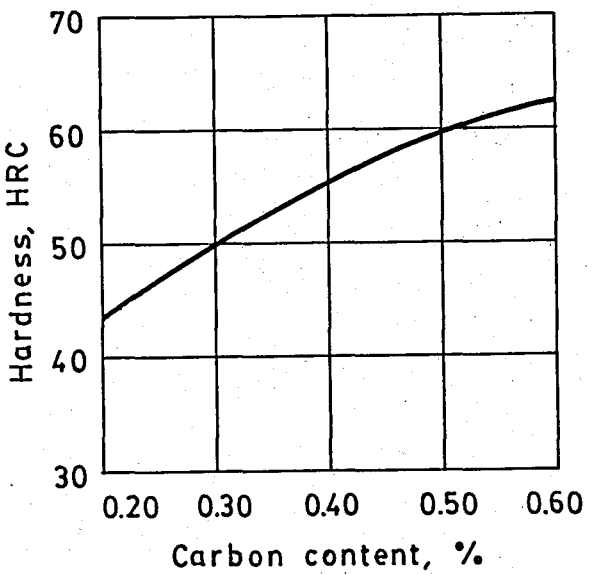

Figure 7. Effect of carbon content on the hardness of fully hardened steels [28].

Austenite transforms to martensite by a diffusionless process in which none of the atoms change place relative to its neighbors. For this reason, it is generally athermal, the amount of transformation depending upon the temperature. The temperature at which the transformation begins on cooling is known as the M_s or "Martensite start" temperature. The temperature at which the transformation is completed is called M_f or "Martensite finish" temperature. The M_s temperature is strongly influenced by composition; practically every element that can be added to steel lowers this temperature.

The austenite-martensite transformation is accompanied by an expansion and involves a shear transformation in the austenite lattice. The structure of martensite may be regarded as a supersaturated solid solution of carbon in α-iron (tetragonal). The dimension of the austenite face-centered cubic lattice and also that

of the martensite of body-centered tetragonal lattice increases progressively with carbon content, the martensite volume increase being considerably greater than the corresponding volume increase in austenite [26].

Umemoto et al. [29] and Kelly and Nutting [30] have studied the structure of martensite in iron-carbon alloys, and found mainly two types. Lath (massive) martensite is characterized by a microstructure composed of many similar sized laths arranged in a parallel fashion to make up a packet (Figure 8 (a)). Several packets are generally found in a single austenite grain. In contrast, plate (acicular) martensite, Figure 8 (a) develops in a non-parallel fashion and neighboring plates vary considerably in size. The substructure of the laths consists of a high density of tangled dislocations while that of plate martensite is made of twins and/or dislocated tangles.

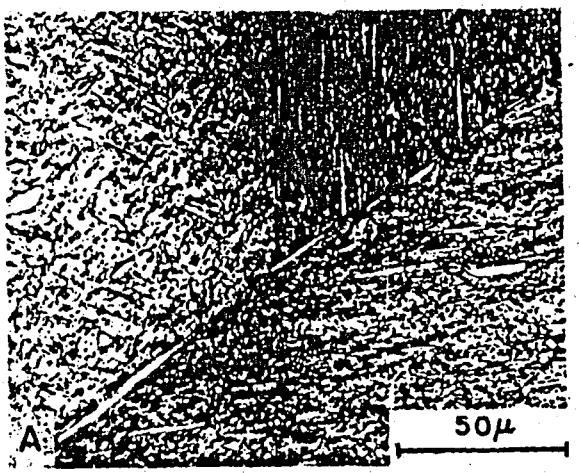

Figure 8 (a) Lath martensite [31].

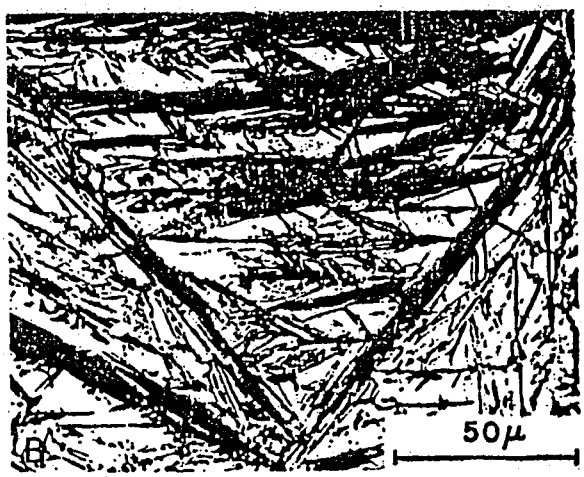

Figure 8 (b) Plate martensite [31].

Although the change to twinned martensite appears to be complete at > 0.5 per cent carbon [31], it is now common to observe a few internally twinned plates in alloys containing only 0.2 per cent carbon [26], and the volume fraction occupied by twin plates appears to increase with carbon content. It therefore seems that between carbon contents of 0.2 and 0.5 per cent, a change is taking place

from dislocated martensite in needles to a twinned acicular martensite arranged in plates [27].

As ferrous martensite is the hardest and strongest metal known, the source of its strength has been the subject of much study. As shown in Figure 7, the hardness and strength of quenched martensite rise rapidly with carbon content. The toughness decreases with about equal rapidity, however. Grain size has some effect but this is not very marked [27], and the main contribution to strength appears to be precipitation hardening from carbides precipitated during the quench, carbon in solid solution, and dislacation arising from the transformation.

The toughness of martensite is greately improved by tempering, because carbon precipitates from the brittle matrix in cementite particles that form on the twin interfaces in a manner akin to lower bainite. In fact, the morphologies of tempered martensite and lower bainite are very similar in strength. The toughness of tempered martensite is greater than that of lower bainite [27], possibly because the cementite particles in the tempered martensite are finer and more uniformly distributed since they are nucleated at a lower temperature.

The strongest and toughest of these structures is dislocated lath (massive) martensite. Where it is not possible to produce dislocated lath martensite because of inadequate hardenability, lower bainite is preferred [27].

Most of the austenite will transform to martensite during quenching to room temperature. The untransformed part is called "retained austenite". Figure 9 shows how the amount of retained austenite in an unalloyed steel varies with carbon content. If the temperature is lowered below room temperature, the transformation to martensite continues.

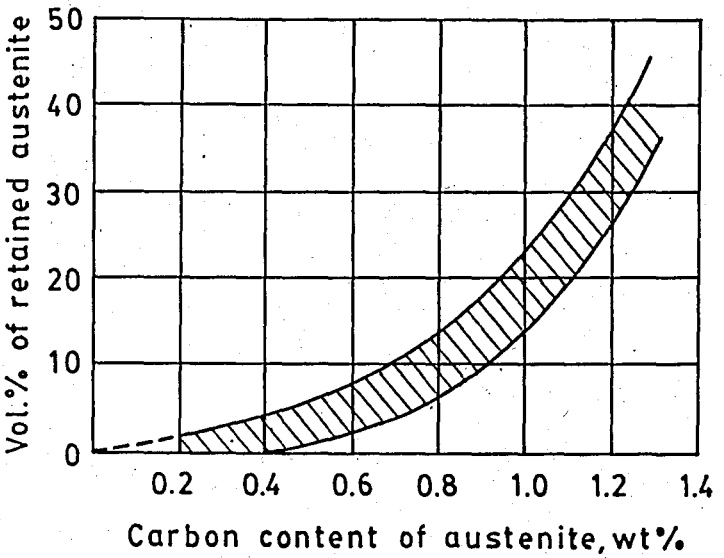

Figure 9. Variation in the amount of retained austenite with carbon content on hardening [31].

2.8. Factors Influencing Transformation Rates

The major factors affecting the rates of transformation of austenite are its composition, grain size, and homogeneity. In general, increasing carbon and alloy content tends to decrease transformation rates. Increasing the grain size of the austenite likewise tends to decrease the transformation rates [24].

2.8.1. Effect of Alloying Elements

The main reason for heat treating an alloy steel is to obtain better strength and toughness that cannot be gained by other means. The ferrite/pearlite structure is the weakest of all structures discussed above and is thus generally avoided in the heat treatment of alloy steels. One way of avoiding this structure, is to apply a high cooling rate (fast enough to avoid cutting the nose of IT curve). This is feasible when the thickness of the steel being heat treated is relatively small, but becomes progressively more difficult as the thickness is increased owing to the relatively low thermal conductivity of the steel and the inadvisibilty of using a fast quench because of the thermal stresses that arise.

The other way of avoiding pearlite is to delay the start of transformation by moving the start lines in CCT diagrams to the right, that is, transformation at all temperature levels starts later and is slower to go to completion. This is characteristic of the effect of alloys in solution in the austenite: in general, increased alloy content delays the start of transformation and increases the time for its completion (24).

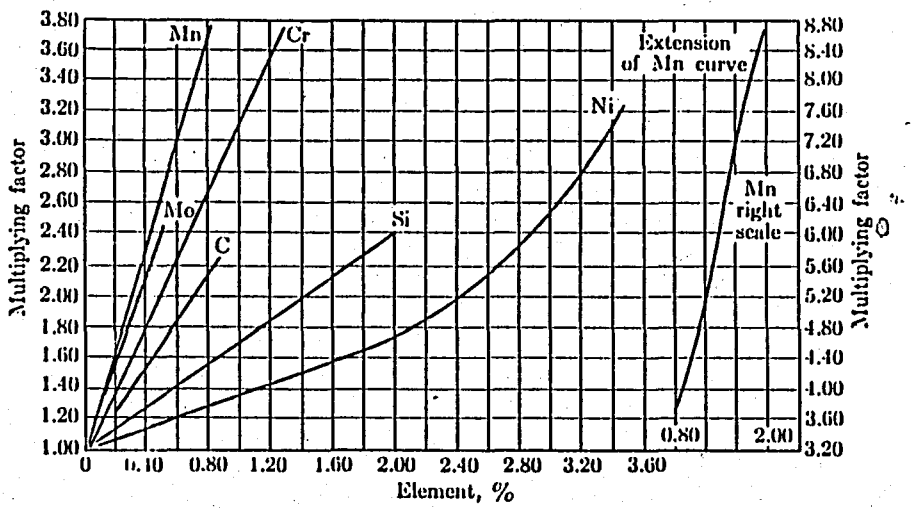

Figure 10. Effect of alloying elements on hardenability (25).

The effect of each alloying element on hardenability which is an indication of transformation rates is shown in Figure 10. The alloying elements that cause the greatest retardation of transformation are molybdenum, tungsten, chromium and manganese. Since the first two of these are more expensive than chromium and manganese, these latter elements are usually preferred (32). Molybdenum is also a strong carbide-former and it is only in solution that it affects the transformation characteristics; it would be somewhat wasteful to add it for this purpose. Vanadium is similar to molybdenum in that it affects transformation characteristics to a marked extend when dissolved but is more useful as a carbide forming element.

Nickel has a moderate effect, less than that of chromium and manganese, but more than that of aluminum titanium and cobalt, which have only a small effect.

Elements such as phosphorus, copper and silicon also exert an influence; phosphorus a very strong one, but this element is usually kept to a very low level in alloy steels because of its effect on toughness. Boron also has a marked effect, particularly in retarding the onset of pearlite transformation; but because of its low solubility in steel, its addition is confined to special applications.

The most common elements added in alloy steel to retard transformation characteristics and facilitate heat treatment are thus chromium, manganese and nickel.

Carbon, of course, itself exerts a strong retarding effect on transformation characteristics, but because of its very great effect on hardness, is usually controlled at the level required for strength and is not used primarily to influence transformation characteristics.

Summarising the effect of alloying elements on transformation behavior, it can be seen that the general effect of increasing the alloy content is to delay both the start and the completion of transformation and that the effect of alloy additions is cumulative. Relatively small amount of several alloying elements are more effective in decreasing transformation rates than larger amount of a single alloy, i.e., more retarding than if they were merely additive (24-26,31).

2.8.2. Effect of Grain Size

As will be described, when a piece is heated above the critical temperature, the ferrite and carbide react with one another to form austenite. The austenite is a crystalline phase differing distinctly from either the ferrite or carbide from which it is formed. The reaction which forms austenite begins at a number of points in the interface of the carbide and ferrite (33). Each of the little islands of austenite grows until finally it reaches the similarly growing neighbors. As the temperature above the critical increases, further grain growth occurs presumably by encroachment of grains into adjacent grains.

The final austenite grain size is, therefore, a function of the temperature above the critical to which it is heated. This grain growth may, however, be inhibited by carbides or by a suitable dispersion of non-metallic inclusions.

The ferrite and carbide formation from the austenite starts at the grain boundary. A fine-grained steel offers more grain boundary area per unit volume on which decomposition can be nucleated than does a coarse-grained steel [35]. Thus, the effect of increasing the grain size of the austenite is similar to that of alloys, it delays both the start and completion of the transformation [24].

2.8.3. Effect of Homogeneity of Austenite

The general effect of inhomogeneous austenite will be to speed up the start of transformation. This occurs because the initial transformation will occur in the portions of the austenite which are "leaner" in alloy. In addition, undissolved carbides may act as nuclei for transformation, thereby hastening the start of transformation [24,26,31].

2.9. Hardenability

Provided the rate of cooling is greater than the critical cooling rate, i.e., the rate at which formation of pearlite or bainite is just prevented, the hardness obtained on quenching depends principally on the carbon content of the steel. If the cooling rate is lower than critical rate, the amount of martensite is reduced, thus lowering the overall hardness of steel. Carbon content in this context means the amount of carbon dissolved in the austenite. Carbon which remains as carbide after the austenitization treatment does not take part in the martensite reaction and has therefore no influence on the hardness of the martensite.

Hardenability is the ability of the steel to harden by the formation of martensite on quenching. The hardenability determines the depth of hardening obtained on quenching. Maximum hardness is dependent almost entirely

upon the carbon content, whereas, hardenability is, in general, far more dependent upon the alloy content and the grain size of the austenite [24,26,31]. (See Figure 11).

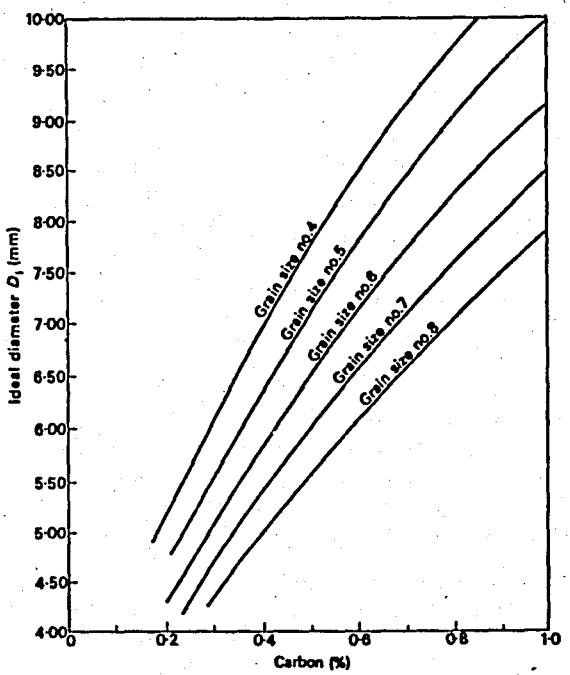

Figure 11. Hardenability (expressed as the ideal critical diameter) as a function of the carbon content and the austenite grain size for plain carbon steels [31].

The characteristic property of a steel possessing high hardenability is that it shows a large depth of hardening or it hardens through in heavy section. The leavier the section to be hardened the smaller is the depth of hardening and the lower is the core hardness. The reason why a steel is harder at the surface than at the centre is explained by referring to a continuous cooling transformation diagram. It is obvious that since the surface cools at a considerable faster rate than the center, the cooling curve representing the surface will past in front of the ferrite and bainite, and as a result, only martensite is formed (Figure 12). At the centre which cools more slowly, some bainite will be formed, as may be inferred from the figure, and this will result in a lower hardness in the core. As the dimensions of the steel increase, the rate of cooling decreases, and the core hardness will be still further reduced, owing to the formation of ferrite and pearlite. The surface hardness will also decrease when the cooling curve is so displaced to the right of the critical cooling curve.

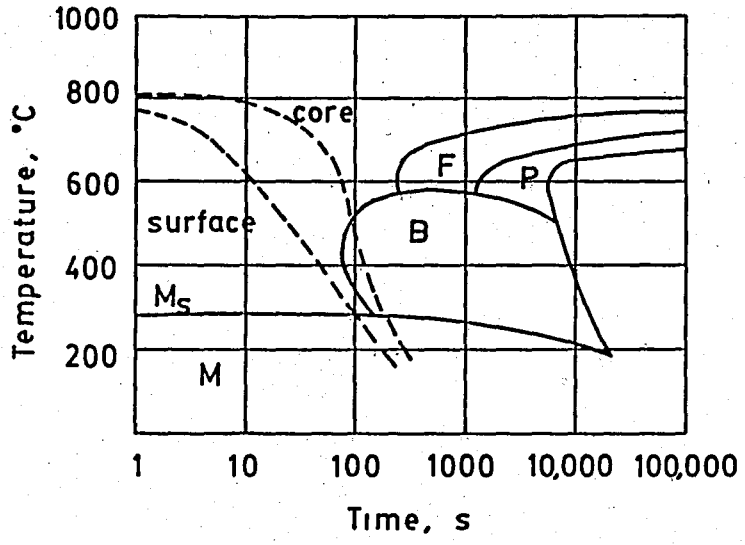

Figure 12. Schematic illustration of the cooling curves for surface and core of an oil-quenched 95 mm diameter bar [31].

2.9.1. Jominy End-Quench Test

The most commonly used method for the measurement of hardenability, at present, has been developed by Jominy [24]. For this test, a round bar specimen is used, 25 mm in diameter and 100 mm in length. The specimen is heated at the hardening temperature of the steel with a holding time of 30 minutes, then placed in a quenching fixture (Figure 13) so that the specimen is held vertically above a water opening in order that a column of water may be directed against the bottom end of the specimen while the

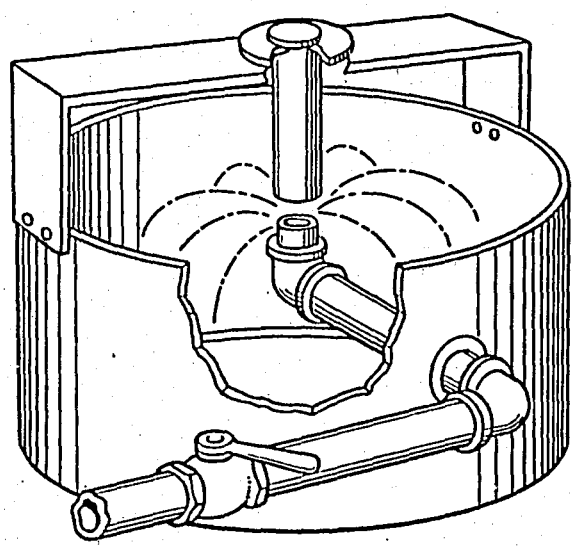

Figure 13. Jominy end-quench test fixture [23].

bottom end is being quenched by the column of water, the opposite end is cooling slowly in air, and intermediate positions along the specimen cool at intermediate rates. When it is cool, two diammetrically opposite flats, 0.4 mm deep and parallel to the axis of the bar are ground and the hardness is measured at intervals of 1/16 inch from the water quenched end to determine how the as-quenched hardness varies with the continuous variation in cooling rate along the length of the specimen. Hardness is then plotted against distance from the quenched end, on standard charts. Figure 14 presents a typical hardenability curve for AISI 5140 steel austenitized at 845°C and 1000°C, plotted on the standard graph.

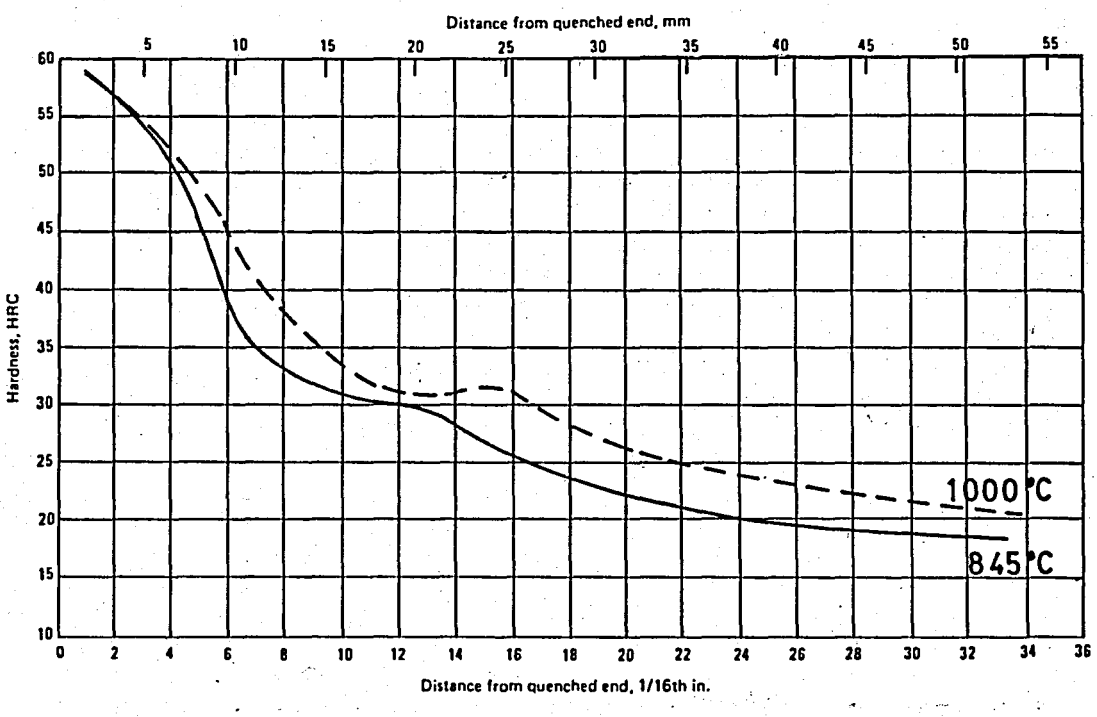

Figure 14. Jominy hardenability curves for AISI 5140 steel auter austenitization at 845°C and 1000°C (22).

The steels having higher hardenability will be harder at a given distance from the quenched end of the specimen than steels having lower hardenability. Thus, the flatter the curve, the greater the hardenability.

For end-quench tests, hardness is not usually measured beyond approximately 2 in. (5 mm), because hardness measurements beyond this distance are seldom of any significance. At about this 2 in. (50 mm) distance from the quenched end, the effect of water on the quenched end has deteriorated, and the effect of cooling from the surrounding air has become significant.

II. HARDENING OF STEEL

The desirable properties of tempered martensitic structures have been emphasized up to now. Quenching and tempering is the heat treatment commonly used to obtain such microstructures, and therefore, represents the final heat treatment ordinarily used to obtain optimum properties in heat-treated materials.

Hardening is defined as "austenitizing and then cooling rapidly enough so that some or all of the austenite transform. to martensite" (34). This method is depicted in Figure 15. It involves a continuous cooling from the austenitizing temperature through the martensite transformation temperature range at a rate rapid enough to prevent any transformation at temperatures above the M_s temperature, followed by tempering to the desired hardness or strength level.

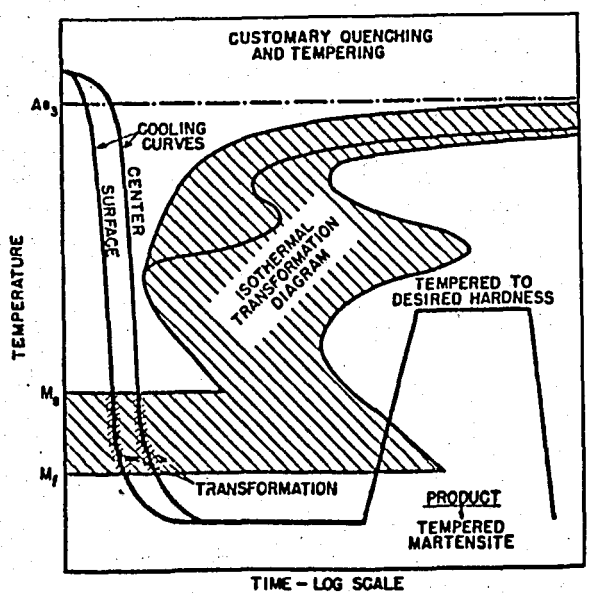

Figure 15. Schematic transformation diagram for quenching and tempering (24).

3.1. Heating

The first step in this heat treatment is the heating of the material to a temperature at which austenite is formed. The actual austenitizing temperature should, in general, be such that all carbides are in solution in order that full advantage may be taken of the hardenability effect of the alloying elements. The temperature should not, however, be so high that pronounced grain growth occurs [24]. The piece should be held at the austenitizing temperature long enough to dissolve carbides, but again, not long enough for excessive grain growth to occur [25].

Too rapid a heating rate may set up high stresses, particularly if irregular sections are involved, and is, therefore generally undesirable [26]. A heating time of one hour per each inch of section is commonly employed, and this is a safe rule [35]. Salt and liquid baths will have generally higher heating transfer coefficient and, therefore, will heat more readily than furnaces in which the heating is in air [32]. Flame hardening, in which rapid heating is obtained by the actual inpingement of a high temperature flame on the surface of the piece being heat treated is also used. These rapid heating practices are the exception, however, and the useful and safe practice is a relatively slow and uniform heating to the austenitizing temperature, followed by a holding period at that temperature long enough to insure that the piece is at a uniform temperature throughout [24].

Unless special precautions are taken, heating will usually result in a certain amount of oxidation or scaling and may also result in decarburization [24,26,28,31,35,36]. Both scaling and decarburization are usually undesirable. Scaling represents a loss of metal, mars the surface finish and may prevent rapid extraction of heat in quenching. Decarburization results in a soft surface and may seriously affect the fatigue life. Special measures are necessary if complete freedom from scaling or decarburization is necessary. These measures include heating in a muffle furnace containing reducing gases such as carbon-monoxide

or methane and hydrogen mixtures; packing in cast-iron chips or in a mixture of charcoal and sodium carbonate or heating in neutral salt or lead bath.

3.1.1. Heating Media [28,31]

During the heating up stage, it is necessary to provide against unintentional carburization or decarburization. Should this happen, the superficial hardness measured after hardening will be misleading, which may result in the choices of an incorrect tempering temperature.

(a) Salt Bath Furnaces: These offer good protection against variations in the superficial carbon content, owing to the short heating time required and the neutral character of the bath. The bath must of course be maintained in good condition. Some typical compositions and working temperatures for neutral salt baths are given below:

45 % NaCl - 55 % KCl	675 - 900 °C
20 % NaCl - 80 % $BaCl_2$	675 - 1060 °C
100 % $BaCl_2$	1025 - 1325 °C

(b) Electrically-Heated Muffle Furnaces: These, if not operated with controlled atmosphere, should be used with annealing boxes in which the steel charge is packed with some protective material, which should be as neutral as possible. One purpose of packing material is to prevent the ingress of air to the steel. For this purpose, cast-iron chips are very suitable since the air that is sucked into the box on account of temperature variations preventially axides the chips. Wood-charcoal or coke tines, borax and some pastes may also be used for protective means.

(c) Controlled Atmospheres: These specially produced protective gases, have shown themselves, both technically and economically to be highly suitable when used for the

heat treatment of costly tools and compound parts. The inert gases generally used for this purposes. Inert gas, is a protective gas that as regard its carbon, oxygen and nitrogen content, remains unreactive to the steel. The most commonly used unreactive gases are argon and nitrogen. A fairly simple method applicable to air-hardening steels is to place the tools in a gas tight box fitted an inlet and outlet tube. The gas is led through the box during the whole treatment cycle.

3.1.2. Hardening Temperature

For each grade of steel, on the basis of a series of practical trials, a range of temperature has been established to which the steel to be heated for hardening. These temperatures are published by American Society for Metals [22]. This temperature range, also called the quenching range, is chosen so as to give the maximum hardness, at the same time maintain a fine-grained structure for steel.

As the temperature increases, so does the grain size, and also the amount of retained austenite [31]. By raising the hardening temperature, the hardenability of steel can be increased. This increase is due to the greatest amount of carbide going into solution and increases in grain size [32]. It is suggested that it may be more practical to use a coarse-grained steel (resulting from high austenitizing temperature) than a more expensive alloy steel to obtain hardenability [32].

3.1.3. Holding Time at Hardening Temperature [28,31]

When the steel has reached the hardening temperature, it is austenitic provided that the temperature has been correctly chosen. The time of holding at the hardening temperature depends on the desired degree of carbide dissolution. Since the amount of carbide is different for different types of steel, the time of holding is also dependent of the grade of steel.

Plain carbon and low alloy structural steel which contain easily dissolved carbides require only a few minutes of holding time after they reached the hardening temperature. In order to be much certain that there has been sufficient carbide dissolution, a holding time of 5-15 minutes is quite sufficient.

3.2. Quenching [28,31]

As has been explained above, the first operation in the heat treatment of alloy steels is to cool sufficiently rapidly from the austenitizing temperature to avoid intermediate transformation to ferrite/pearlite and ensure transformation to either martensite or bainite depending upon the section size and the rate of cooling employed. There is very strong interaction between the quenching medium used to obtain the required amount of cooling and the shape and size of steel section to be treated. Because the normal contraction that takes place during cooling and the expansion that occurs during the austenite-martensite transformation, severe internal stresses are often set up and a substantial amount of distortion of the dimension of the treated component can take place. If this component has a complex shape, then very great care has to be taken in the selection of the appropriate quenching medium to avoid distortion being severe as to render the part useless for further application, or to avoid internal stresses of sufficient severity to cause quench cracks.

The various types of conventional quenching techniques in practice are direct quenching, time quenching, selective quenching, spray quenching, fog quenching and interrupted quenching.

Direct quenching is the most widely used method, the parts are plunged into the appropriate medium be it water, brine, oil or fused salt. Time quenching is applied when the cooling rate of the part being quenched has to be changed abruptly at some time during the cooling cycle. The change in cooling rate may be either an increase or decrease.

The usual practice is to quench in one medium for a short time until the "pearlite nose" has been passed, and then to quench the part in a second medium so that it cools more slowly through the martensitic or bainitic transformation ranges. Time quenching is most often used for minimizing distortion, cracking and dimensional changes. Selective quenching is adopted when it is required that certain areas remain unaffected by the quenching medium and this is accomplished by insulating these areas from the quench. In spray-quenching, spray of quenching liquids are directed at high pressures to local areas. Fog-quenching employes a fine fog or mist of liquid droplets and the gas carrier as cooling agent. Interrupted quenching pertains to quenching in a molten bath maintained at a constant temperature. This is used in the austempering and martempering processes.

3.2.1. Mechanism of Quenching

Stage A (See Figure 16), called "vapor blanket cooling stage", is characterized by the formation of an unbroken vapor blanket that surrounds the test piece. This stage is one of slow cooling, because the vapor envelope acts as an insulator and cooling occurs principally by radiation through the vapor film.

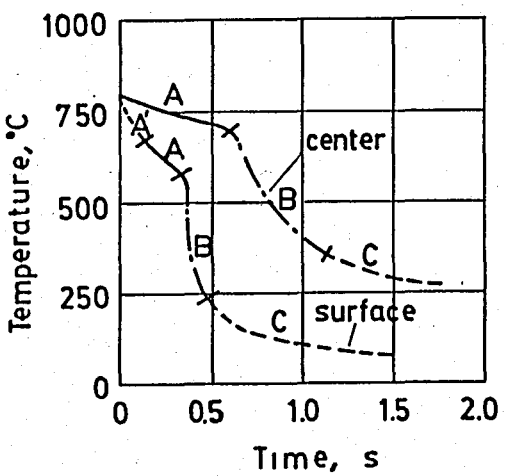

Figure 16. Typical surface and center cooling curves indicating the stages of heat transfer from a hot solid to a cold liquid (28).

Stage B, the vapor transport cooling stage, which produces the highest rates of heat transfer, begins when the temperature of the surface of the metal has been

reduced somewhat and the continuous film collapses, violent boiling of the quenching liquid then occurs and heat is removed from the metal at a rapid rate, largely as heat of vaporization.

Stage C is called the "lequid stage", the cooling rate in this stage is slower than that developed in stage B. Stage C begins when the temperature of the metal surface is reduced to the boiling point of the quenching liquid. Below this temperature, boiling stops and slow cooling takes place thereafter by conduction and convection.

3.2.2. Factors Affecting Cooling Rate

Agitation, that is, externally produced movement of the quenching liquid, has an extremely important influence on the heat transfer characteristics of the quenching liquid. It causes an earlier mechanical disruption of the vapor blanket in stage A. It mechanically disrupts or dislodges gels and solids, whether they are on the surface of the test piece or suspended at the edge of the vapor blanket, thus producing faster heat transfer in liquid cooling (stage C). In addition to the above effects, agitation also brings cool liquid to replace heat-laden liquid.

Another factor which affects the cooling rate is the temperature of the liquid. Higher liquid temperatures lower the characteristic temperature and thus lengthen the time at stage A. However, the boiling point is not changed. Higher liquid temperatures may decrease viscosity, affect the bubble size, or influence the breakdown and flush point of certain oils or compounds. Other factors being equal, higher temperatures decrease the rate of heat transfer in stage C.

Increasing the temperature of the test piece has relatively little effect on its ability to transfer heat to the quenchant. The rate of heat transfer may be increased simply because a greater temperature difference exists [8]. The most noticeable change in ability to transfer heat

probably comes from the more rapid oxidation of the surface of the test piece. This can either increase or decrease the heat transfer ability, depending on the thickness of the oxide developed.

3.2.3. Quenching Mediums

Water is probably the oldest cooling medium used for hardening and it has remained the major coolant throughout the ages. Pure water, however, is rather unsuitable as a cooling medium since its greatest cooling efficiency occurs at 300°C, i.e., the temperature at which martensite formation starts in many steels. By adding 10 per cent common salt or soda to the water (then, it is called brine solution), its cooling capacity is increased very considerably and at the same time its greatest heat-extracting capacity now occurs at 500°C. These points are illustrated in Figure 17, which shows the rapid fall in cooling capacity as the temperature of the water rises about 60°C. The overall best result is obtained when the water temperature is between 20°C and 40°C.

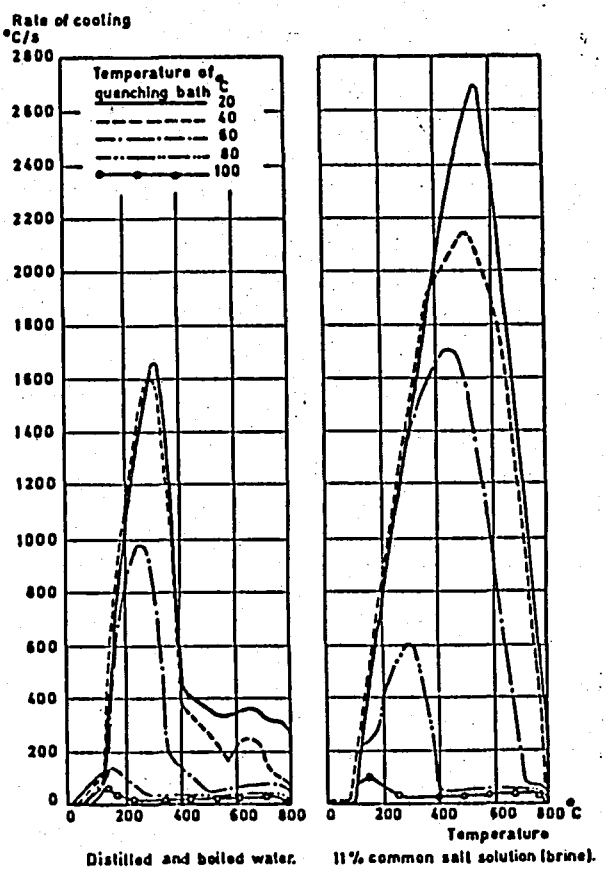

Figure 17. Cooling capacity of pure water and brine (31)

The great drawback of water, as mentioned above, is that the rate of cooling is high in the temperature range of martensite formation. This exposes the steel to the simultaneous influence of transformation stresses and thermal stresses, the combined effect of which will increase the risk of crack formation.

Oil cooling is much slower than water cooling. The rate of cooling is greatest at about 600°C and is relatively slow in the range of martensite formation. Since oil has rather low capacity for heat extraction relative to water, its use as a coolant for medium to low alloy steels is restricted to light section. A reliable and tested way of increasing the cooling capacity of oil is by agitating vigorously the bath or the charge. Another way of increasing the cooling potential is to raise the temperature of oil to 50-80°C. This increase in temperature makes the oil more fluid and hence increase its cooling capacity. Figure 18 shows how the cooling capacity of a conventional mineral oil and a fast quenching oil are influenced by their respective temperatures.

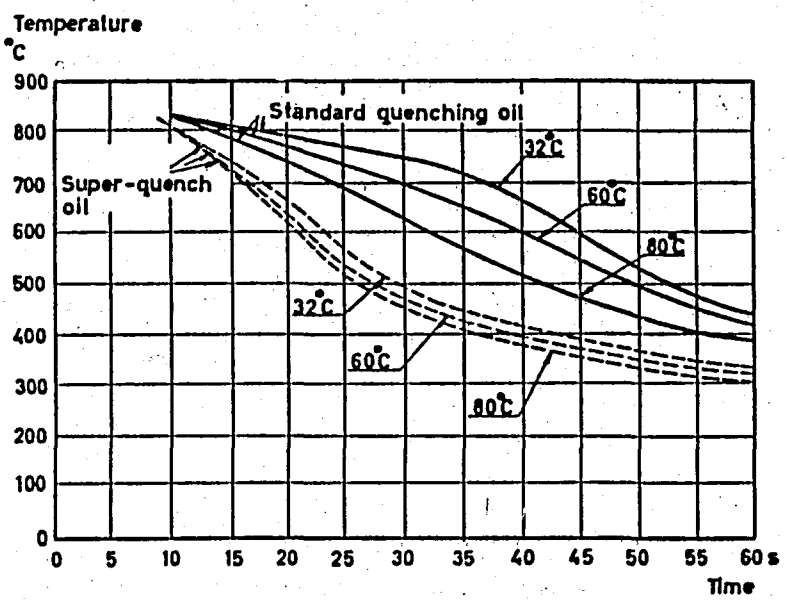

Figure 18. Influence of quenching oil temperature on quenching rate of plain carbon steel (25 mm diameter and 75 mm long test specimen) (31).

Mixtures of water and oil (emulsions) are a third type of oil quenchant and their characteristics can vary considerably depending upon the percentage content of water and oil.

Low alloy steels in light sections and high alloy steels may be successfully hardened by means of compressed air or still air. The advantages of using air are that distortion is negligible and that the steel can easily be straightened during the cooling process.

The last kind of quenching medium is salt bath which consists of approximately equal parts of sodium nitrite and potassium nitrate. They are used in the temperature range 150-500°C. A salt bath is the ideal quenching medium for a steel having a reasonably good hardenability and not too heavy a section. The cooling capacity down to about 500°C is high and then decreases as the temperature of the steel continues to fall. The lower the temperature of the bath and the greater the agitation, the better is its cooling capacity.

3.3. Tempering

The martensite formed by quenching is very hard and very brittle and, as described above, its formation leaves high residual stresses. The purpose of tempering is to relieve these stresses and to improve ductility, which it does at the expense of strength or hardness.

Tempering is defined as "reheating a quenched or normalized ferrous alloy to a temperature below the transformation range (A_1) and then cooling at any desired rate" (34). Steels are tempered by reheating after hardening to obtain specific values of mechanical properties and to relieve quenching stresses and ensure dimensional stability. Tempering usually follows quenching from above the critical temperature, however, tempering also be used to relieve the stresses and to reduce the hardness developed during welding, and to relieve stresses induced by forming and machining.

The stress relief and recovery of ductility by tempering after quenching are brought about through precipitation of carbides from the super-saturated unstable alpha-iron solid solution (martensite) and through diffusion and coalescence of the carbides as the tempering operation proceeds. For a better understanding of the mechanism of the tempering process, the stages [31] that a hardened carbon steel passes through when subjected to a continuous rise in temperature are now briefly discussed.

1. 80-160°C
   - Precipitation of carbon-rich phase called epsilon-carbide.
   - Transformation of tetragonal martensite progressively to cubic martensite.
2. 230-280°C
   - Decomposition of retained austenite to bainite like product.
3. 160-400°C
   - Formation and growth of cementite at the expense of epsilon-carbide.
4. 400-700°C
   - Continued growth and spheroidization of cementite.

The tempering of martensite results in a contraction and if the heating is not uniform, stresses will be set up by this unequal contraction which will cause distortion or even cracking. Similarly, too rapid a heating for tempering may be dangerous because of the sharp temperature gradient set up between the surface and interior of the piece. Recirculating air furnaces are ideal for obtaining uniform heating desired for tempering and are very commonly used for tempering temperatures up to 250°C. Oil or salt baths are very commonly used for tempering and are generally safe in spite of their rapid rate of heating, since the temperature differential is low.

3.3.1. Principal Variables

Variables associated with tempering that affect the microstructure and the mechanical properties of a tempered steel include temperature, time at temperature, cooling rate from the tempering temperature and composition of steel including carbon content, alloy content and residual elements . In a steel quenched to a microstructure consisting essentially martensite, the iron lattice is strained by the carbon atoms, producing the high hardness of quenched steels. On heating, the carbon atoms diffuse and react in a series of distinct steps that eventually form Fe_3C or an alloy carbide in a ferritic matrix of gradually decreasing stress level. The properties of tempered steel are determined primarily by the size, shape, composition and distribution of carbides that form, with a relatively minor contribution from solid solution hardening of the ferrite. These changes in microstructure usually decrease hardness, tensile strength and yield strength, but increase the ductility and toughness. Temperature and time are interdependent variables in the tempering process, within liminta, lowering temperature and increasing time usually can produce the same result as raising temperature and decreasing time.

(a) Tempering Temperature: Figure 19 shows the effect of tempering temperature on hardness, tensile and yield strength, elongation, reduction in area and Charpy impact energy of a plain carbon steel (AISI 1050). Note that both room temperature hardness and strength decrease as the tempering temperature is increased. Ductility at ambient temperatures, as measured by either elongation or reduction in area, increases with tempering temperatures.

Whereas elongation and reduction in area increase continuously with tempering temperatures, toughness as measured by a notch-bar impact test, varies with most steels as shown in Figure 19 (e). Tempering at temperatures from 260 to 320°C decreases both impact energy to a value below than that obtained at about 150°C. Above 320°C, impact energy again increases with increasing tempering temperatures.

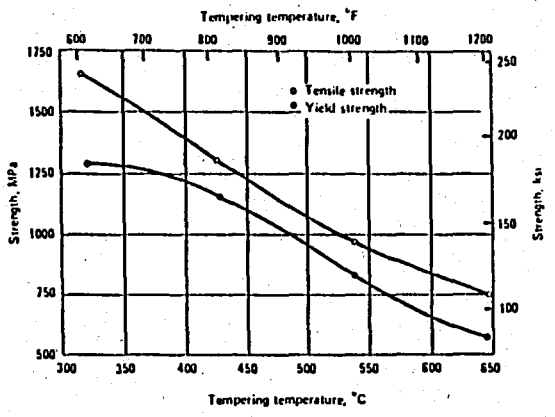

(a)

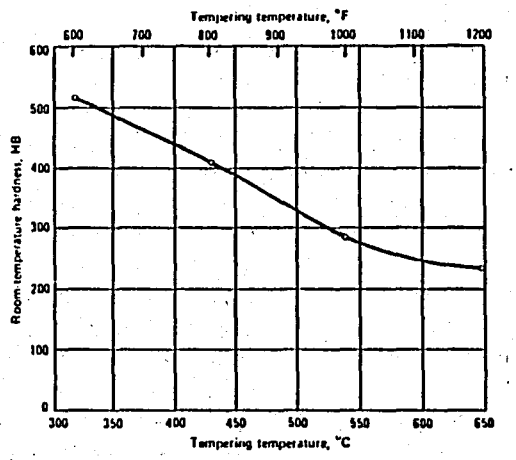

(b)

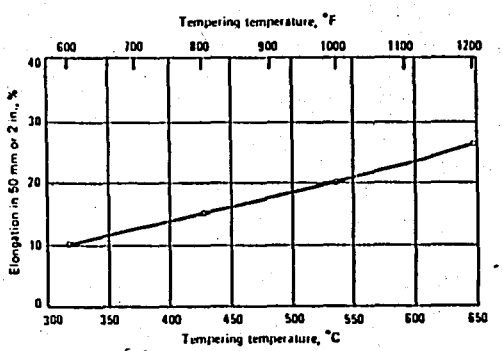

(c)

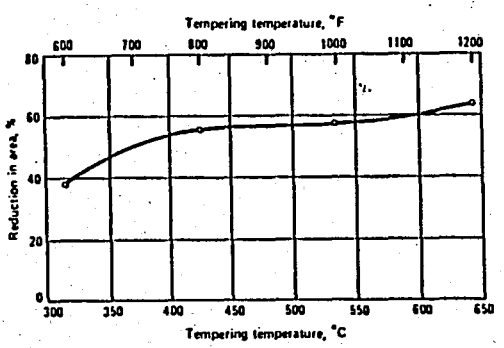

(d)

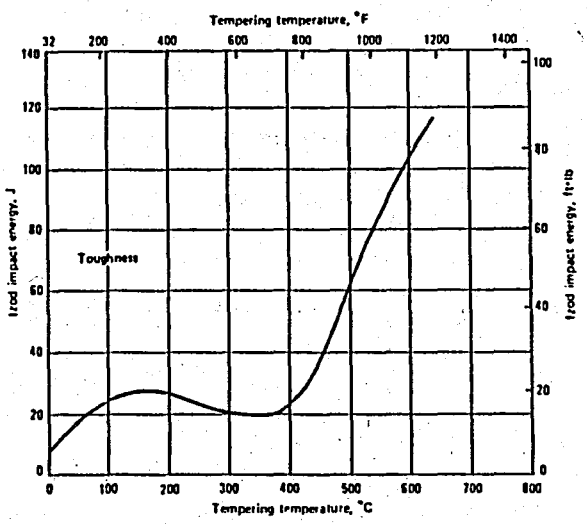

(e)

Figure 19. Effect of tempering temperature on room temperature mechanical properties of 1050 steel (38 mm in diameter, water quenched) [28].

Both plain carbon and alloy steels respond to tempering in this manner. The phenomenon of impact energy minima centered around 350°C is called "500°F embrittlement" [28]. At the same time, the loss in toughness is accompanied by a change from a predominantly "tough" shear type of fracture to a more brittle cleavage type. The tough or shear type of fracture seems to take place across grains (transgranular), whereas the brittle or cleavage type seems to take place in grain boundaries (intergranular). The intergranular nature of the fracture is believed to occur by the precipitation of film-like carbides on grain boundaries [13].

(b) Tempering Time: The diffusion of carbon and alloying elements necessary for the formation of carbides is temperature and time dependent. In general, lowering temperature and increasing time usually can produce the same result as raising temperature and decreasing time.

(c) Cooling Rate: Another factor that can affect the properties of a steel is the cooling rate from the tempering temperature. Although tensile properties are not affected by cooling rate, toughness (as measured by notched-bar impact testing) can be decreased if steel is cooled slowly through the temperature range from 370 to 575 °C, especially in steels that contain carbide-formin elements. Elongation and reduction in area may also be affected. This phenomenon is called "temper embrittlement". The embrittlement - a loss of cohesion at prior austenite grain boundaries - is believed to be caused by segregation of antimony and phosphorus and, to a lesser extend of arsenic and tin to prior austenite grain boundaries during austenitization of the steel [37]. The susceptibility of a steel to temper embrittlement is also enhanced by segregation of alloying elements, particularly manganese and chromium, to prior austenite grain boundaries. Apparently the embrittling elements are arranged near the grain boundaries and move to the embrittling configuration only in the temperature range 370 to 575°C. Below about 370°C,

the mobility of the embrittling elements is restricted and above 575°C, they return to the unembrittling configuration [13].

(d) Alloy Content: The addition of alloying elements which increase hardenability may be very helpful in decreasing the magnitude of the internal stresses resulting from the quench, since they all permit the attainment of a martensitic structure with a less drastic quench. For this reason, the use of an alloy steel and a mild quench for an application requiring high hardness, and therefore, a low tempering temperature with an accompanying relatively low degree of stress relief may be very advantageous.

The alloying elements will however, have a direct and significant effect upon the second behavior, that of crystallization and coalescence of carbides. In general, the effects of alloying elements will be the retardation of the rate of softening. This means that an alloy steel will customarily require higher tempering temperature or longer time at temperature, to obtain a given hardness. Alloying elements can be characterized as carbide forming and non-carbide forming. Elements such as nickel, silicon, aluminum and manganese, which have little or no tendency to occur in the carbide phase, remain essentially in solution in the ferrite and have only a minor effect on tempered hardness. Hardening due to the presence of these elements occurs mainly through solid-solution hardening of the ferrite. The carbide forming elements such as chromium, molybdenum, tungsten, vanadium, tantalum, niobium and titanium retard the softening process by formation of alloy carbides. The effect of the carbide-forming elements is minimal at low tempering temperatures where Fe_3C forms, however, at higher temperatures alloy carbides are formed and hardness decrease slowly with tempering temperatures. Under certain conditions, such as with highly alloyed steels, hardness may actually increase. This latter effect is known as "secondary hardening".

IV. HIGH TEMPERATURE AUSTENITIZATION

Commercial low alloy steels are conventionally austenitized at the lower end of the austenite range, quenched fast enough to produce martensite and tempered to produce fine prior austenite grain sizes, insuring good strength and relatively low or moderate fracture toughness.

In 1970's however, there has been considerable interest in employing much higher austenitization temperatures (up to 1200°C) to increase the fracture toughness of such steels without loss in strength [1-21].

4.1. Increasing Toughness with High Temperature Austenitization

The first comprehensive investigation to improve the fracture toughness of as-quenched or lightly tempered alloy steels (like 4340) by non-conventional heat treating procedure is attributed to Zackay et al. [7]. They studied the effect of high temperature austenitization, i.e., 1000°C, 1100°C and 1200°C, either direct or stepped quench (step quenching : after the austenitization at high temperature, furnace cooling to a lower temperature and holding at that temperature for a determined time before quenching) and quenching in different media, i.e., iced brine, water or oil. They arrived in nearly two-fold increase in fracture toughness values after quenching from 1200°C when compared to conventional treatment at 870°C. They also concluded that the austenitization temperature is more important than quenching rate for optimizing toughness. They attributed the effectiveness of a high austenitization

temperature in reducing brittleness to the fact that grain boundary nucleation of a second phase is retarded when the high energy grain boundaries associated with small grains are eliminated by grain growth.

Wood [9] studied the effect of high austenitization temperatures on different materials and showed that while the conventionally heat treated as-quenched and low temperature tempered fracture toughness of alloy steels were very low, large increase in fracture toughness could be achieved, without sacrificing strength by altering the heat treatment (See Table 1). For alloys with very limited hardenability, the high austenitizing temperatures resulted in very large grains which provided added hardenability. This when combined with more rapid quenching rates, eliminated large amounts of non-martensitic decomposition products which provided essential sites for crack initiation. However, the alloys with inherently greater hardenability such that the microstructure should be essentially martensitic for all the heat treatments employed, also underwent dramatic increase in toughness when given high temperature heat treatments. They suggested that the other factors such as possibly retained austenite or segregation effects should be involved.

Table 1. As-quenched fracture toughness of several alloy steels as a function of austenitizing temp. [9].

Alloy	Austenitizing Temp. (°C)	Quench	K_{1c} (MPa$\sqrt{m}$)
4130	1200	Oil	96.5
	1200-870*	Oil	80.3
	870	Oil	61.6
4140	1200	Oil	56.1
	1200-870*	Oil	36.3
	870	Oil	29.7
4340	1200	Oil	69.3
	1200-870*	Oil	67.1
	870	Oil	40.7

(*) Step quenching

Lai [38] supported the results of Wood [9] by examining the structures resulted from both high and conventional austenitizing treatments by transmission electron micrographs. The undesirable austenite decomposition products such as proeutectoid ferrite and upper bainite were eliminated by high temperature austenitizing. He also pointed out the possible role of increasing amount of retained austenite with austenitizing temperatures to enhance fracture toughness.

Clark et al.[19] have associated the improvement in fracture toughness by high temperature austenitizing with the prevention of segregation of impurity elements such as antimony, phosphorus and bismuth with so high temperatures, since the increase in fracture toughness is rapid at a described temperature as shown in Figure 20. They stressed on the point that if the tempering temperature is such that the martensite temper embrittlement could occur, the reduced grain boundary area might lead to greater concentrations of segregate and hence to a reduction in toughness in high temperature austenitized structures.

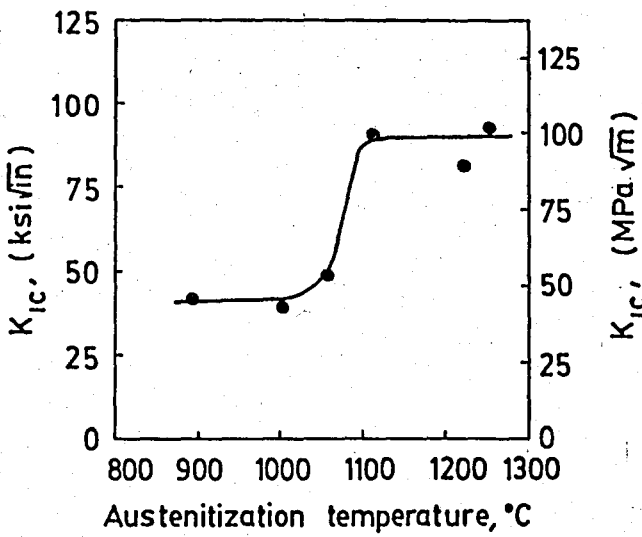

Figure 20. Variation of K_{Ic} with austenitizing temperature (5 % Mo, 0.6 % mn, 0.3 % C steel) (2).

McDarmaid [20] reported the results of high temperature austenitization, step quenching and rapid austenitization on fracture toughness of 300M steel. As shown in Figure 21, the beneficial effects of high temperature austenitization is obvious at low tempering

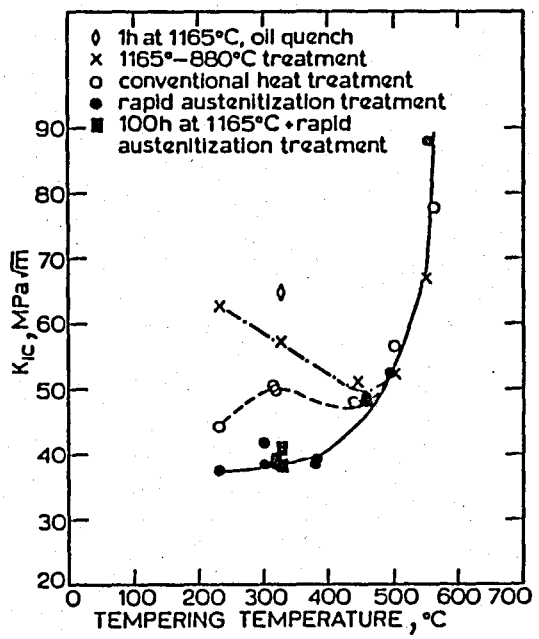

Figure 21. Effect of austenitization and tempering temperatures on K_{1c} of 300M steel (20).

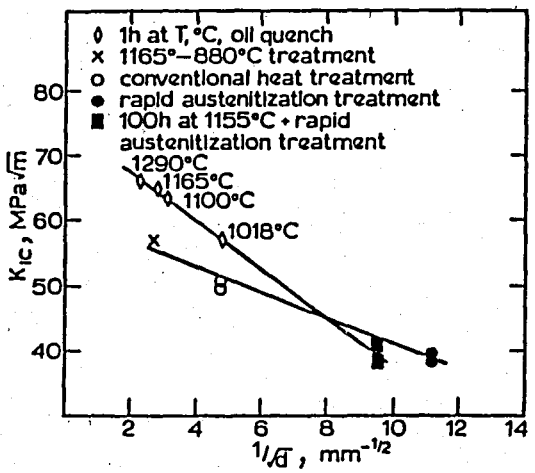

Figure 22. Effect of grain size on K_{1c} of 300M steel tempered at 320 C (20).

temperatures. Above the tempered martensite embrittlement temperature (450°C for 300 M steel), the fracture toughness was independent of the hardening treatment. He also observed a linear relationship between the grain size and austenitization temperature (Figure 22). The increase in fracture toughness was believed to be the result of the chemical homogeneity by reducing segregation of the alloy elements and impurities such as P, S, Sb and As; microstructure and fracture mode.

It has been shown by Khan and Wood (17) that a consistent drop in fracture toughness values was observed as the intermediate holding temperature decreased or the holding time at this temperature increased during step quenching. While direct evidence for segregation has not been found, the observed facts were consistent with segregation effects during austenitization treatment. The fracture toughness properties of AISI 4340 steel were affected not only by the amount and distribution of retained austenite, but also by the extend of segregation during austenitization.

Lai et al.[13] have examined the effect of austenitization temperatures such as 870°C, 1000°C, 1100°C and 1200°C on the fracture toughness as well as the impact strength of as-quenched 4340 steel. Since direct quench from high austenitizing temperature might have resulted in quench cracking (in water), they have also studied the effect of step quenching on toughness characteristics. Their results were:

(a) Fracture toughness increased, but Charpy V-notch impact energy slightly decreased with increasing austenitization temperatures (See Table 2),

(b) Step quenching gave similar results with the direct quench from the same initial temperature,

(c) Yield and tensile strengths were nearly independent of the austenitizing temperature,

(d) Ductility was better with the conventional treatment,

(e) High austenitizing temperature caused 10-fold increase in prior austenite grain size,

(f) There was no need for a faster medium than oil for 1200°C treatment.

Microstructural observations concomitant with the increase in K_{1c}, fairly continuous films of 100-200°A thick of retained austenite were present between the martensite laths. Additionally, specimens austenitized at 870°C contained twinned martensite plates, while those austenitized at 1200°C showed no twinning.

Table 2. Room temperature fracture properties for 4340 steel in the as-quenched condition [13].

Austenitization temp. (°C)	Quench	K_{1c} (MPa$\sqrt{m}$)
1200	Oil	64.5
1100	Oil	44.0
1000	Oil	34.2

It has been proposed by Parker and Zackay [21] that the fracture toughness of quenched and tempered steels such as 4340, 4140 and 300M can be increased by 50-100 per cent by minor changes in heat treating procedures. They argued that certain microstructural features, particularly blocky ferrite, upper bainite and twinned martensite plates, are deleterious to fracture toughness. Similarly, the presence of undissolved carbides and sulfide inclusions which act as crack nuclei, can lower the fracture toughness. Other microstructural constituents such as lower bainite, auto-tempered martensite, and retained austenite can enhance fracture toughness. Disappearance of undissolved carbides at high austenitizing temperatures may increase K_{1c}. But if the steel is such that it does not contain any undissolved carbides after 870°C austenitization, e.g., 4340, the main reasons are the increased amount of retained austenite and elimination of twinned martensite during 1200°C austenitization.

Youngblood and Raghavan [10] made an extensive study on the effect of both the austenitization and tempering temperatures on fracture toughness and the tensile ultimate and yield strengths of 300M steel. Results indicated that substantial improvement in toughness with no loss in strength could be accomplished in quenched and tempered steel by austenitizing at 1000°C or higher. Low fracture toughness in conventionally austenitized 300M steel (at 870°C) appeared to be caused by undissolved precipitates seen both in the submicrostructure and on the fracture surface which promoted failure by quasi-cleavage. These precipitates appeared to dissolve in the range 950-1000°C.

The effect of austenitizing temperature upon the microstructure and mechanical properties of Fe-Cr-C steels with and without titanium were investigated by Carlson et al. [3]. For the ternary Fe-Cr-C alloys, the results were consistent with the earlier investigations, but the fracture toughness did not change with increasing austenitizing temperatures after 0.2 per cent titanium was added. The titanium formed carbides (TiC) that did not dissolve, providing a roughly constant number of crack nucleation

sites and preventing austenite grain growth up to 1100°C. If titanium has not been added, the ternary Fe-Cr-C alloy contained submicron size chromium carbides that dissolve at about 1000°C and do not prevent linear increase in grain size with austenitizing temperature. They stressed on the role of grain size to effect fracture toughness.

Toughness of lath martensite structure has been shown to be higher than that of plate martensite by Yokota and Lai [39]; and Khan and Wood [17], Lai et al.[13], Parker and Zackay [8] and Padmanabhan and Wood [15] have associated the increase in fracture toughness by the decreasing amount of plate martensite which contained twinning during high temperature austenitization.

Youngblood and Raghavan [10] argued that after tempering around 350°C, the observed decohesion along prior austenite grain boundaries suggested that the micromechanism propagating the failure was definitely at the grain boundary rather than in the matrix. It has been reported by Ferguson et al.[21] that, because of the increased grain size and hence reduced grain boundary area that results from high temperature austenitizing, the toughness during subsequent tempering could be reduced if an embrittling species segregated to the prior austenite grain boundaries, for the reduced grain boundary area would lead to a greater concentration of segregate. Thomas and Yen-Yung Chen [40] and Sarıkaya et al.[6] have linked the severity of 350°C embrittlement with the decomposition of retained austenite to carbide at the martensite lath boundaries, and since the high temperature austenitized structure contained more retained austenite than conventionally austenitized structures, they showed more pronounced embrittlement.

4.2. Conflicting Results in K_{1c} and CVN Impact Energy in High Temperature Austenitization

Although the fracture toughness, K_{1c}, of low alloy steels may be increased by as much as a factor of two with no loss in strength, by austenitizing temperatures greater

than 1000°C, a corresponding increase in Charpy impact energy cannot always encountered. Results for 4340, Fe-Cr-C, En 25 and 300M steels have shown either no increase or decrease in impact energy [1-5,15,41] after austenitization at high temperatures in both as-quenched and quenched and tempered (<350°C) conditions. Increase in impact energy have also been reported for lower carbon 4330 and 4130 alloys [42,43]. Since K_{1c} and Charpy impact energy are both measures of material toughness, it appears paradoxical that high temperature austenitizing gives greater toughness when rated by K_{1c}, while low temperature austenitization gives the greater toughness when rated by Charpy impact energy.

In the face of this conflicting evaluation of toughness, it is tempting for the scientist to simply adopt the results of the K_{1c} test and disregard the results of Charpy test as "inadequate", since it is no doubt true that K_{1c} test is based on a theoretical foundation of greater solidity than in the Charpy impact test. In reality, however, the contradictory results of the two technique for measuring toughness appear to be a real phenomenon and are indeed indication of important difference between fracture induced by sharp crack and blunt notches. These differences may be summarized as follows [1]:

(a) The Charpy test measures the energy required to cause complete failure of the specimen and therefore will include a contribution from plane stress, shear lip formation. The fracture toughness, on the other hand, measures a critical rate of the stress intensity, $\dot{K}$, at the crack tip necessary to cause plane strain unstable fracture. In a test piece of valid thickness, this value will be virtually independent of shear lip formation.

(b) The strain rate in an impact test is several order of magnitude greater than in a K_{1c} test. In fact, when expressed in terms of rate of increase in stress intensity at the notch tip ($\dot{K}$), $\dot{K}$ for impact testing is of the order of 10^5-10^6 MPa$\sqrt{m}$/s compared with <3 MPa$\sqrt{m}$/s for static K_{1c} test.

(c) There is a marked difference in the root radius (ρ) of the stres concentrator in the two tests. Charpy test-pieces contain a V-notch ($\rho \sim 0.25$ mm), whereas K_{1c} test-pieces contain a fatigue precrack ($\rho \rightarrow 0$).

Ritchie et al.[1] wished to find an explanation for the discrepancy in fracture toughness and Charpy impact energy data resulted from high temperature austenitizing in the as-quenched 4340 steel. They studied the effect of shear lip, strain rate and notch root radius, and found that there was no measurable difference in shear lip portions of the fracture surface, thus, the first possible reason failed. In order to observe the effect of strain rate, they tested fatigue precracked Charpy specimens in an instrumented Charpy machine (dynamic fracture toughness testing, K_{1d}), and found that, although there was a reduction in toughness for high temperature austenitized specimens, they showed superior toughness on 870°C specimens. Since this result occurred at the strain rate as in standard Charpy test, which showed the opposite result in terms of which structure was tougher, it was clear that strain rate sensitivity did not provided an explanation for the contradictory toughness results.

To determine how measured toughness varies with notch root radius for each austenitizing treatment, a series of Charpy test pieces were prepared with notch root radii ranging from a fatigure precrack to a 0.58 mm radius V-notch. The specimens were broken at room temperature in an instrumented Charpy machine, an impact energy and "apparent" dynamic fracture toughness, K_A, measured in each case. (Apparent fracture toughness refers to the value of K_{1c} or K_{1d} measured ahead of a rounded notch of radius ρ, and is generally varies as a mean of estimating the fracture toughness without recourse to fatigue cracking). The apparent fracture toughness is shown as a function of the square root of the notch radius, $\rho^{1/2}$ „ for both microstructures (Figure 23).

The important feature of this figure is that for small root radii $\rho \leq 0.05$ mm, the toughness of the 1200-870°C structure (step quenched) exceeds that of the 870°C

structure, whereas at larger radii ($\rho > 0.05$ mm) the reverse is the case. Thus, it can be seen that in fracture toughness tests, where $\rho \rightarrow 0$, the 1200-870°C structure will have the higher K_{1c} value, but for Charpy tests, where $\rho = 0.25$ mm, the 870°C structure will fracture at the larger K_{1c} value, and thus show the larger impact energy. For each structure the toughness is proportional to $\rho^{1/2}$ when ρ is greater than a critical radius ρ_o.

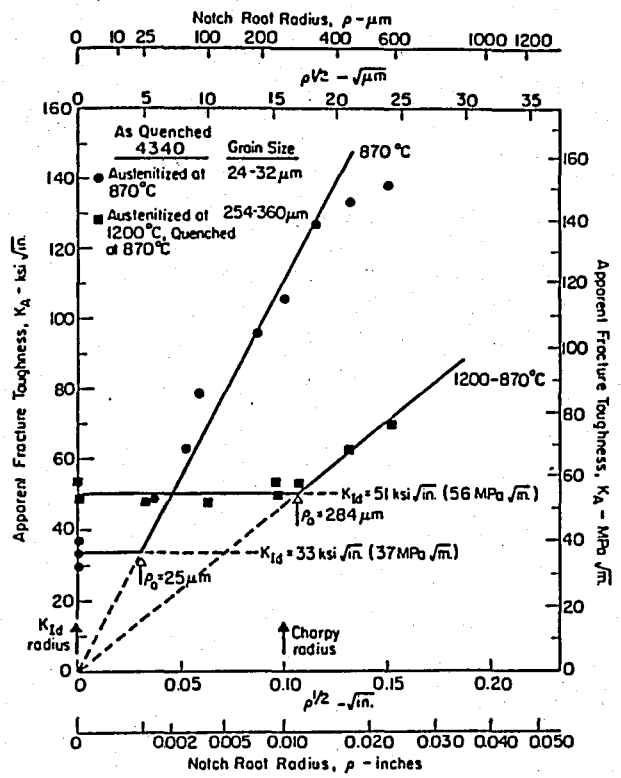

Figure 23. Relationship between the apparent toughness, K_A, and notch root radius [1].

By considering only the stress controlled fracture mechanism, i.e., quasi-cleavage and intergranular fracture, Ritchie et al.[1] developed a model to account for the influence of notch root radius (ρ) on fracture. They proposed that failure occurs when the maximum tensile stress σ_{yy}^{max} located at the plastic-elastic interface exceed a critical fracture stress, σ_f , for failure and arrived in

$$K_A \simeq 2.9\, \sigma_y \left(\exp\left(\sigma_f/\sigma_y - 1\right)\right)^{1/2} \rho_o^{1/2} \qquad (1)$$

The parameter ρ_o, the effective or limiting root radius, is a measure of the extent of the process zone ahead

of the crack, the "characteristic distance" over which the critical stress σ_f must exists to cause failure, and is related to the microstructural feature which controls fracture (such as grain size for cleavage fracture or inclusion or precipitation spacing for ductile fracture). The characteristic distance " l " represents the minimum distance from the notch where the critical fracture event can occur (i.e., where $\sigma_{yy} > \sigma_f$) and is only important where the maximum tensile stress (σ_{yy}^{max}) is very close to the notch tip. This is the case of ahead of sharp crak, where σ_{yy}^{max} at fracture is located at a distance ahead of the crack tip which is generally smaller than the characteristic distance. Ahead of rounded notches ($\rho > \rho_o$), however, σ_{yy}^{max} is located at, or just behing the plastic-elastic interface, and thus at failure „ the critical fracture event is occurring at a distance from the crak tip which is large compared with the characteristic distance.

Examination of Figure 24 in the light of the above theory reveals:

(i) The critical fracture stress, σ_f , is smaller in the 1200-870°C structure compared to 870°C structure, as indicated by the differing slopes of the equation (1),

(ii) The limiting root radius, ρ_o , is larger for the 1200-870°C structure compared to 870°C structure,

(iii) For both structures, the value of ρ_o is the same order as the prior austenite grain size. These observations indicate that the higher austenitization treatments have caused a reduction in critical fracture stress, but increased the critical distance over which it must be exceeded for failure. The increase in characteristic distance appears to be associated with the larger grain size. The decrease in σ_f is probably the result of grain boundary embrittlement due to segregation of impurity elements to the smaller grain boundary area of the larger grain sized material.

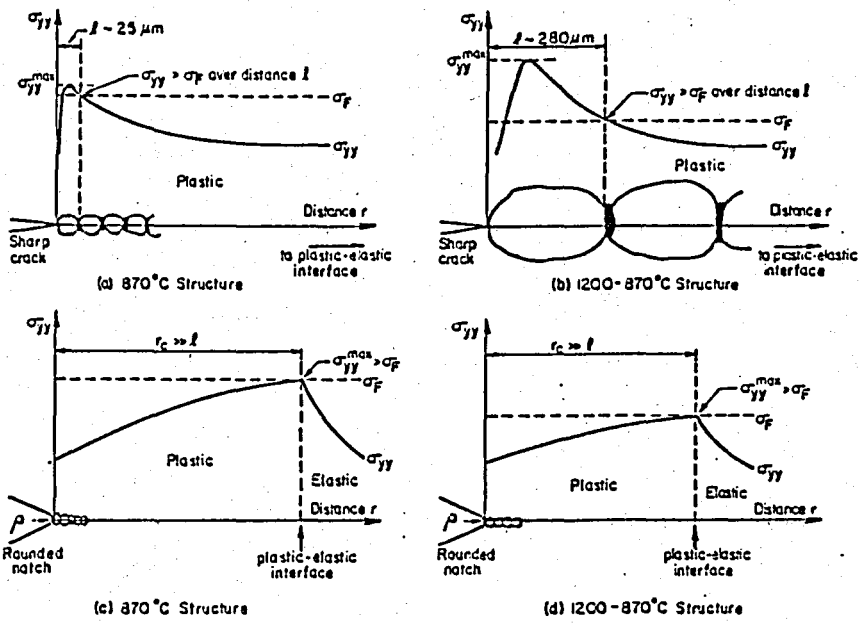

Figure 24. Schematic representation of the distribution of tensile stress (σ_{yy}) at distance (r) ahead of stress concentrator at failure for (a) 870 °C structure with sharp crack ($\rho < \rho_o$), (b) 1200-870 °C with sharp crack, (c) 870 °C structure with rounded notch ($\rho \geq \rho_o$), (d) 1200-870 °C structure with rounded notch [1].

By considering the strain controlled ductile rupture (microvoid coalescence) of quenched and tempered (at 200 °C) of 4340 steel, Ritchie and Horn [2] have arrived an expression for the fracture toughness ahead of notch for strain controlled fracture:

$$K_A = \left((3/2)\, \sigma_y\, E\, \varepsilon_f \right)^{1/2} \rho_o^{1/2} \qquad (2)$$

The parameter ρ_o, the effective or limiting root radius, can be considered in this instance as a measure of the characteristic distance or gage length over which the critical strain must be exceeded to cause failure. This distance is likely to be closely associated with the particle spacing or distribution. The slope of K_A versus $\rho^{1/2}$ plot is now a function of the critical fracture strain which is a measure of ductility. The observed decrease in slope with

increasing austenitizing temperature and thus a reduction in V-notch toughness (Charpy energy) when $\rho > \rho_0$ can be attributed to a decrease in ductility found with increasing austenitizing temperatures. The increase in sharp crack toughness K_{1c} on the other hand, has been associated with an increase in the characteristic distance over which the fracture strain must be exceeded ahead of the crack tip, apparently brought about by dissolution of carbide particles and sulfide inclusions with high temperature austenitization.

McDarmaid [41] have investigated the effect of notch-root radius, austenitization temperature and austenitization time on the room temperature impact strength and the ductile-brittle transition characteristics of tempered 300M steel and showed that the impact strength is increased with increasing austenitizing temperature if the notch root radius is less than 0.13 mm, but for blunter notches, it is decreased when the treatment temperature is above 1000°C (Figure 25). He argued that the impact strength depended on the energy required to nucleate a crack and the energy to propagate a crack. The impact energy required to fracture the precracked test-piece is a measure of the propagation energy, since virtually no energy will be required to nucleate the impact fracture. As it increases with increasing austenitizing temperatures, degradation of impact energy must be related to the changes in nucleation energy.

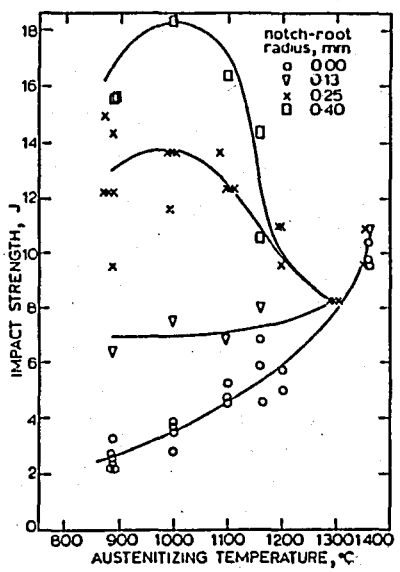

Figure 25. Effect of austenitization temperature and notch root radius on impact strength of 300M steel [41].

He also arrived in that for the standard notch, the transition temperature was increased with increasing austenitization temperature and this resulted in a decrease in the room temperature impact strength. This was not unexpected since DBTT is known to increase with grain size.

The increase in impact energy when the austenitization time is increased (Figure 26) proved that the observed increase in the material toughness, i.e., plane strain fracture toughness with austenitization temperature may be attributed to an improvement in steels, chemical homogeneity by resolution of residual elements, a reduction in segregation effects and supression of impurity segregation.

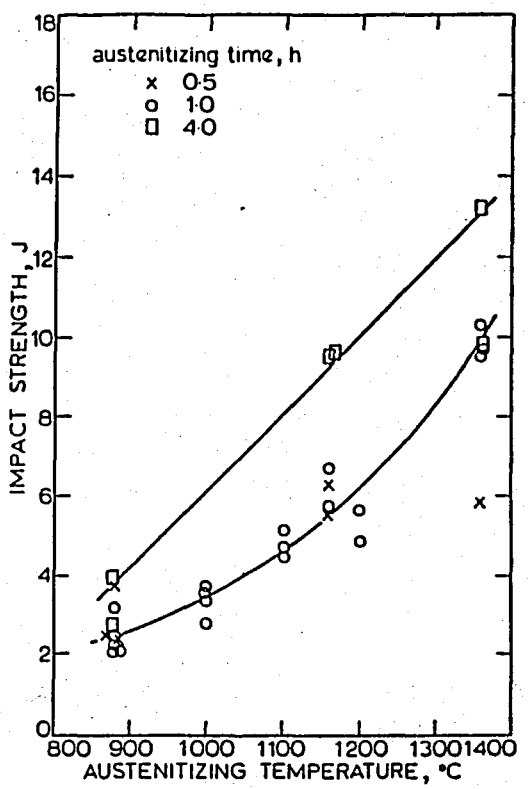

Figure 26. Effect of austenitization time on impact strength [41].

V. EXPERIMENTAL PROCEDURE

5.1. Material

The AISI 5140 low alloy steel used in the present study was obtained from "ASİL ÇELİK San. ve Tic. A.Ş." in a fully annealed condition. Its chemical composition has been determined by "ARL 34000 Spectrometer" as given in Table 3. About 225 kg. of steel was obtained in three different forms:

(a) 24 mm in diameter x 10 m in length,
(b) 36 mm in diameter x 10 m in length,
(c) 60 mm in diameter x 5 m in length.

Table 3. Chemical composition (weight per cent) of AISI 5140 steel used in this study.

C	Si	Mn	P	S	Cr	Mo	Ni	Al	Cu	Sn
0.41	0.29	0.80	0.022	0.021	0.75	0.03	0.14	0.028	0.26	0.029

5.2. Mechanical Testing

5.2.1. Tensile Testing

The room temperature longitudinal tensile properties were determined using a 12.5 mm in diameter and 62.5 mm in gage length ASTM specified [44] round specimens as shown in Figure 27. These specimens were machined oversized from the center of the 24 mm diameter bar, and after the heat treatments, were ground to the final dimensions. Duplicate tests were performed.

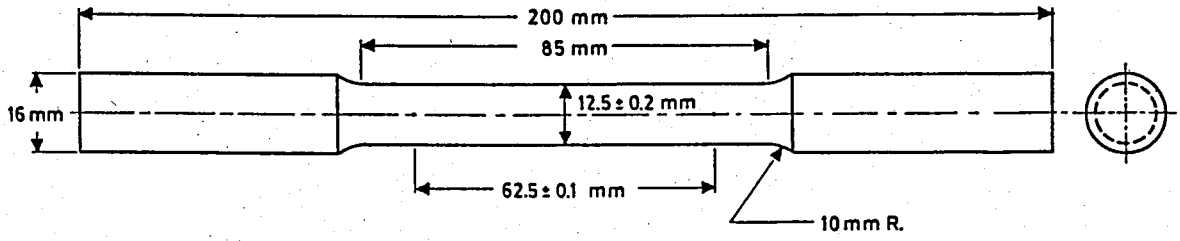

Figure 27. Tension test specimen.

A 400 kN capacity West Germany made "Wolpert Tensile Testing Machine" (Figure 28) was used to test the specimens at a loading rate of 1.7×10^{-5} m/s. The 0.2 per cent offset yield strength was determined from the load versus elongation curve.

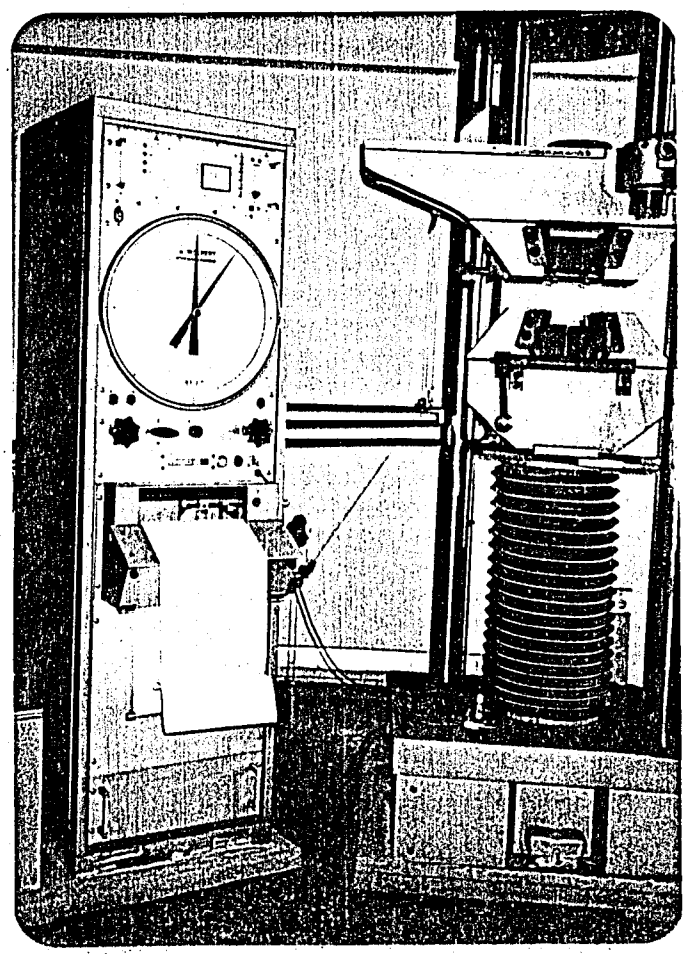

Figure 28. Wolpert Tensile Testing Machine.

5.2.2. Impact Testing

The room temperature longitudinal impact properties were determined using the standard ASTM [45] Charpy V-notch specimens as shown in Figure 29. The specimens were oversized machined from 24 mm diameter bar (See Figure 30 for specimen orientation). Following the heat treatmens, Charpy specimens were ground off 0.3 mm on each side and the notches were machined. Duplicate tests were done for all heat treatments on a pendulum type West Germany made "Wolpert Impact Testing Machine" (Figure 31) adjusted to 150 joules.

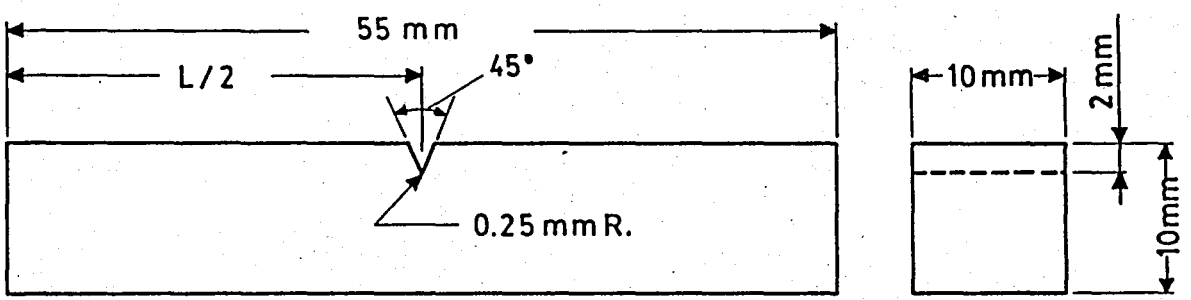

Figure 29. Charpy impact specimen, type A.

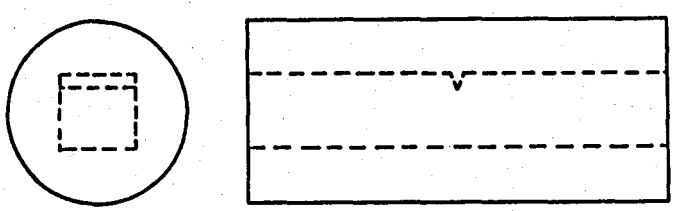

Figure 30. The schematic representation of the orientation of Charpy V-notch impact specimen.

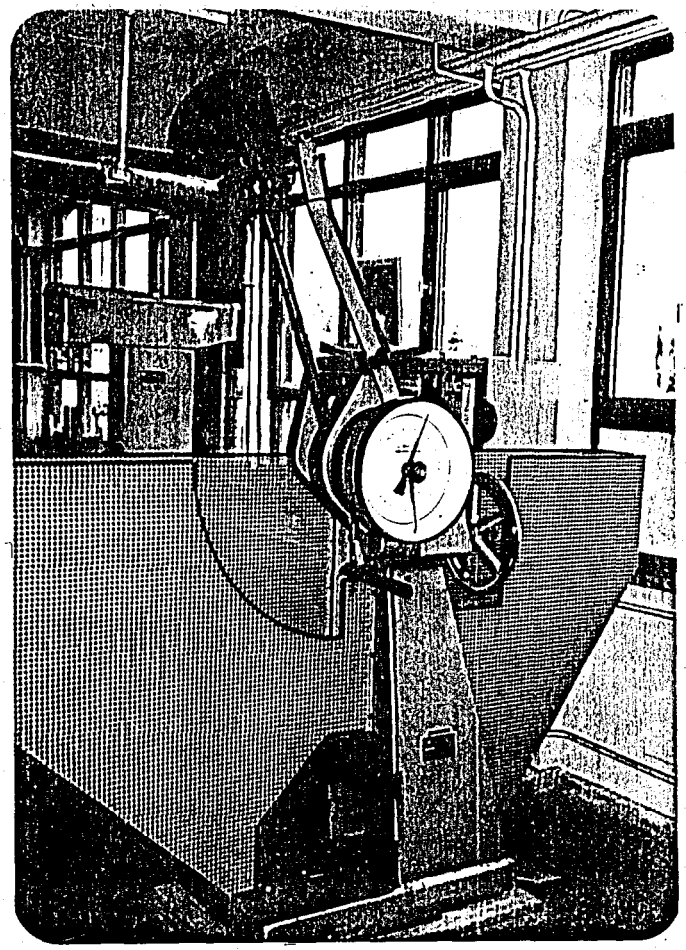

Figure 31. Wolpert Impact Testing Machine.

5.2.3. Fracture Toughness Testing

The room temperature plane strain fracture toughness (L-R direction) was determined using the ASTM specified [46] bending specimens (Figure 32) of 31.0 mm thickness. (See Figure 33 for specimen orientation).

The procedure followed in fracture toughness testing was:

(a) Bend test fixture design: Since no fixture was available for three-point bending testing, a fixture in accordance with the specifications of ASTM [46] was designed and machined (Figure 34).

(b) Specimen preparation: The specimens were machined oversized from 36 mm bar. The thickness of the specimens was decided as 31.0 mm from the existing K_{1c} results of similar low alloy steels such as AISI 4340 and 300M. The hole was drilled and the slot was machined.

(c) Heat treatment.

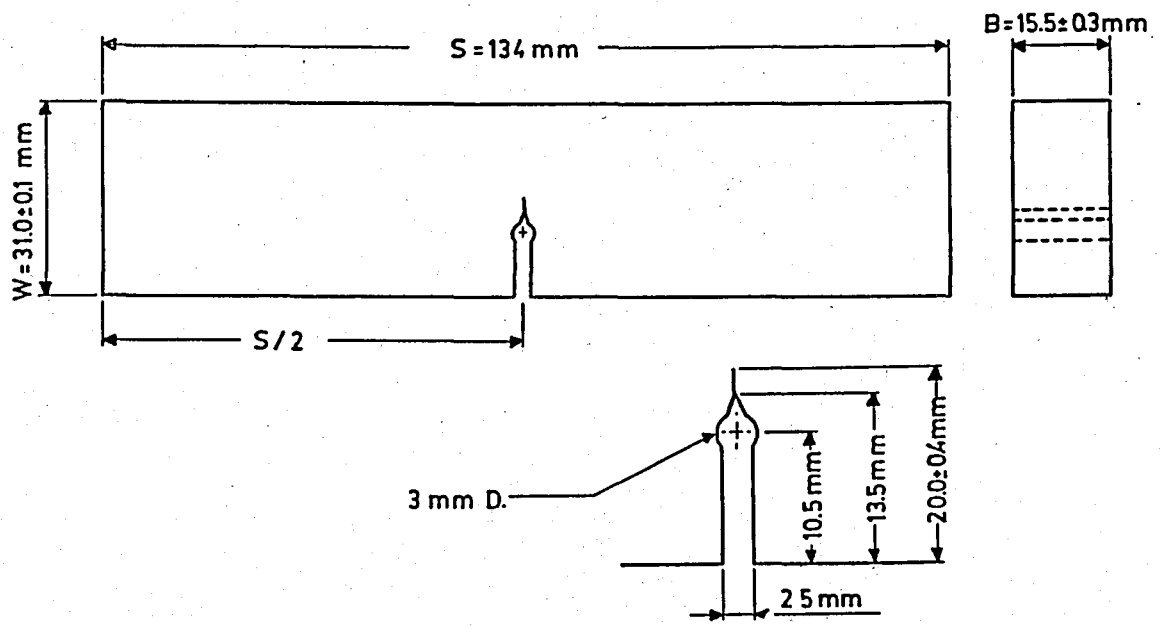

Figure 32. Bend specimen.

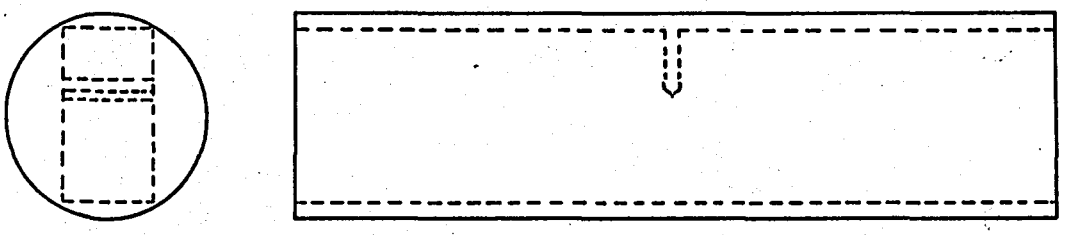

Figure 33. The schematic representation of the bending specimen orientation.

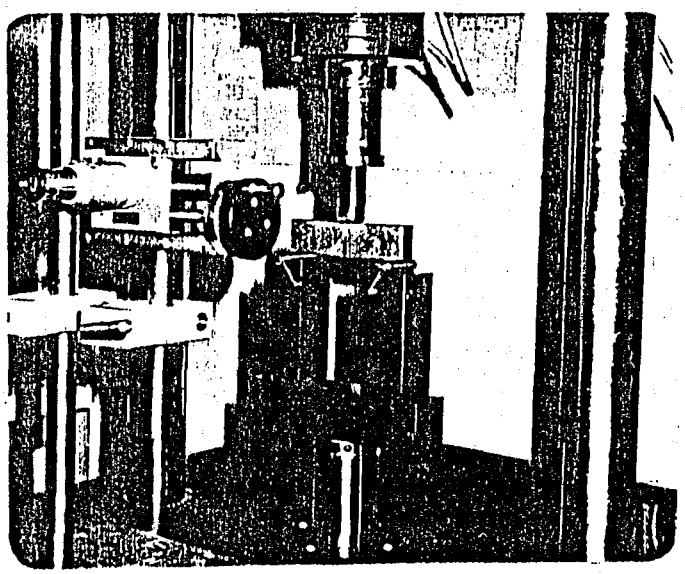

Figure 34. Three-point bending fixture (with the bending specimen attached on it).

(d) After the heat treatment, 0.3 mm was ground off each side of the specimens.

(e) Crack starter notch: A straight through fatigue crack starter notch with a root radius of 0.10 mm was made with electro-erosion. This was a costly operation, but crack starter notches which are made by electro-erosion reduce the precracking fatigue cycle when compared to the machined ones because of their sharp root radii.

(f) Fatigue cracking: Fatigue precracking was performed at 6 cycles/sec on the electro-hyraulic closed loop MTS 812 fatique testing machine with a maximum capacity of 10 tons (Figure 35) under load control with sinuzoidal waveform. The initial value of maximum fatique load was selected from the estimated K_{1c} value such that the maximum stress intensity factor in the initial portion of the fatigue cycle did not exceed 80 per cent of the estimated K_{1c} value. The minimum load was selected so that the stress ratio is 0.09. During fatigue cycling, the crack was carefully observed using a Gaetner travelling microscope (10x).

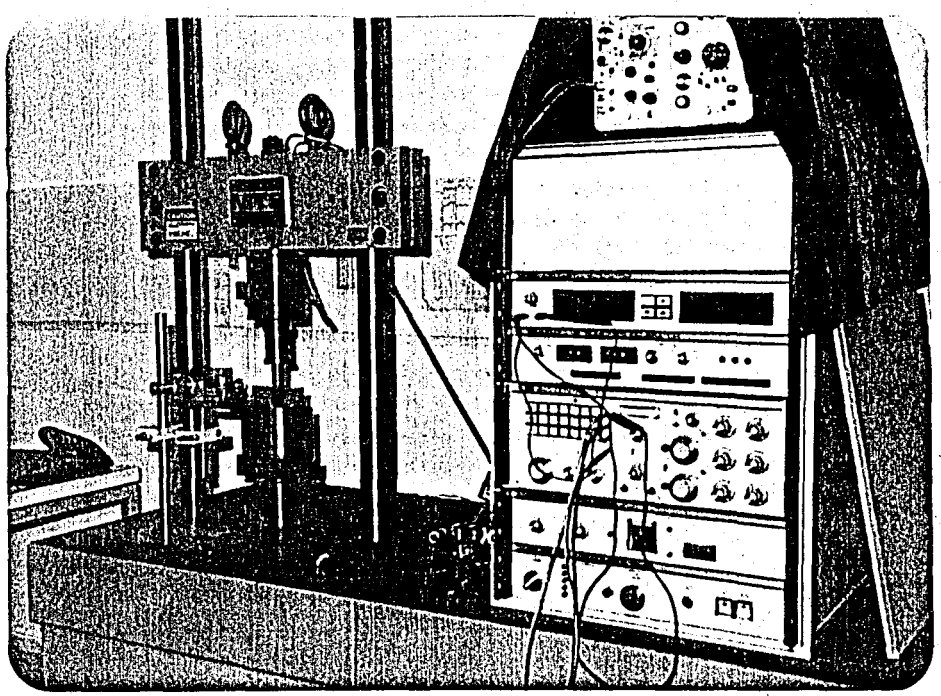

Figure 35. The electro-hydraulic MTS 812 fatigue testing machine for for fracture toughness testing.

When the crack has reached the last 2.5 per cent of the total crack length (0.5 mm in our case), the maximum load was reduced so that the terminal value of K_{max} did not exceed 60 per cent of the estimated K_{1c} value. The minimum load was then adjusted so that the stress ratio was 0.09. Fatigue precracking was interrupted when the crack has reached the ASTM specified length (2 mm in our case).

(g) These precracked specimens were tested on a electro-hydraulic MTS machine with a crosshead movement rate of 0.02 mm/sec which corresponds to a loading rate of 50 kgf/sec in the linear region, and the load versus displacement was recorded by a Hewlett-Packard X - Y recorder.

(h) The analysis of the load-displacement plots has been made by drawing the secant line OP_5 , shown in Figure 36, through the origin of the test record with slope $(P/v)_5 = 0.95\ (P/v)_o$, where $(P/v)_o$ is the slope of the tangent OA of the initial linear part of the record. The load P_Q was then defined as follows: If the load at every point on the test record which precedes P_5 is lower than P_5, then P_5 is P_Q (Type 1); if however, there is a maximum load preceding P_5 which exceeds it, then this maximum load is P_Q (Type II and III).

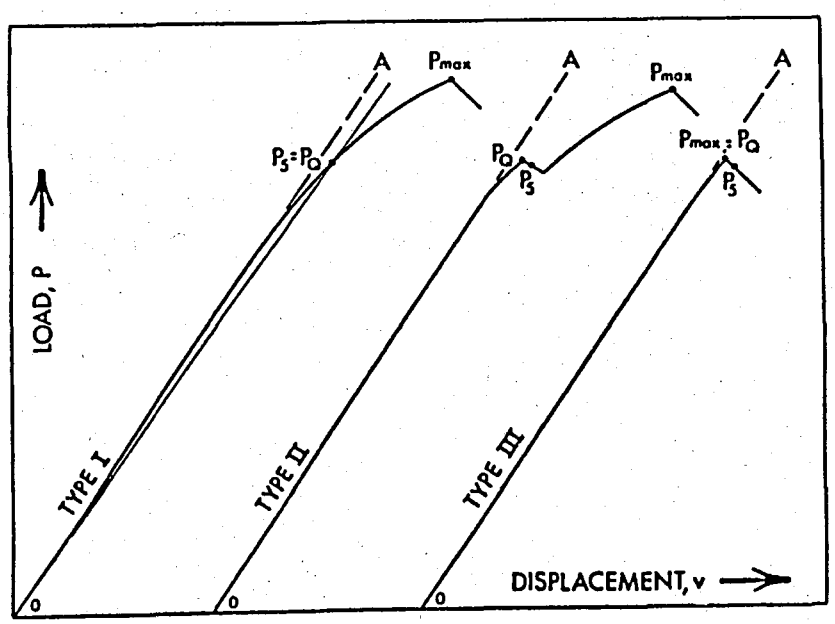

Figure 36. Principal types of Load-Displacement records.

(1) The stress intensities for the bending specimens then could be determined from the following equation [46]:

$$K_Q = \frac{P_Q S}{BW^{3/2}} \cdot f(a/W) \qquad (3)$$

where

$$f(a/W) = \frac{3(a/W)^{1/2}\left[1.99-(a/W)(1-a/W) \times (2.15-3.93a/W+2.7a^2/W^2)\right]}{2(1+2a/W)(1-a/W)^{3/2}} \qquad (4)$$

where K is the stress intensity, P_Q is the load, B is thickness, S is span, W is width and a is crack length.

5.2.4. Hardenability Testing

Jominy end-quench test specimens (Figure 37) were machined from 36 mm bar in accordance with ASTM standards [47], i.e., 25 mm in diameter and 100 mm in length.

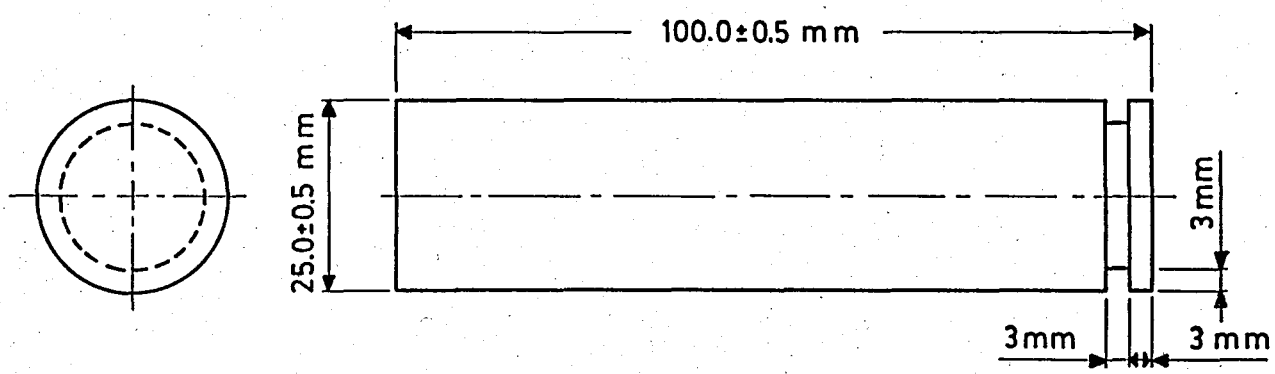

Figure 37. Jominy end-quench test specimen.

The procedure followed for end-quench testing was:

(a) Normalizing at 870°C for 1 hour followed by air cooling.

(b) The specimens were then austenitized in a electrically heated muffle furnace at either 845°C, 1000°C, or 1100°C for 50 minutes.

(c) The water quenching device was adjusted so that the stream of water rised to a free height of 63.5 mm above the 12.7 mm orifice, without the specimen in position. The support for the specimen should be dry at the beginning of each test. Then the austenitized specimens were immediately (in 5 sec) placed in the support so that its bottom face is 12.7 mm above the orifice and the water was turned on by means of quick-opening valve. The stream of water (at a temperature of around 20°C) was directed against the bottom face of the specimen for 15 minutes. (The supporting fixture is shown in Figure 38).

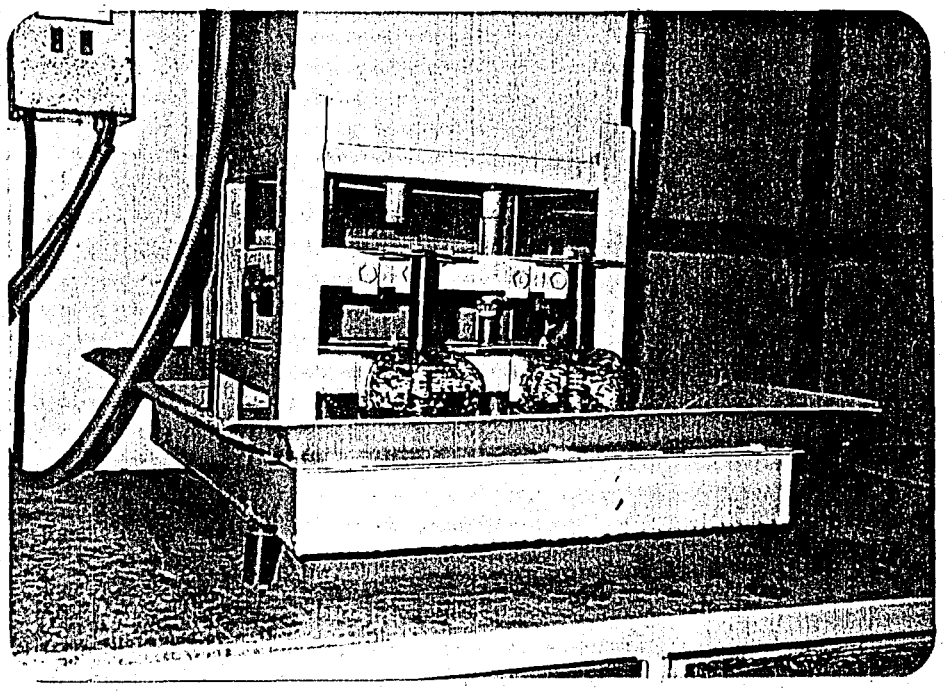

Figure 38. The supporting fixture for end-quench test (with two specimens attached on it).

(d) Two diammetrically opposite flats, 0.4 mm deep and parallel to the axis of the core were ground, and the hardness (Rockwell C) was measured along the flats with a Karl-Frank hardness tester. The resulting hardness values were plotted on a standard hardenability chart in which the ordinate represents Rockwell hardness value and the abscissa represents the distance from the quenched end of the specimen at which the hardness determinations were made.

Since the electrically heated muffle furnace for Jominy end-quench test specimens had a maximum heating capacity up to 1100°C, a set of round bars of increasing diameter, i.e.,

(a) 24 mm in diameter x 96 mm in length,

(b) 36 mm in diameter x 144 mm in length,

(c) 60 mm in diameter x 240 mm in length,

were prepared in order to observe the effect of high austenitization temperatures (especially 1200°C) on hardenability.

These set of bars were austenitized at either 845°C, 1000 C, 1100°C or 1200°C and oil quenched. After the oil quenching, 10 mm thick section from the mid-length of each bar was cut and the hardness distribution was measured in two diameters (Figure 39).

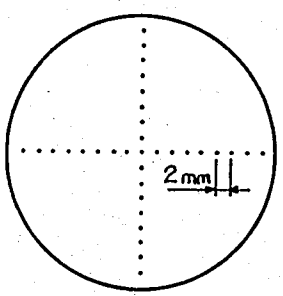

Figure 39. Hardness distribution data points.

5.3. Heat Treatment

The heat treatments were performed at "PANKURT San. A.Ş.", and are sketched in Figure 40 and tabulated in Table 4.

The austenitization was done at either 845°C, 1000°C, 1100°C or 1200°C, and the resulting structures will be referred as the 845°C, 1000°C, 1100°C and 1200°C structures, respectively. The austenitization treatment was performed in neutral salt bath with a temperature control of ± 5°C. During austenitizing, each of the specimens was inserted into the bath individually, then the specimens were quenched in agitated oil at room temperature. The austenitizing times are shown in Table 5.

Table 4. The heat treatments schedule.

	Austenitizing Temperature (°C)	Tempering Temperature (°C)	Second Austenitizing Temperature (°C)	Tempering Temp. (°C)
1.	845	200	---	---
2.	1000	200	---	---
3.	1100	200	---	---
4.	1200	200	---	---
5.	845	570	---	---
6.	1000	570	---	---
7.	1100	570	---	---
8.	1200	570	---	---
9.	1200	200	845	200
10.	1200	200	845	570

Table 5. The austenitizing times, t_1

1.	Tensile, Charpy and toughness specimens	20 min.
2.	24 mm round bars	25 min.
3.	36 mm round bars	30 min.
4.	60 mm round bars	35 min.

Half of the specimens austenitized at each temperature were tempered at 200°C, and the other half were tempered at 570°C. Tempering at 200°C was performed in a electrically heated muffle furnace, and tempering at 570°C was done in salt bath. The tempering time was 30 minutes for tensile, Charpy and fracture toughness specimens.

Double austenitization (designed by Thomas and Ten-Lung Chen [40]) was also employed. It consisted of 1200°C austenitization followed by oil quenching. After the oil quenching, the specimens were tempered at 200°C, and then reaustenitized at 845°C, and oil quenched. After this reaustenitization, the specimens were tempered at either

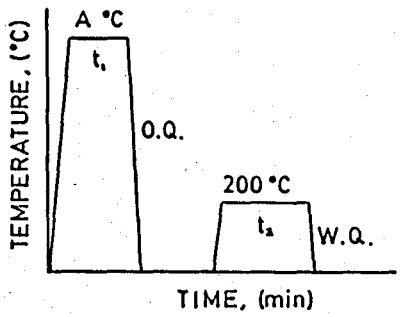

(a)

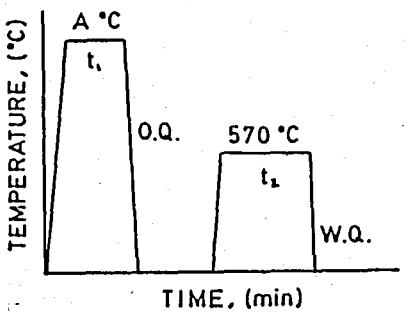

(b)

For heat treatment (1) A = 845°C
" (2) A = 1000°C
" (3) A = 1100°C
" (4) A = 1200°C

For heat treatment (5) A = 845°C
" (6) A = 1000°C
" (7) A = 1100°C
" (8) A = 1200°C

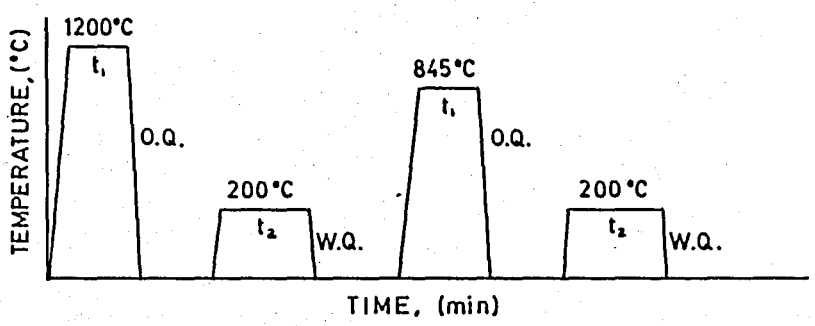

(c) Heat treatment (9)

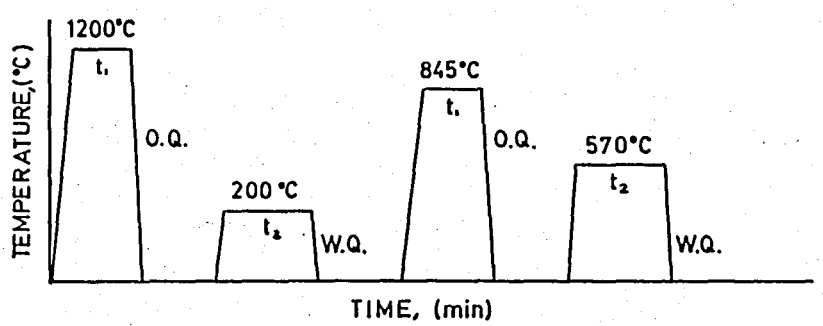

(d) Heat treatment (10)

Figure 40. Schematic of heat-treatment schedules (See Table 4). (The austenitizing times, t_1, are indicated in Table 5, and the tempering time, t_2, is 30 minutes for the tensile, Charpy and toughness specimens).

200°C, or 570°C. The resulting structures will be called as double austenitized or 1200-845°C structures. (Figure 40 (c) and (d)).

5.4. Metallography

Sections to be used for metallography were cut from the mid-thickness of the broken fracture toughness specimens. They were ground on successively 80, 320, 400 and 600 grit abrasive papers under flood to prevent heating and then polished to 7.5 and 3 μ finish successively using a diamond paste. All specimens for microstructural study were etched in a 3 per cent nital solution and the structures viewed on an Olympus optical microscope (Figure 41).

Sections to be used for prior austenite grain size determinations were cut from the water quenched 24 mm diameter bars and prepared in the same way as the metallographic specimens. The etchant consisted of 5 gr picric acid in 95 ml water and a few drops of "pril". The etchant and the specimens were heated to 50-60°C and the specimens were held 15 minutes in the heated solution. The surfaces after the etching were lightly polished and the grain sizes examined through optical microscope.

For estimating the average prior austenite grain sizes, the circular intercept method, Abrams procedure [48] has been applied. In this method, the test pattern consisted of three concentric and equally spaced circles having a total circumference of 500 mm [48]. First, a cursory examination of the microstructure performed and ASTM grain size number was roughly estimated. Using these estimated sizes, a rational magnification yielded approximately 100 intercepts for the 500 mm circular test pattern was selected and the microscope was resetted for this magnification. A transparency of the pattern was applied directly to the ground-glass screen of the metallurgical microscope (Figure 41), and the intercepts were counted on three blindly selected fields. Then, the average of these intercepts, $\bar{N}$, were entered into Figure 42, and the corresponding ASTM

grain sizes were determined. The mean intercept distance, "$\bar{l}$", has been determined by entering the average intercept counts, $\bar{N}$, to Figure 43.

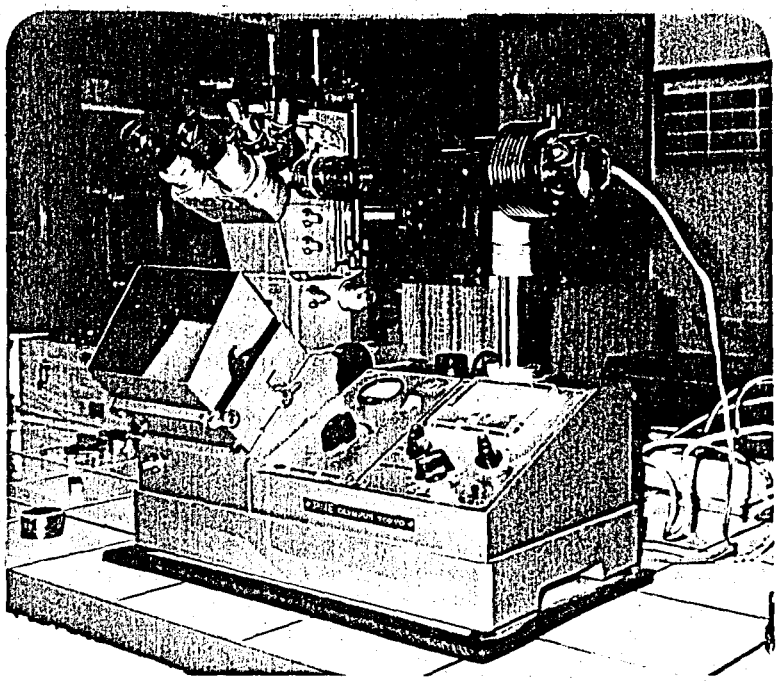

Figure 41. Olympus optical microscope used in this study.

5.5. Scanning Electron Microscopy

The fracture surfaces of the fracture toughness specimens were examined with a 25 kV "Cambridge Stereoscan" (Figure 44).

After the fracture toughness testing, the fracture surfaces were coated with grease. This prevented contamination during storage or when they were sliced from the test-pieces for fractographic analysis in SEM. The specimens were then sectioned to fit in the SEM. Afterwards, they were cleaned with CCl_4 and acetone, subsequently.

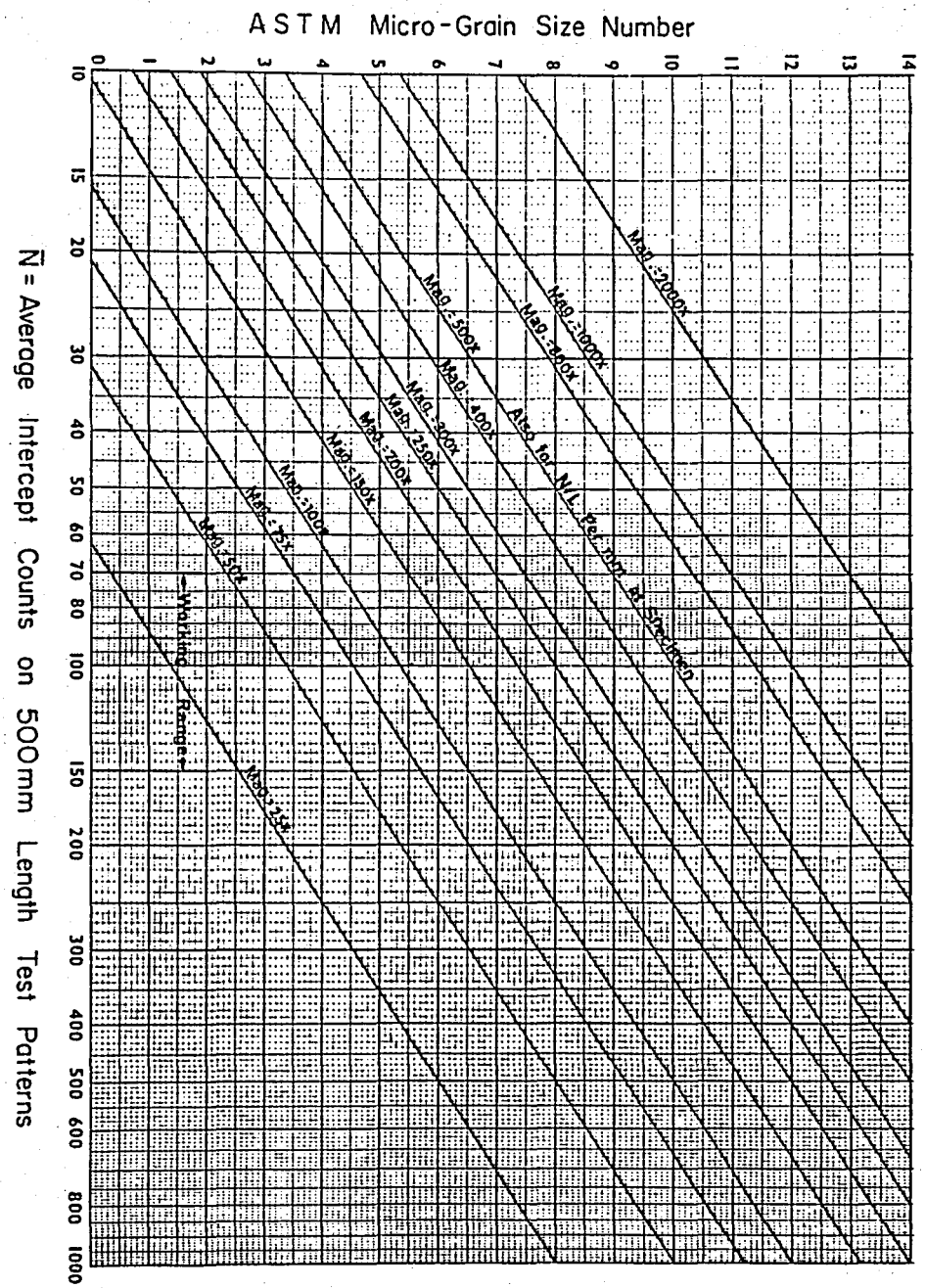

Figure 42. Chart for direct determination of ASTM micro-grain size number from the intercept count on 500 mm test pattern [48].

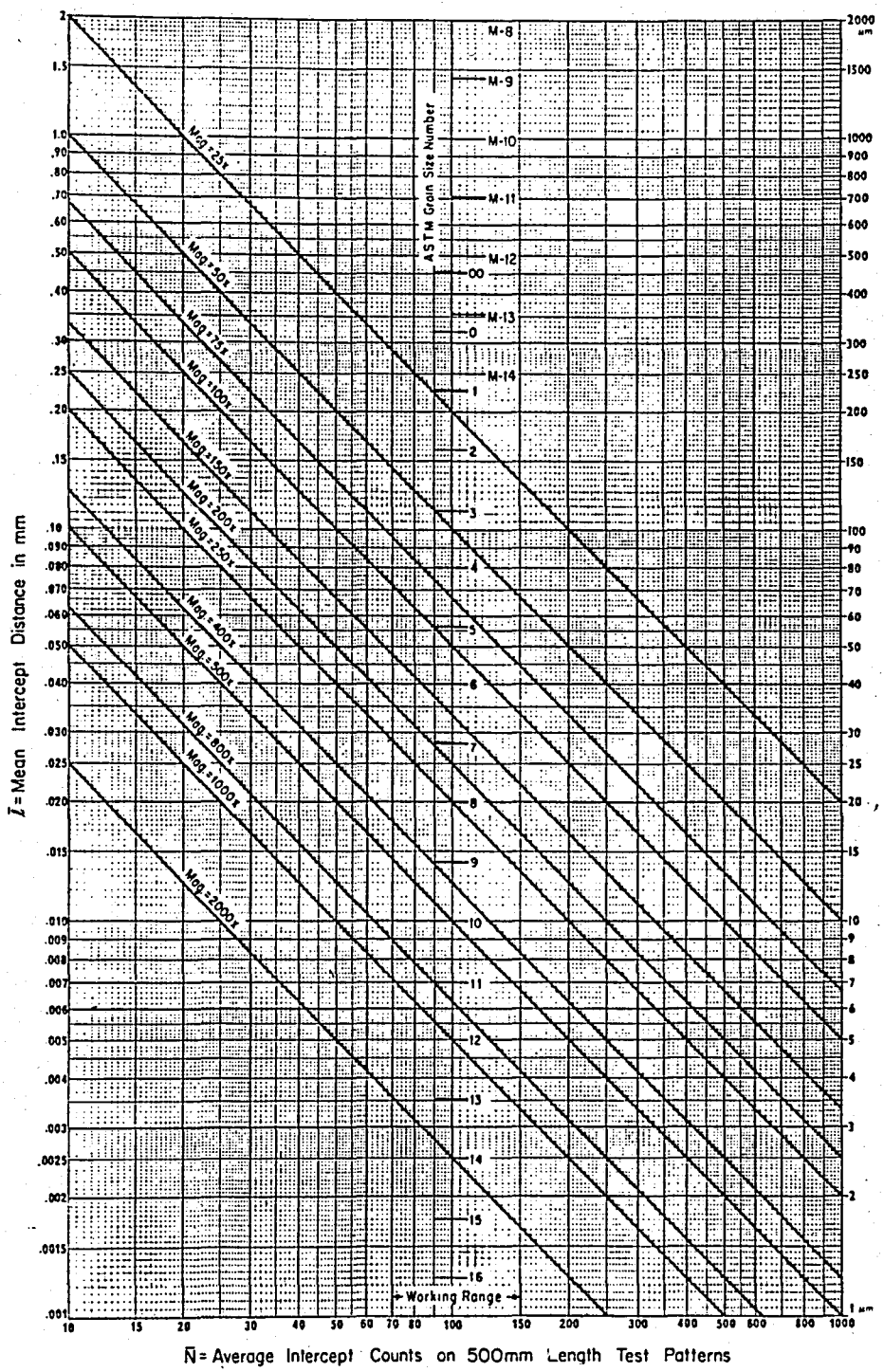

Figure 43. Chart for direct determination of mean intercept distance from the intercept count on 500 mm test pattern [48].

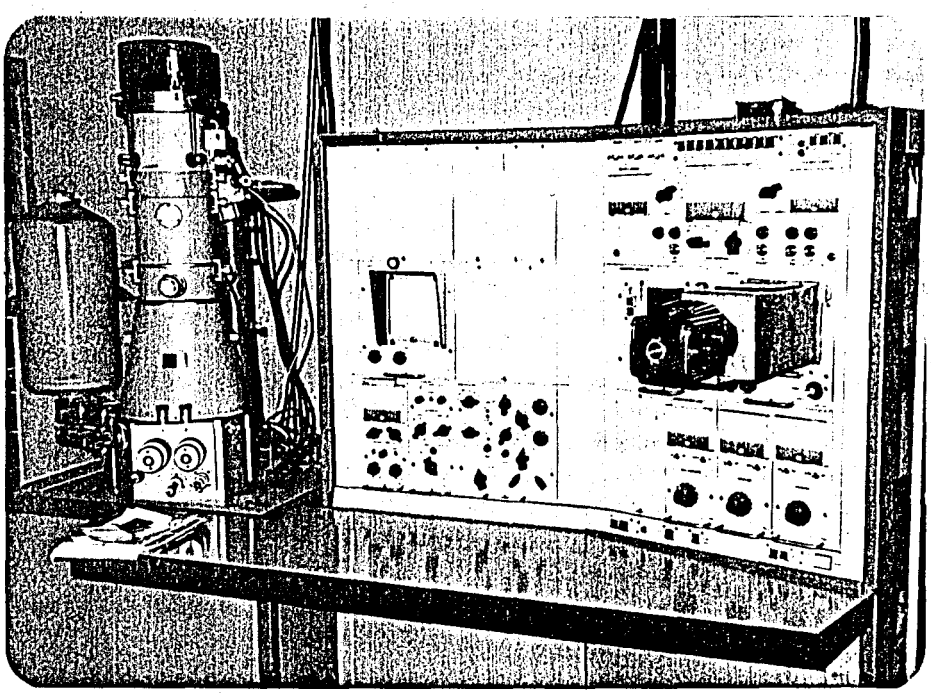

Figure 44. The scanning electron microscope (SEM) used in this study.

VI. RESULTS

6.1. Tensile Properties

The general shape of the tensile curves obtained after both 200°C and 570°C tempering is shown in Figure 45.

The room temperature tensile properties are listed in Table 6 and 7, and plotted in Figures 46-49 for 200°C and 570°C tempered structures, respectively. From these data it is evident that varying the austenitizing temperature

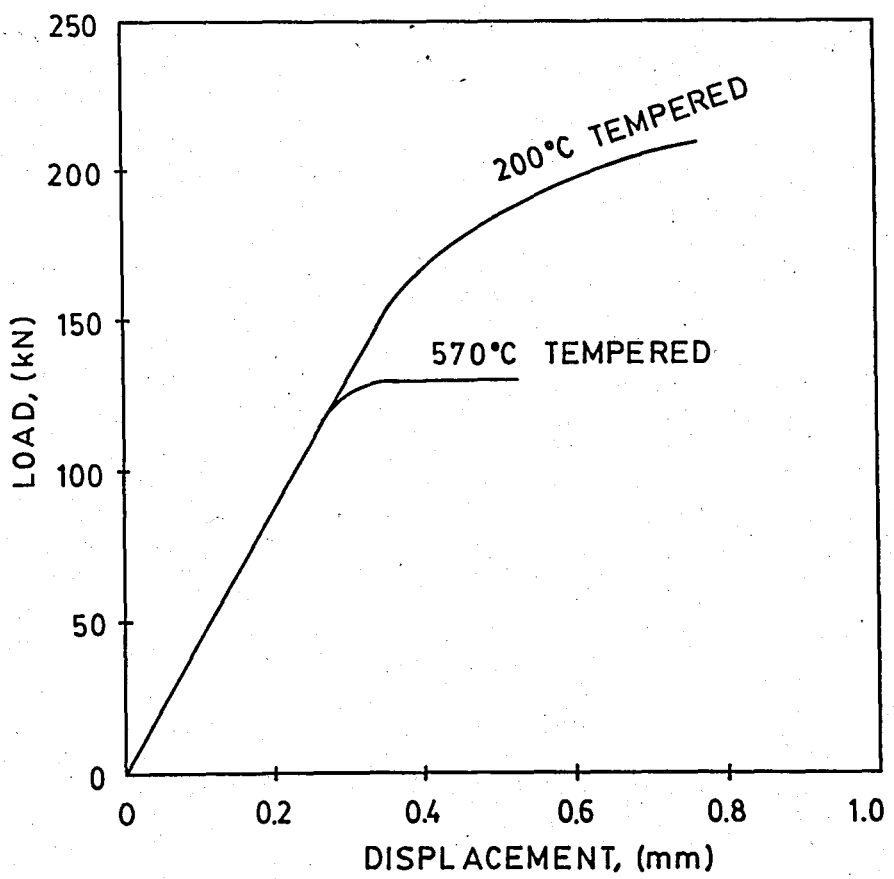

Figure 45. The general shape of load - displacement curve for 200°C and 570°C tempered specimens.

between 845°C and 1200°C has little effect on either yield or ultimate tensile strength. However, the ductility (elongation and reduction in area) was better with the conventional austenitizing temperature.

Table 6. Room temperature tensile properties for AISI 5140 steel tempered at 200°C.

Austenitizing Temperature (°C)	Yield Strength (MPa)	Tensile Strength (MPa)	Elongation (%)	Reduction in area (%)
845	1515	1934	8.7	16.3
"	1525	1974	9.2	15.6
1000	1530	1957	7.5	13.7
"	1560	1963	7.7	13.2
1100	1540	1993	7.5	12.4
"	1570	2000	7.5	12.6
1200	1572	2000	7.4	9.6
"	1501	1987	7.2	9.9
1200-845	1660	1986	5.6	6.4
"	1680	1987	6.3	7.4

Table 7. Room temperature tensile properties for AISI 5140 steel tempered at 570°C.

Austenitizing Temperature (°C)	Yield Strength (MPa)	Tensile Strength (MPa)	Elongation (%)	Reduction in area (%)
845	989	1075	15.0	32.2
"	985	1073	15.6	32.2
1000	973	1066	14.4	29.0
"	973	1066	15.3	28.4
1100	940	1060	13.3	24.5
"	940	1068	12.2	23.8
1200	964	1080	11.9	19.8
"	966	1086	11.6	21.3
1200-845	999	1076	14.8	32.4
"	991	1072	15.6	32.4

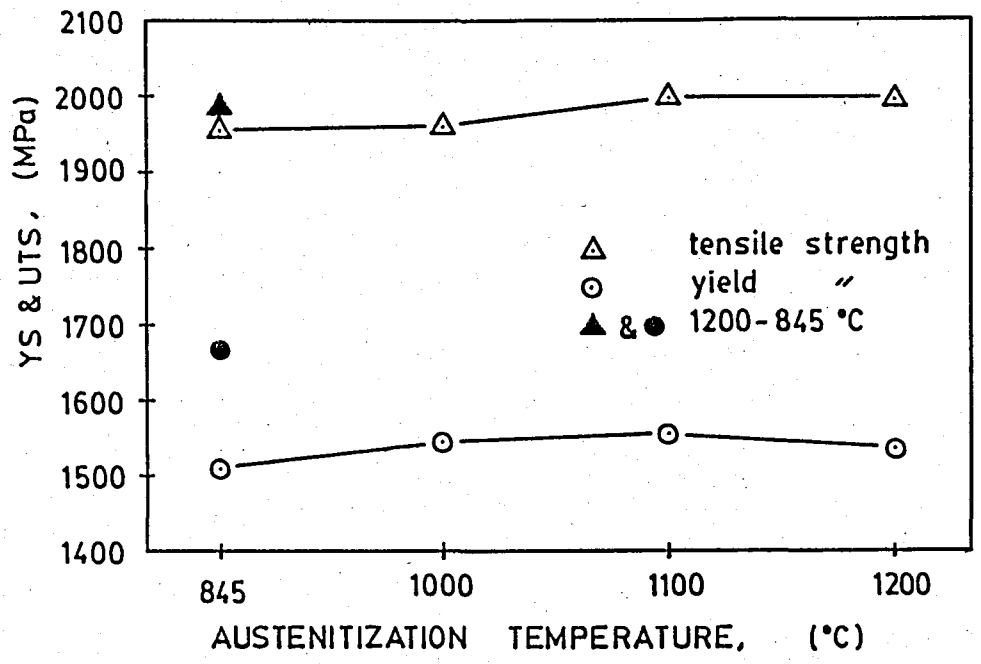

Figure 46. Yield and tensile strength versus austenitization temperature for 200°C tempered specimens.

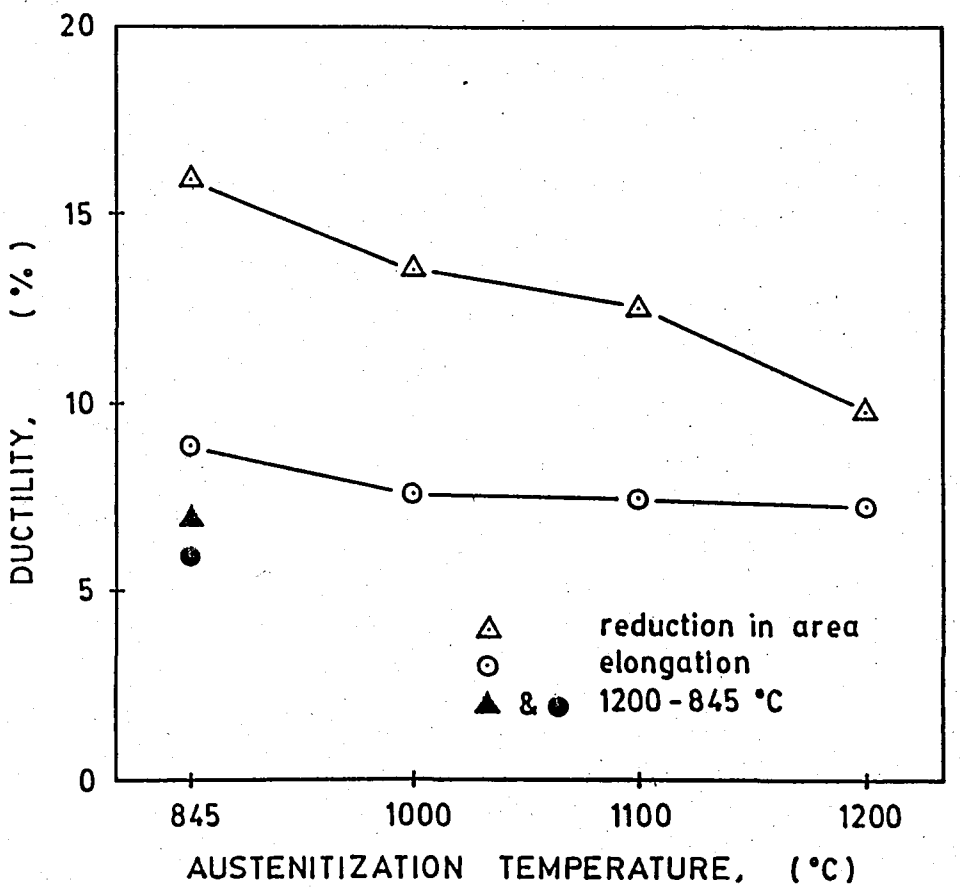

Figure 47. Ductility versus austenitization temperature for 200°C tempered specimens.

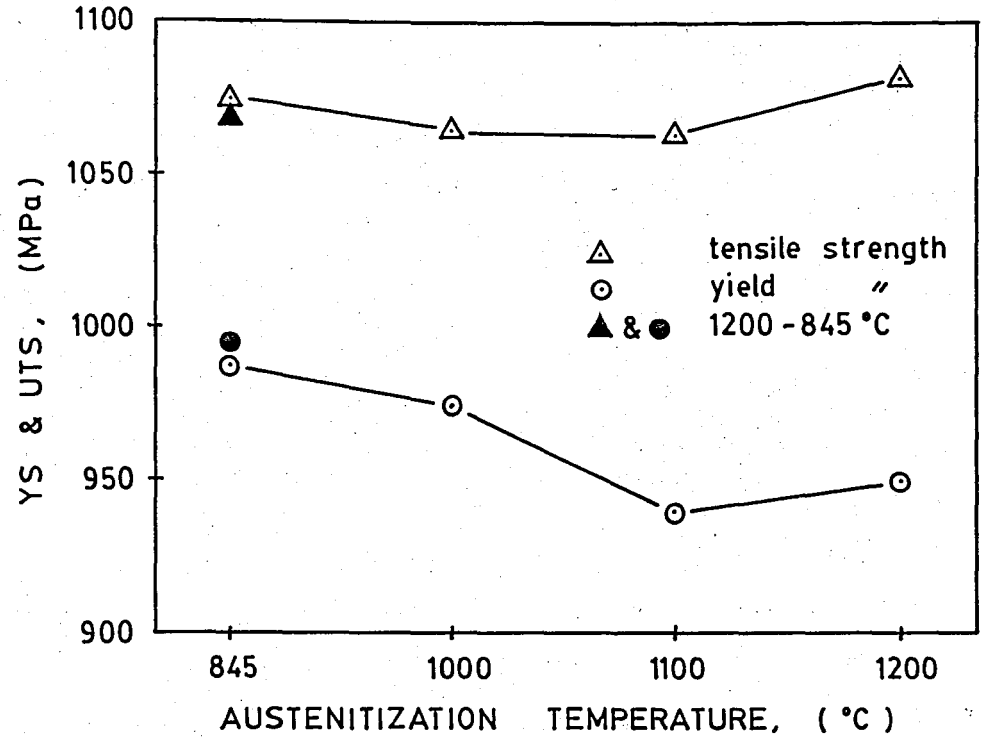

Figure 48. Yield and tensile strength versus austenitization temperature for 570°C tempered specimens.

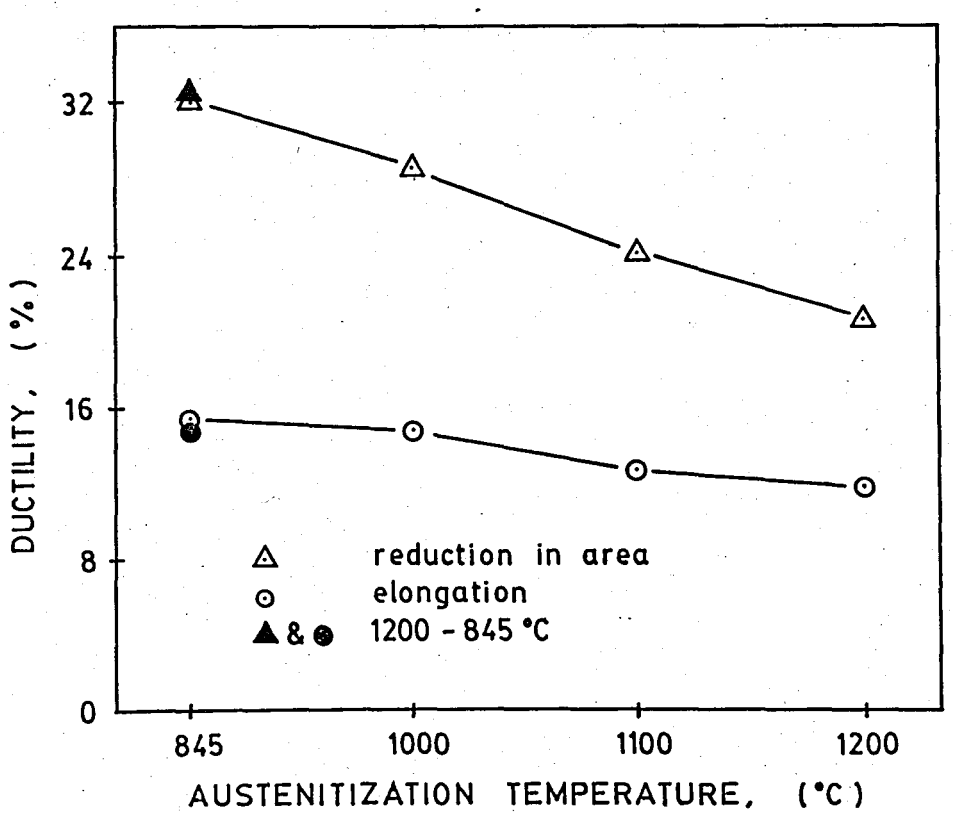

Figure 49. Ductility versus austenitization temperature for 570°C tempered specimens.

6.2. Toughness Properties

The initial and terminal loads and the total number of cycles during fatigue precracking for each specimen are given in Table 8 and 9 for 200°C tempered and 570°C tempered structures, respectively.

The general shape of "load - displacement" curve for plain strain fracture toughness testing is shown in Figure 50.

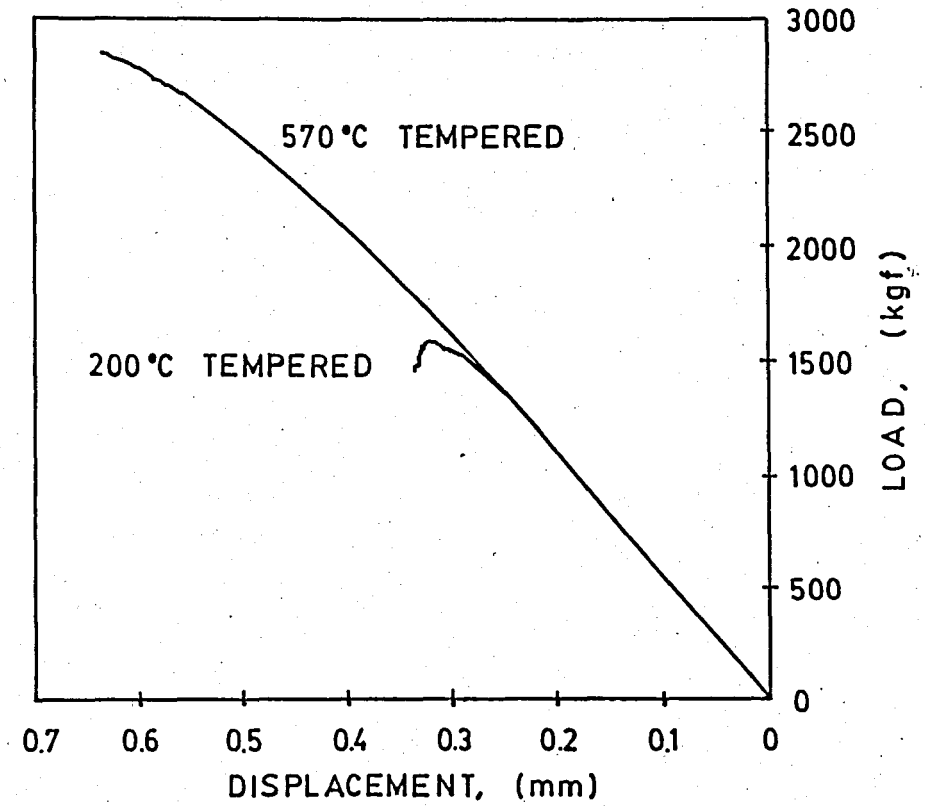

Figure 50. The general shape of "load-displacement curve" for plane strain fracture toughness testing.

The room temperature plain strain fracture toughness testing results are given in Table 10 and 11. In these tables, $\bar{a}$ is the average of the crack length measured at the center of the crack front, midway between the center and at the end of the crack front on each side and at each surface.

For the K_Q value to be considered the valid plane strain fracture toughness, K_{1c}, the following conditions must be met [46].

Table 8. Fatigue precracking data for 200°C tempered specimens.

Austenitization Temperature (°C)	Initial loads (kgf)	Terminal loads (kgf)	Terminal cracking beginning cycle	Final cycle
845	800 - 70	500 - 40	15,000	16,900
1000	900 - 80	550 - 50	7,400	8,500
1100	1100 - 100	650 - 60	7,300	9,300
1200	1350 - 120	800 - 70	7,500	9,200
1200-845	1100 - 100	650 - 55	4,200	8,300

Table 9. Fatigue precracking data for 570°C tempered specimens

Austenitization Temperature (°C)	Initial loads (kgf)	Terminal loads (kgf)	Terminal cracking beginning cycle	Final cycle
845 C	1500 - 120	900 - 80	6,250	8,200
1000	1500 - 120	900 - 80	9,500	11,600
1200	1500 - 120	900 - 80	6,500	8,000
1200 -845	1500 - 120	900 - 80	7,000	9,000

Table 10. Plain strain fracture toughness testing results for 200°C tempered specimens.

Austenitization Temperature (°C)	YS (MPa)	B (mm)	$\bar{a}$ (mm)	W (mm)	P_5 (kgf)	P_{max} (kgf)	P_Q (kgf)	P_{max}/P_Q	K_Q (MPa$\sqrt{m}$)	K_{1c} (MPa$\sqrt{m}$)	min.req. B (mm)
845	1520	15.5	15.66	31.0	1075	1075	1075	1.00	41.7	41.7	1.9
1000	1545	"	15.66	"	1175	1175	1175	1.00	45.6	45.6	2.2
1100	1555	"	15.33	"	1490	1590	1490	1.02	56.1	56.1	3.3
1200	1537	"	15.33	"	1840	1960	1840	1.07	69.3	69.3	5.1
1200-845	1670	"	15.93	"	2025	2125	2025	1.05	81.2	81.2	5.9

Table 11. Plain strain fracture toughness testing results for 570°C tempered specimens.

Austenitization Temperature (°C)	YS (MPa)	B (mm)	$\bar{a}$ (mm)	W (mm)	P_5 (kgf)	P_{max} (kgf)	P_Q (kgf)	P_{max}/P_Q	K_Q (MPa$\sqrt{m}$)	K_{1c} (MPa$\sqrt{m}$)	min.req. B (mm)
845	987	15.5	16.00	31.0	1890	3025	1890	1.60	75.8	--	38
1000	973	"	16.00	"	2075	3060	2075	1.47	83.2	--	40
1200	965	"	15.66	"	2200	3170	2200	1.44	85.4	--	41
1200-845	995	"	15.66	"	2125	3200	2125	1.51	82.5	--	39

1. $P_{max} / P_Q \leqslant 1.1$

2. $B \geqslant 2.5 (K_Q / \sigma_y)^2$

3. $a \geqslant 2.5 (K_Q / \sigma_y)^2$

where P_{max} is the maximum load achieved during the test, P_Q and K_Q are the load and stress intensity obtained using the procedures described by the ASTM [46]. "B" is the thickness and σ_y is the 0.2 per cent yield strength.

For 200°C tempered structures, the above conditions are met, but for the 570°C tempered structures, the first condition is violated.

The plain strain fracture toughness values and Charpy V-notch impact energies are given in Table 12 and 13 for 200°C and 570°C tempered structures, respectively. K_{1c} versus austenitization temperature and Charpy V-notch versus austenitization temperature are plotted in Figures 51 and 52, respectively.

For AISI 5140 steel, the conventional heat treatment is to austenitize at 845°C followed by oil quenching. This resulted in a fracture toughness of 41.7 MPa$\sqrt{m}$ for 200°C tempered specimens. By raising the austenitization temperature from 845°C to 1200°C followed by oil quenching, the toughness increased to 69.3 MPa$\sqrt{m}$. Double austenitizing gave better results than the 1200°C austenitization.

The same trend has also been observed for Charpy V-notch impact energies. The conventional 845°C treatment gave a value of 10.5 joule. By raising the austenitizing temperature, we obtained a rapid increase in impact energy, especially after 1100°C treatment. At 1200°C austenitization, the impact energy increased to a value of 21.5 joule. Double austenitization indicated better result than that of 1200°C austenitization.

For 570°C tempered specimens, there was nearly no change in impact energy and plane strain fracture toughness values when the austenitization temperature is changed as has been observed earlier by Youngblood and Raghavan [10] and MacDarmaid [20].

Table 12. Plain strain fracture toughness, K_{1c}, and Charpy V-notch energies for 200°C tempered specimens

Austenitization Temperature (°C)	Charpy impact energy (Joule)	Plain strain fracture toughness (MPa$\sqrt{m}$)
845	11.0	41.7
"	10.0	----
1000	12.0	45.6
"	13.0	----
1100	18.5	56.1
"	19.0	----
1200	20.0	69.3
"	23.0	----
1200-845	25.0	81.2

Table 13. Plain strain fracture toughness, K_{1c}, and Charpy V-notch energies for 570°C tempered specimens

Austenitization Temperature (°C)	Charpy impact energy (Joule)	Plain strain fracture toughness (MPa$\sqrt{m}$)
845	65.0	75.8
"	67.0	----
1000	68.0	83.2
"	68.0	----
1200	57.5	85.4
"	58.5	----
1200-845	67.0	82.5
"	68.0	----

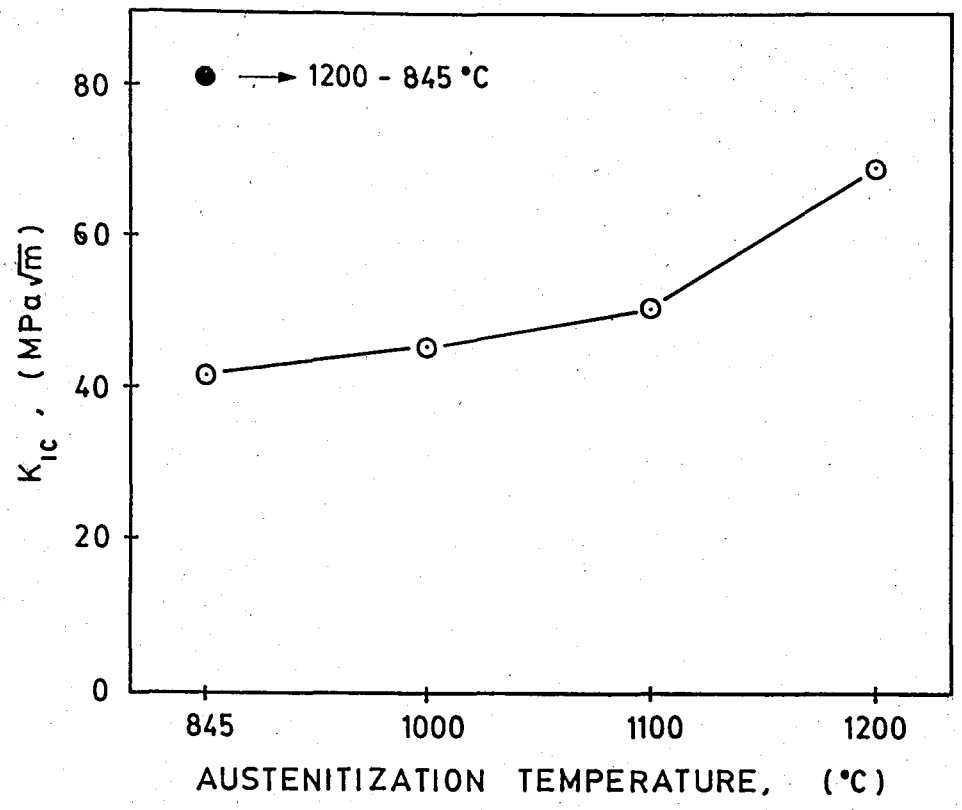

Figure 51. K_{Ic} versus austenitization temperature for 200°C tempered specimens.

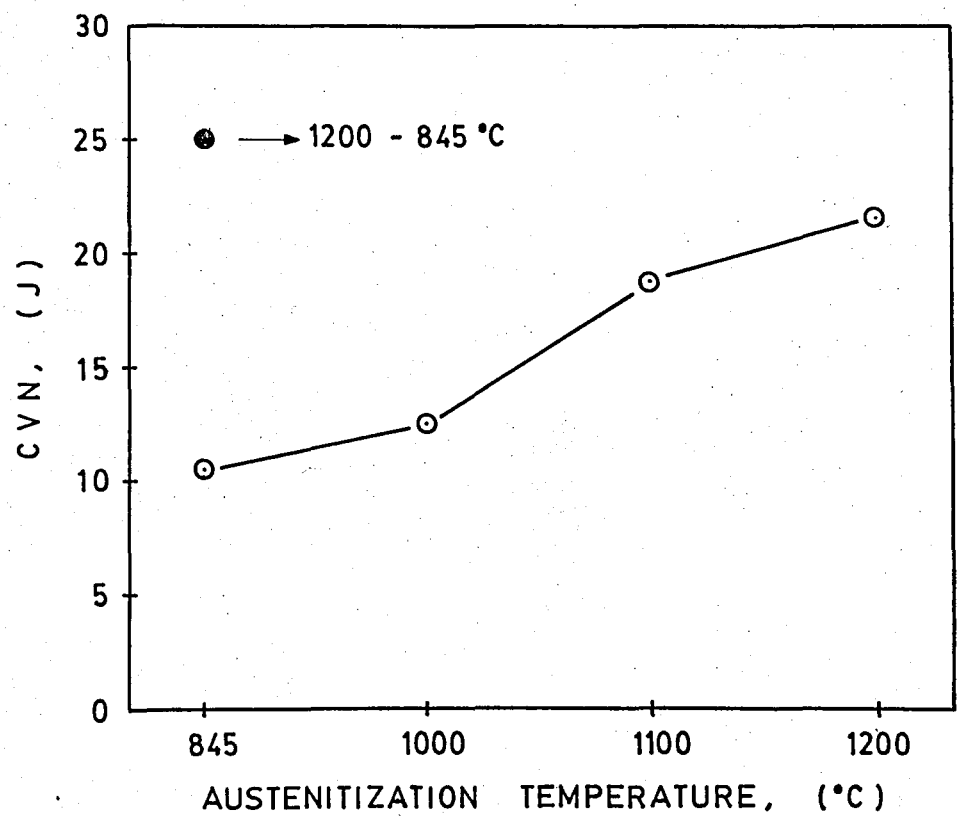

Figure 52. Charpy impact energies versus austenitization temperature for 200°C tempered specimens.

6.3. Hardenability Results

Results for Jominy end-quench test after austenitizing at 845 °C, 1000 °C and 1100 °C are presented in Table 14 and plotted in Figure 54.

Hardness distribution results for 24 mm, 36 mm and 60 mm diameter bars after 845 °C, 1000 °C, 1100 °C and 1200 °C austenitizing are given in Table 15 and plotted in Figure 53.

As it can be seen from Figure 54, when we increase the austenitization temperature from the conventional 845 °C to 1200 °C, the curve becomes flatter, indicating the increase in hardenability.

High austenitization temperatures cause an increase not only in the center hardness, but also on the surface hardness. This improvement on the surface hardness becomes more evident as the diameter of the bar increases. (Figure 53). These results are consistent with Jominy end-quench test results.

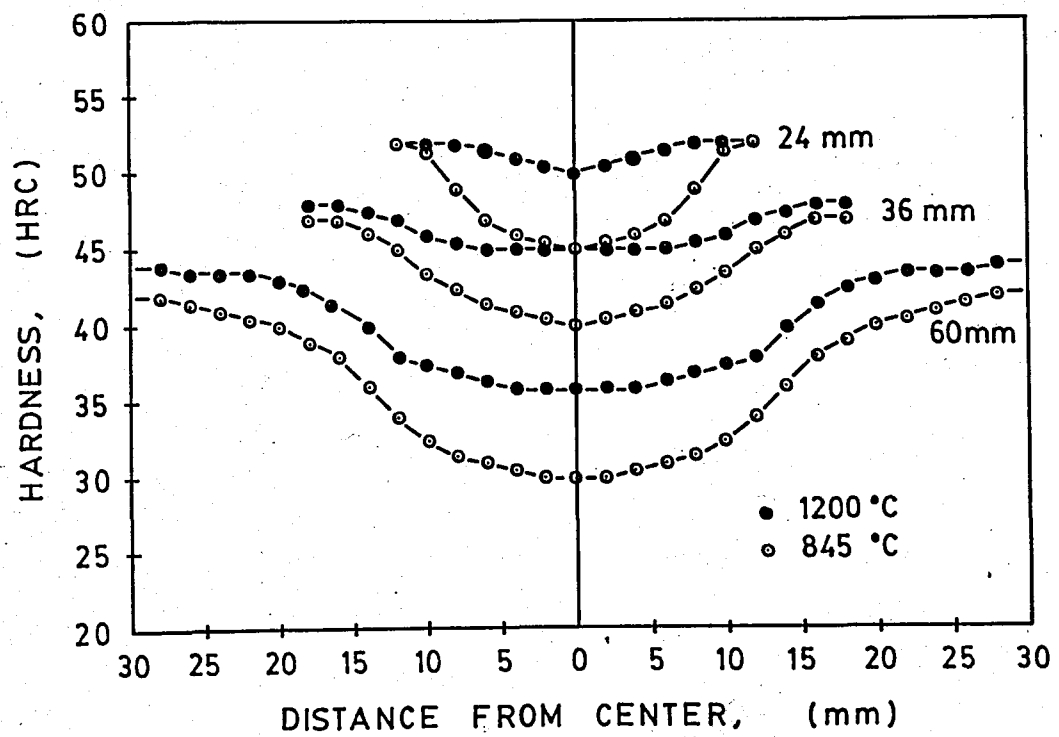

Figure 53. Hardness distribution after 845 °C and 1200 °C austenitization for 24 mm, 36 mm and 60 mm diameter bars.

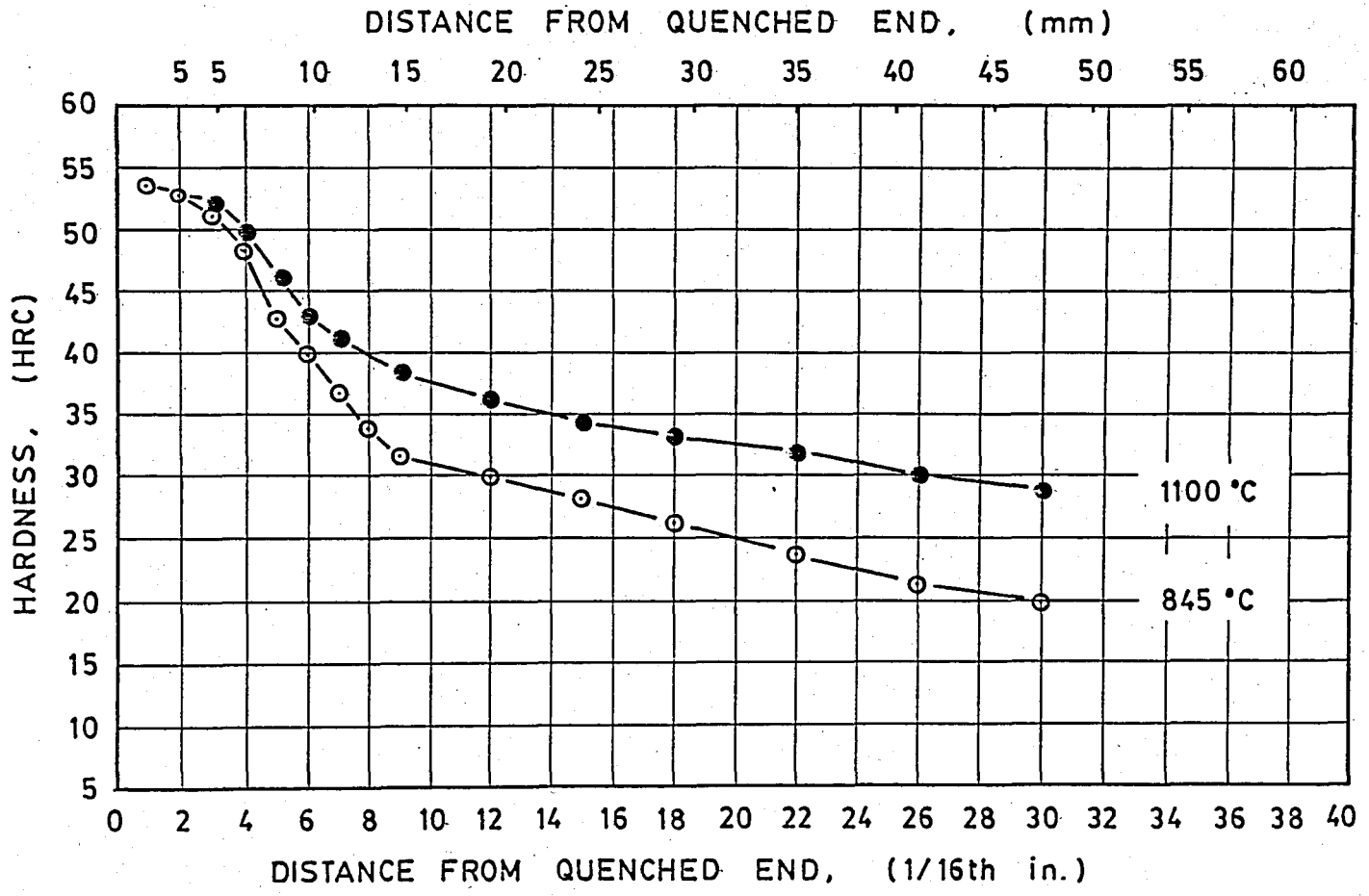

Figure 54. Jominy end-quench test measurements after 845°C and 1100°C austenitization.

Table 14. Jominy end-quench test results.

Austenitization Temperature (°C)	Jominy Hardness Measurements (HRC)															
	J_1	J_2	J_3	J_4	J_5	J_6	J_7	J_8	J_9	J_{12}	J_{15}	J_{18}	J_{22}	J_{26}	J_{30}	(1/16 inch)
845	54	53	51	49	43	40	37	34	32	30	28	26	24	21	20	
1000	54	53	51	49	43	41	37	36	34	32	30	28	26	23	22	
1100	54	53	52	50	47	44	41	40	39	37	35	34	32	31	29	

Table 15. Hardness distribution after austenitization at different temperatures for 24 mm, 36 mm and 60 mm diameter bars.

	Austenitization Temperature (°C)	Distance from surface (mm)															
		0	2	4	6	8	10	12	14	16	18	20	22	24	26	28	30
24 mm bar	845	52.0	51.5	49.0	47.0	46.0	45.5	45.0									
	1000	52.0	51.5	50.0	48.5	47.0	46.5	46.0									
	1100	52.0	52.0	51.5	50.5	49.5	49.5	49.0									
	1200	52.0	52.0	52.0	51.5	51.0	50.5	50.0									
36 mm bar	845	47.0	47.0	46.0	45.0	43.5	42.5	41.5	41.0	40.5	40.0						
	1000	47.0	47.0	46.5	45.5	44.0	43.0	42.5	42.0	41.5	41.0						
	1100	48.0	47.0	47.0	46.0	45.0	44.5	44.0	44.0	43.5	43.5						
	1200	48.0	48.0	47.5	47.0	46.0	45.5	45.0	45.0	45.0	45.0						
60 mm bar	845	42.0	42.0	41.5	41.0	40.5	40.0	39.0	38.0	36.0	34.0	32.5	31.5	31.0	30.5	30.0	30.0
	1000	42.0	42.0	42.0	41.5	41.0	40.0	39.0	37.5	37.0	35.5	34.5	33.0	32.0	31.5	31.0	31.0
	1100	43.5	43.5	43.0	43.0	42.5	42.0	41.0	40.0	38.5	37.0	36.0	35.5	35.0	34.5	34.0	34.0
	1200	44.0	44.0	43.5	43.5	43.5	43.0	42.5	41.5	40.0	38.0	37.5	37.0	36.5	36.0	36.0	36.0

6.4. Metallography

6.4.1. Prior Austenite Grain Size

The prior austenite grain sizes after different hardening treatments are tabulated in Table 16 and plotted in Figure 55. The prior austenite grain sizes at 100x magnification are given in Figure 56.

It is quite clear that increasing the austenitization temperature from the conventional 845°C to 1200°C resulted in a 10-fold increase in the austenite grain size. Double austenitization refined the prior austenite grain size. These results are consistent with the results of Khan and Wood [3], Padmanabhan and Wood [18] and Youngblood and Raghavan [10].

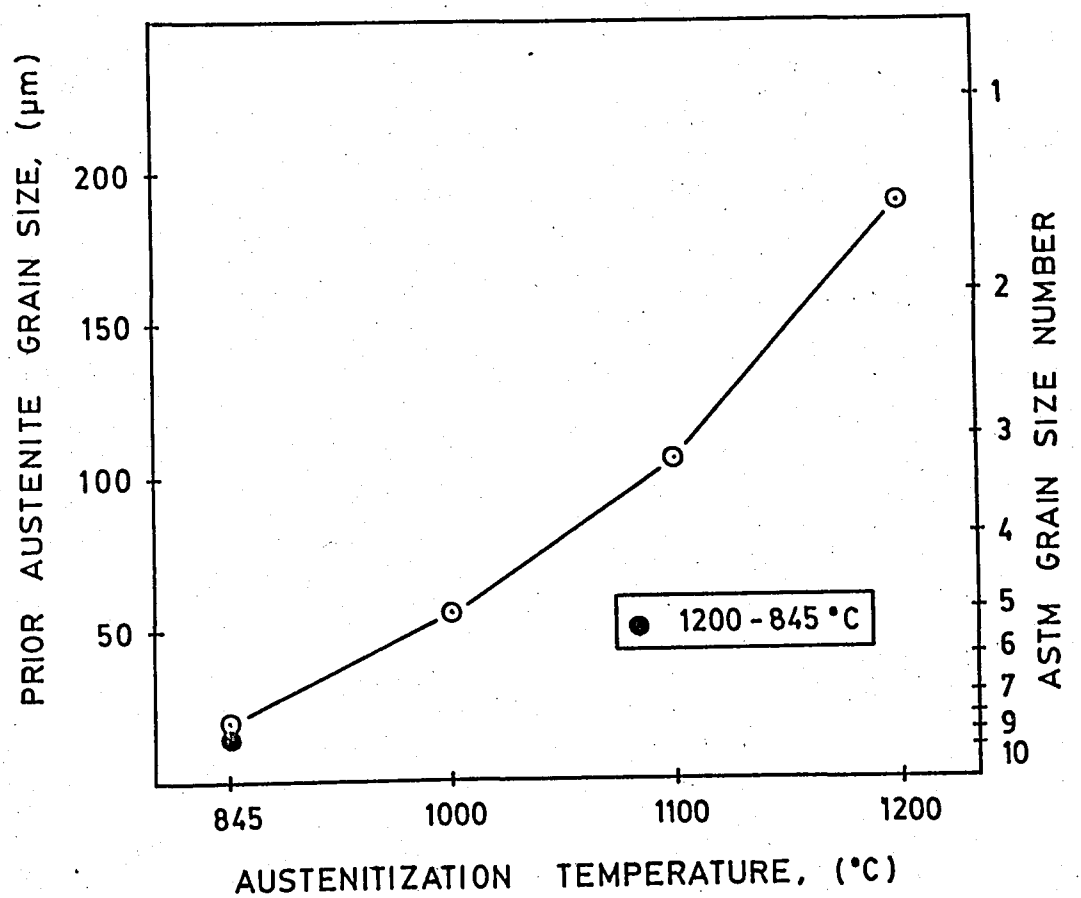

Figure 55. The change in prior austenite grain sizes with austenitizing temperatures.

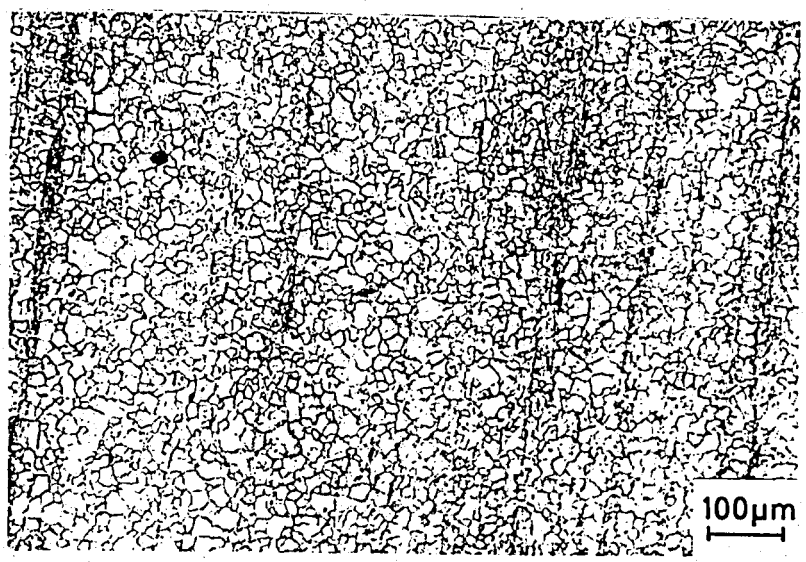

Figure 56 (a)
845°C
ASTM No 8.5

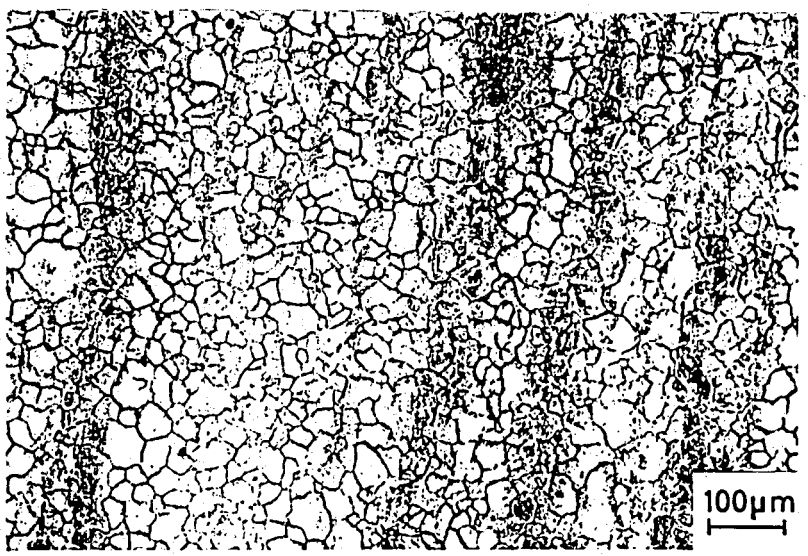

Figure 56 (b)
1000°C
ASTM No 7.0

Figure 56 (c)
1100°C
ASTM No 3.3

Figure 56 (d)
1200°C
ASTM No 1.7

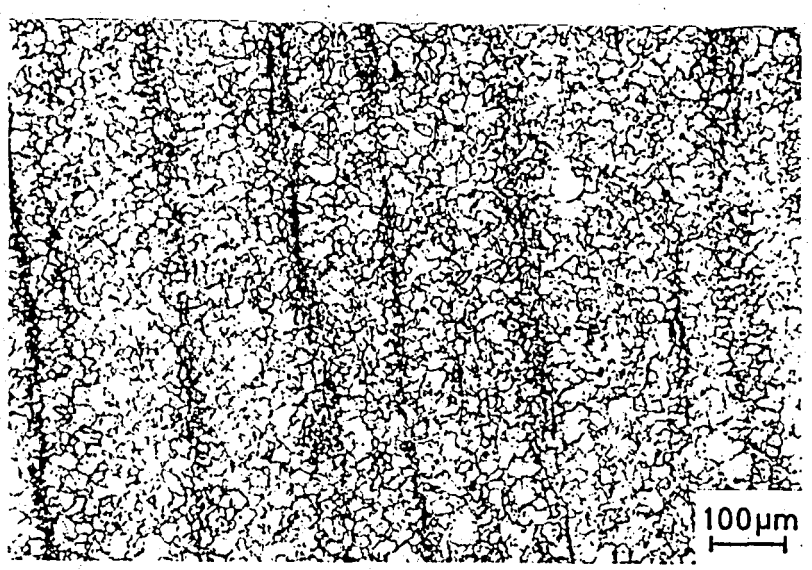

Figure 56 (e)
1200-845°C
ASTM No 9.0

Figure 56. Prior austenite grain sizes after (a) 845°C, (b) 1000°C, (c) 1100°C, (d) 1200°C, (e) 1200-845°C austenitization treatment.

Table 16. Prior austenite grain sizes after different austenitization treatments for AISI 5140 steel (calculated by Circular Intercept, Abrams Procedure [47]).

Austenitization Temperature (°C)	Magnification	$\bar{N}$(*)	ASTM no	$\bar{l}$(**) (μm)
845	200x	145	8.5	17
1000	100x	90	7.0	56
1100	50x	98	3.3	105
1200	50x	57	1.7	190
1200-845	400x	90	9.0	13

(*) $\bar{N}$ is the average intercept counts on 500 mm length test pattern.

(**) "$\bar{l}$" is the mean intercept distance.

6.4.2. Microstructure

Optical metallography was done to determine the as-quenched, 200°C tempered and 570°C tempered structures of AISI 5140 steel. The photographs were taken in all heat treated specimens on sections cut from actual fracture toughness specimens except as quenched ones which were taken from mid-portions of 24 mm hardenability bars. The as-quenched structures are shown in Figure 57, 200°C tempered ones in Figure 58, and 570°C tempered ones in Figure 59.

The 1200°C heat treatment resulted in mainly martensite with the formation of upper bainite through nucleation along prior austenite grain boundaries. The alternating sheets of ferrite and iron-carbide are clearly visible and characteristics of upper bainite [9]. Upper bainite is indicated by arrows. The microstructure with a fine grain size resulted from 845°C austenitization is shown in Figure 57 (a). This figure reveals that this heat treatment resulted in the formation of ferrite and very

coarse upper bainite in which the ferrite laths are very wide, in a martensitic structure. The upper bainite is shown with arrows and are nucleated along the grain boundaries.

The 1000°C and 1100°C structures are just transition between these two cases.

The observed microstructures agree well with the observations of Wood [9], and of Wood et al. [11] for similar AISI 4140 and 4130 steels.

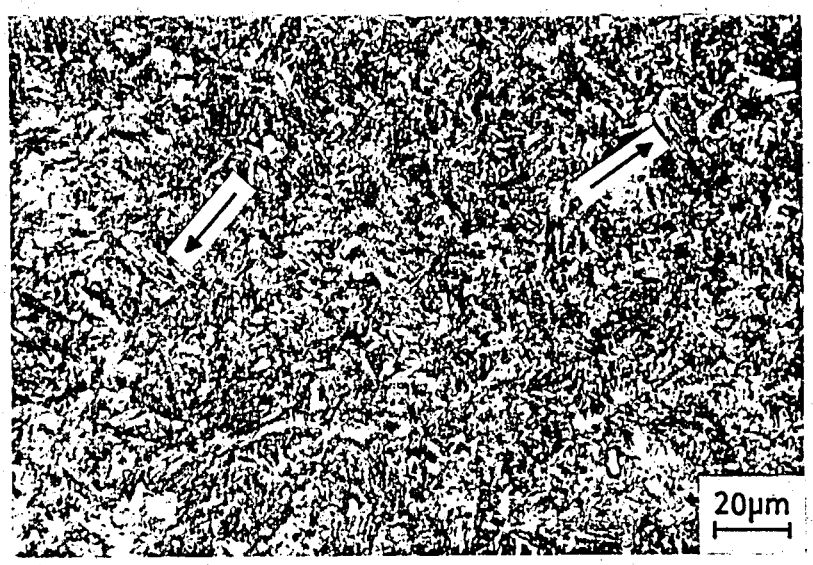

Figure 57 (a)
845°C

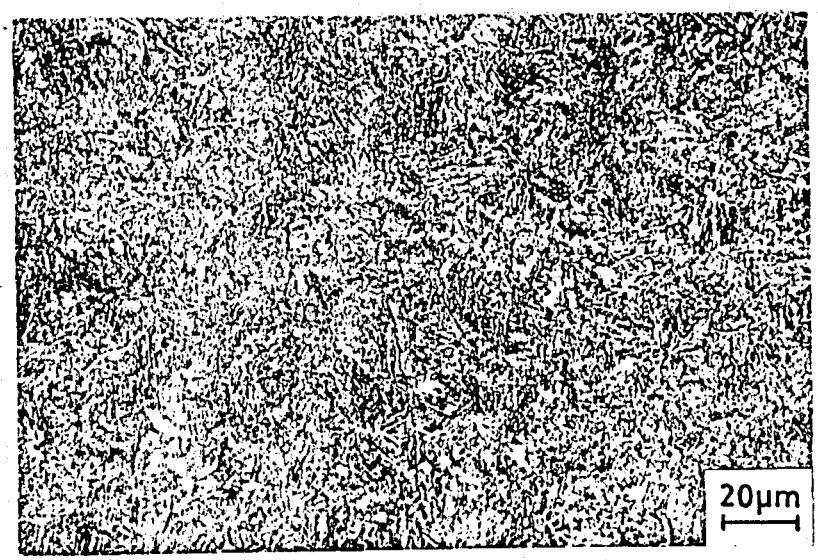

Figure 57 (b)
1000°C

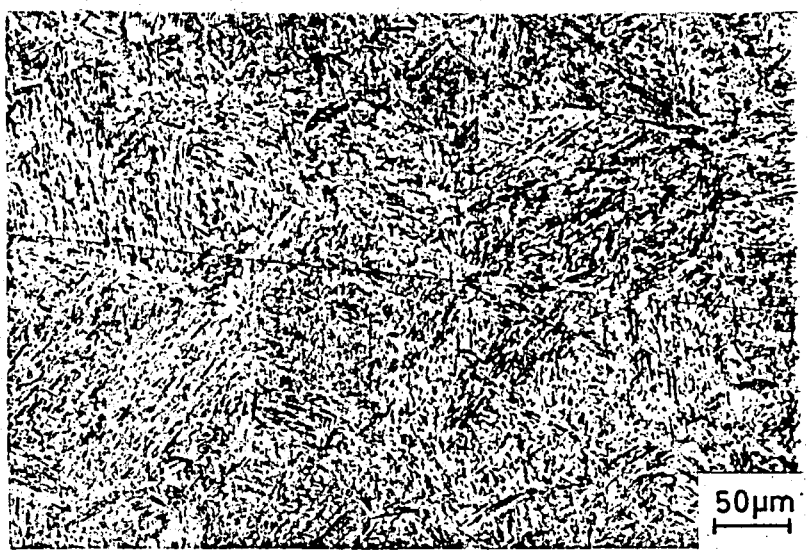

Figure 57 (c)
1100 C

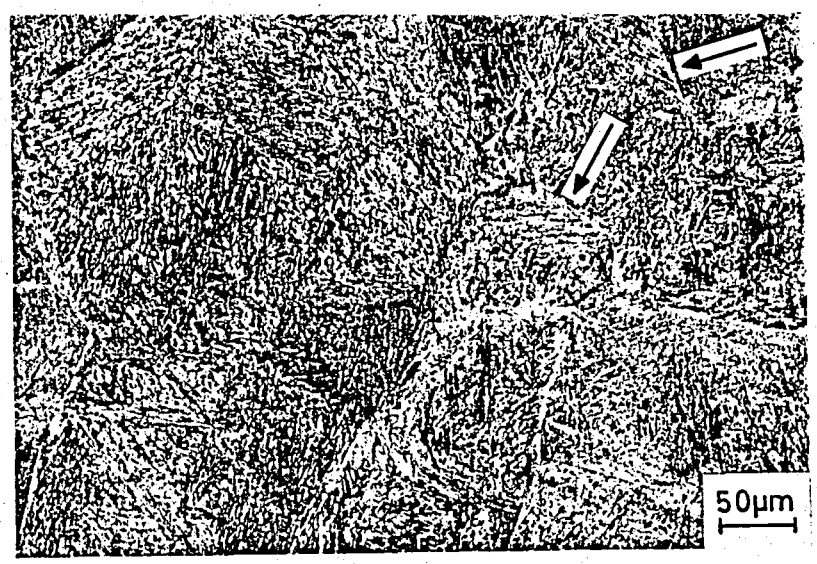

Figure 57 (d)
1200 C

Figure 57. As-quenched microstructures after (a) 845°C, (b) 1000°C, (c) 1100°C, (d) 1200°C austenitization treatments.

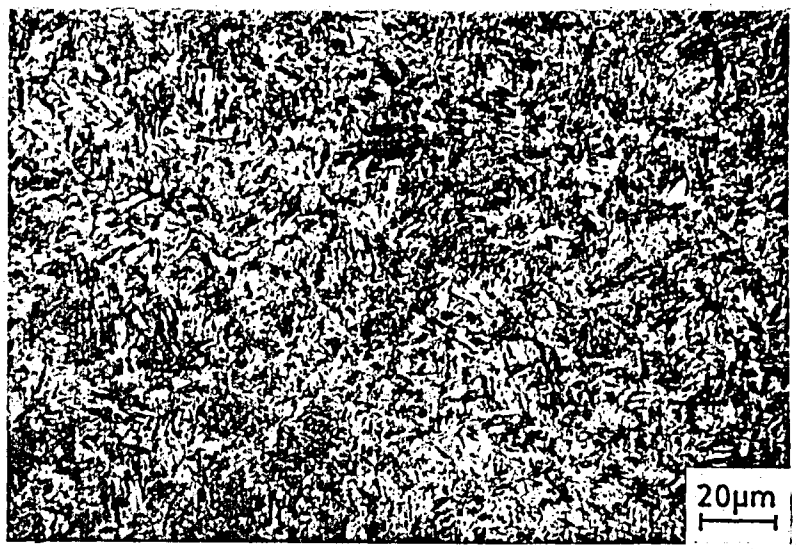

Figure 58 (a)
845°C

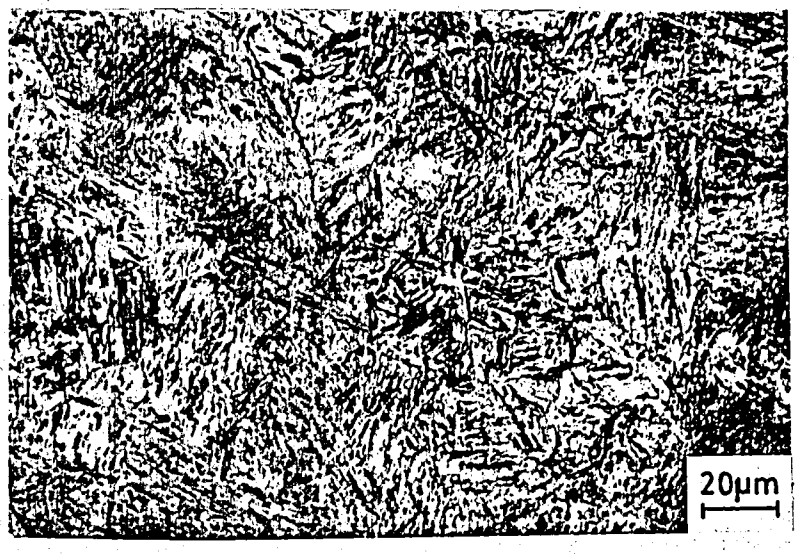

Figure 58 (b)
1000°C

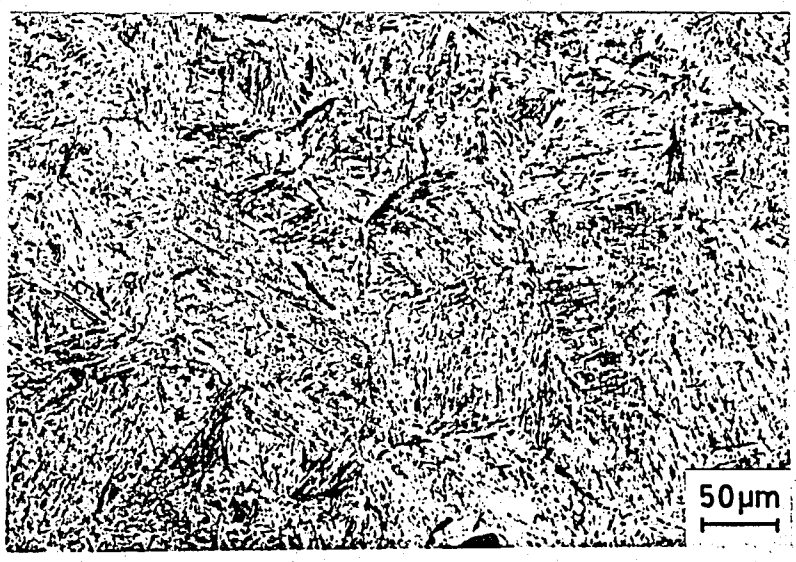

Figure 58 (c)
1100°C

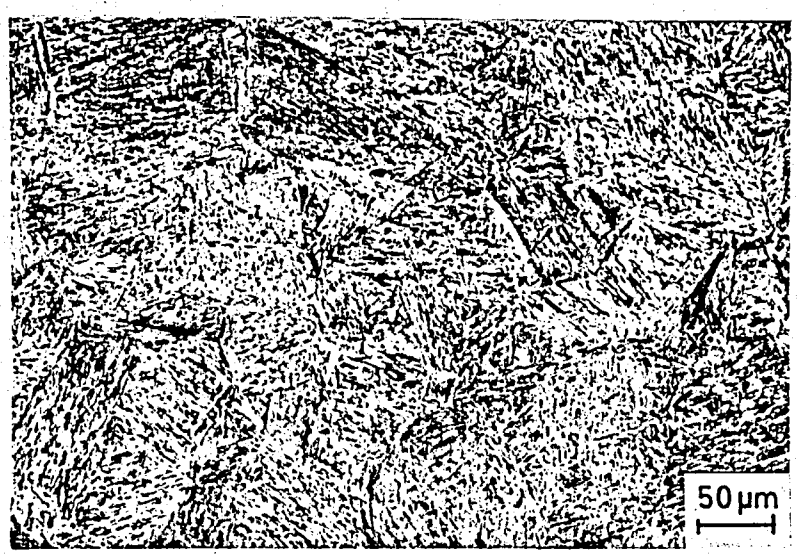

Figure 58 (d)
1200°C

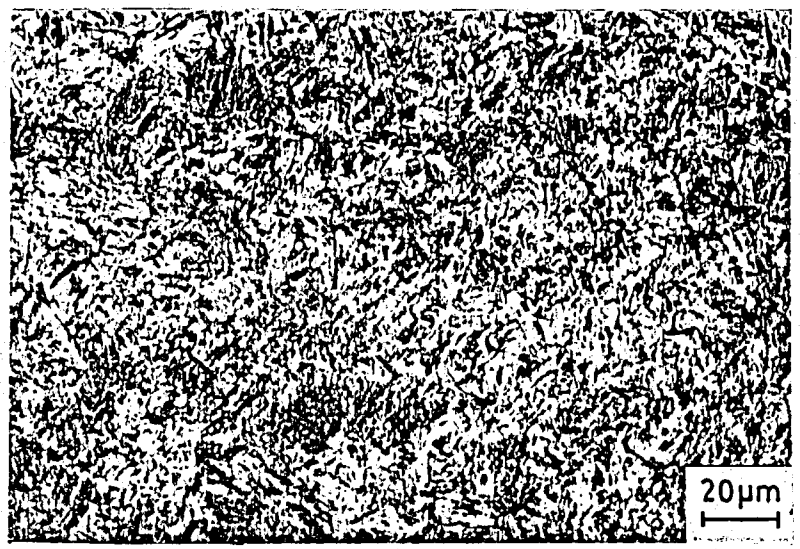

Figure 58 (e)
1200-845°C

Figure 58. 200°C tempered microstructures after (a) 845°C, (b) 1000°C, (c) 1100°C, (d) 1200°C, (e) 1200-845°C austenitization treatment.

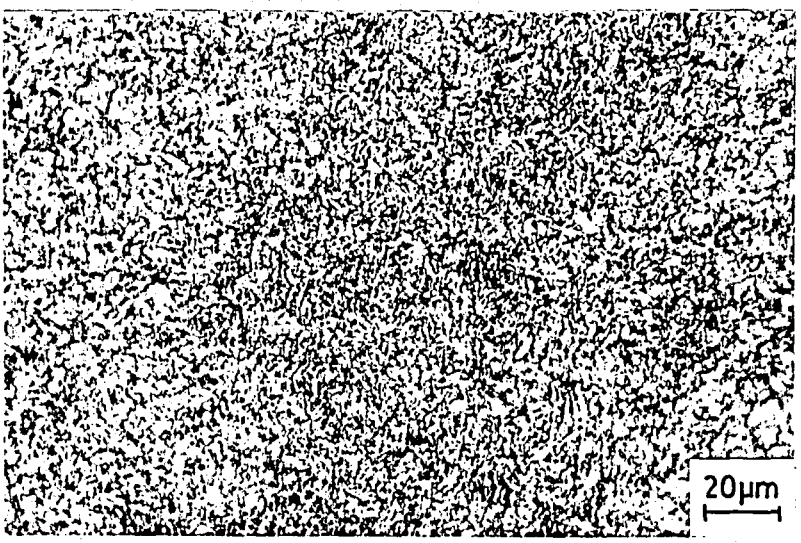

Figure 59 (a)
845°C

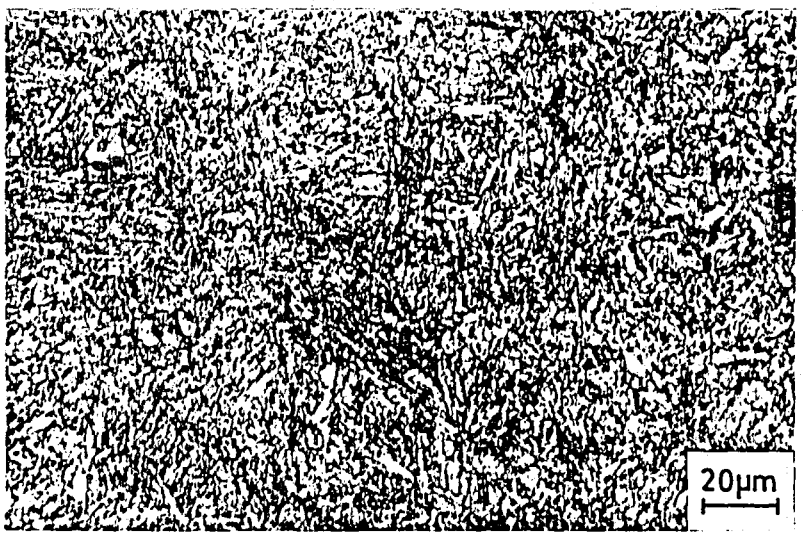

Figure 59 (b)
1000°C

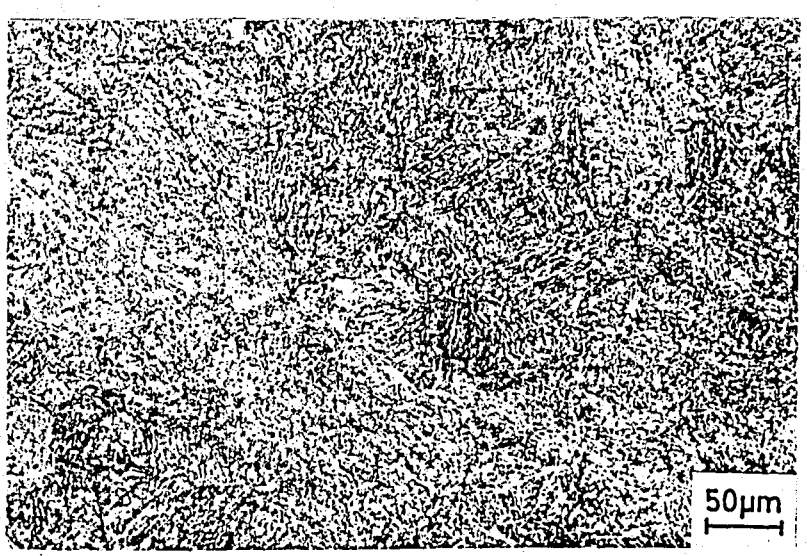

Figure 59 (c)
1100°C

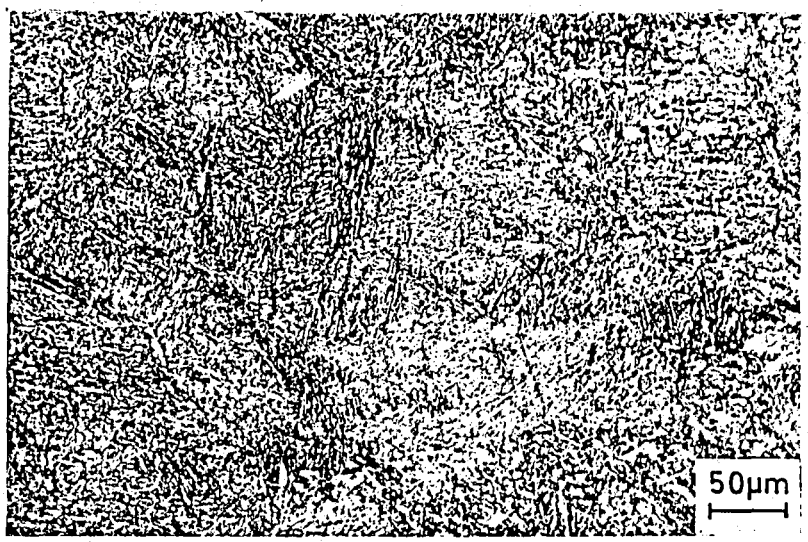

Figure 59 (d)
1200°C

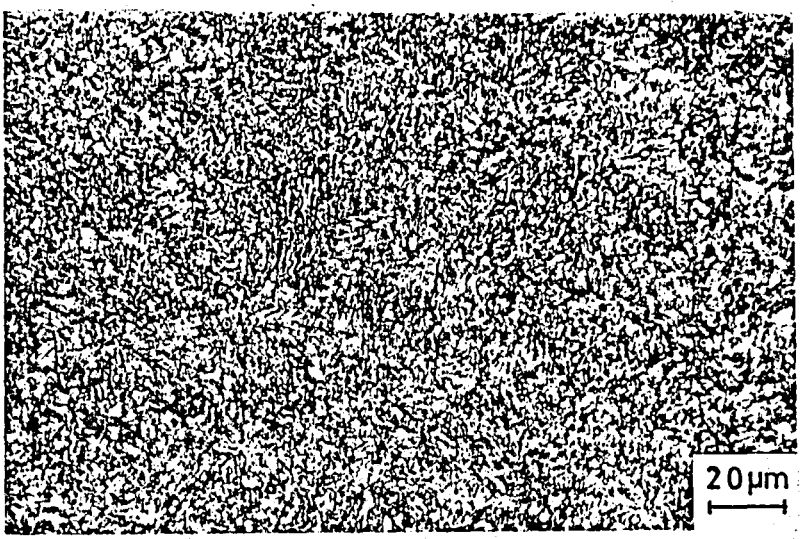

Figure 59 (e)
1200-845°C

Figure 59. 570°C tempered microstructures after (a) 845°C, (b) 1000°C, (c) 1100°C, (d) 1200°C, (e) 1200-845°C austenitization treatment.

6.5. Fractography

The macro-photographs of fracture surfaces of Charpy and fracture toughness specimens which are tempered at 200°C are shown in Figure 60 and 61, respectively. Here, the only characteristic feature that can be identified is the increase in austenite grain sizes with increasing austenitizing temperatures.

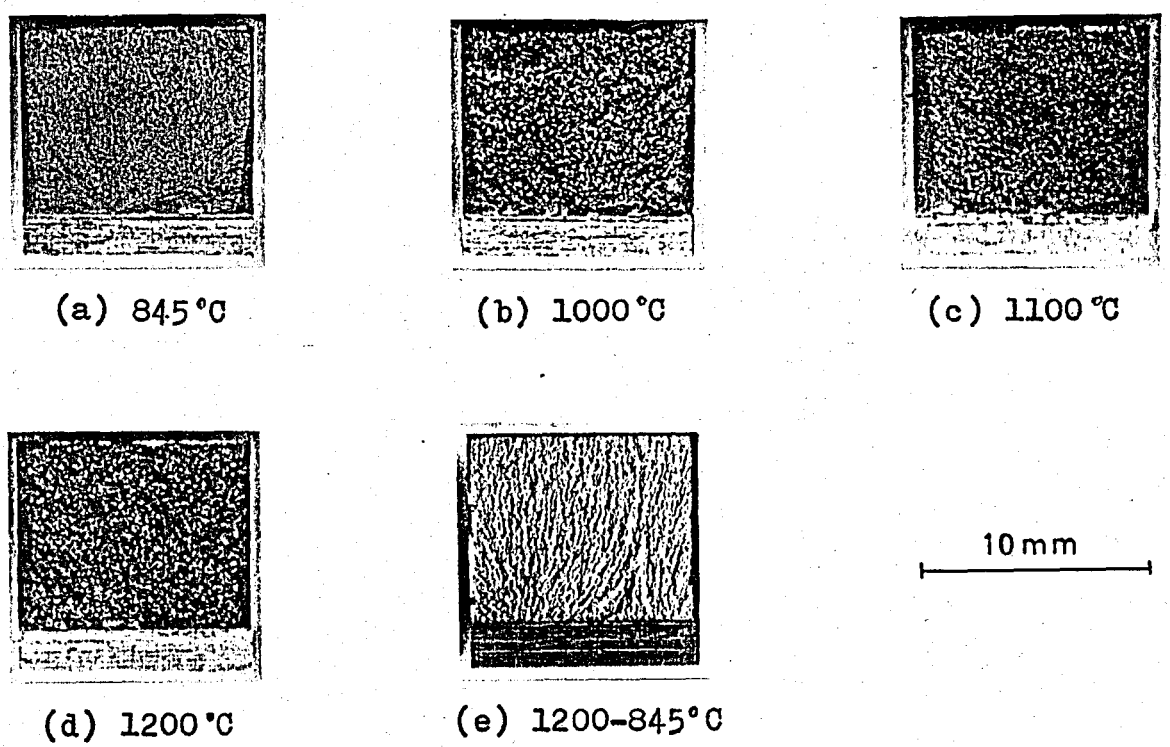

Figure 60. The fracture surfaces of Charpy V-notch specimens which are tempered at 200°C. (The austenitization temperatures are indicated underneath the photographs).

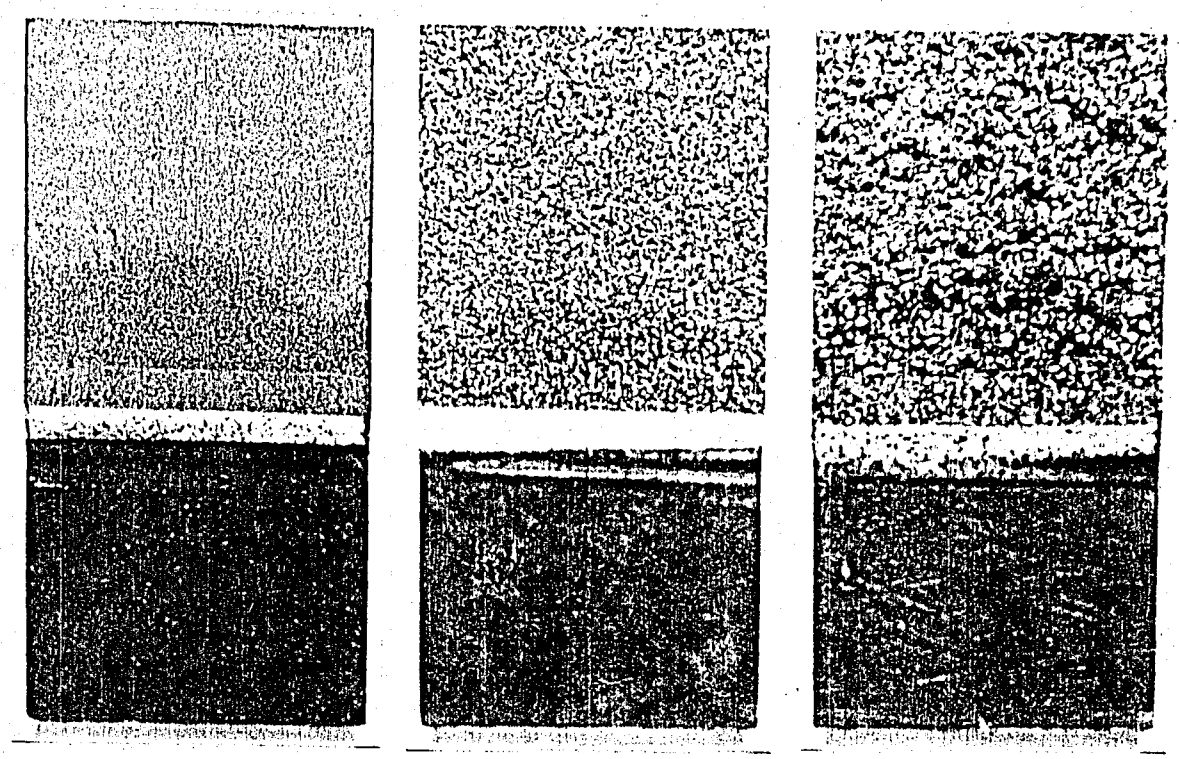

(a) 845°C (b) 1000°C (c) 1100°C

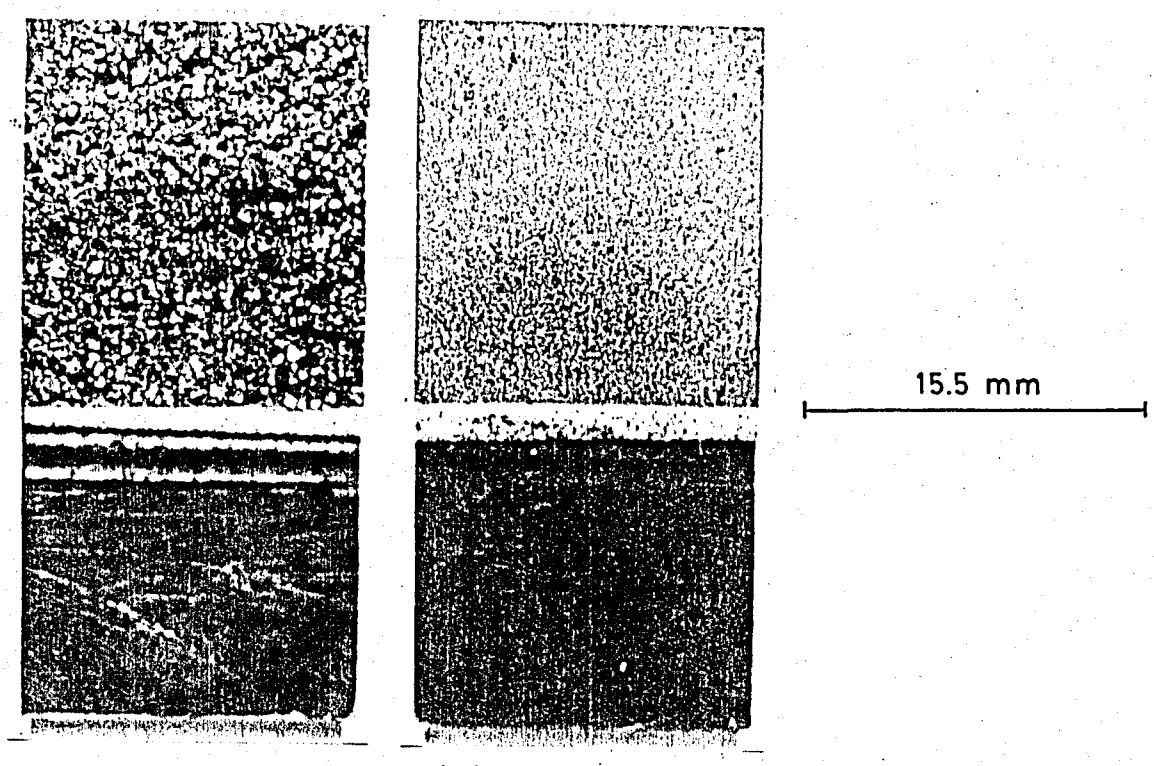

(d) 1200°C (e) 1200-845°C

Figure 61. The macro-photographs of the fracture surfaces of the fracture toughness specimens (200°C temper).

Figure 62 shows the scanning electron microscope photographs of crack initiation regions of fracture toughness specimens (200°C tempered ones).

Photomicrographs 62 (a) is of the specimen austenitized at 845°C. The fracture surface is quasi-cleavage with scattered packets of ductile rupture. Photomicrographs 62 (c) is of the fracture surface from a specimen austenitized at 1100°C. This surface exhibited extensive amounts of dimpled rupture. Figure 62 (d) is from a specimen austenitized at 1200°C. It shows completely dimpled rupture.

By increasing the austenitization temperature from the conventional 845°C to 1200°C, the fracture surface changed from quasi-cleavage and dimpled rupture to an entirely dimpled rupture. Figure 62 (b), which presented intergranular (white), transgranular (gray) and very little dimpled fracture did not obey this trend.

Fracture surface of Figure 62 (d) has greater ductility, hence greater energy absorbtion than that of Figure 62 (a) [13].

These results agree well with the fracture thoughness values for these structures, and also with the observations of Carlson et al. [3], Datta [4] and Lai et al.[13].

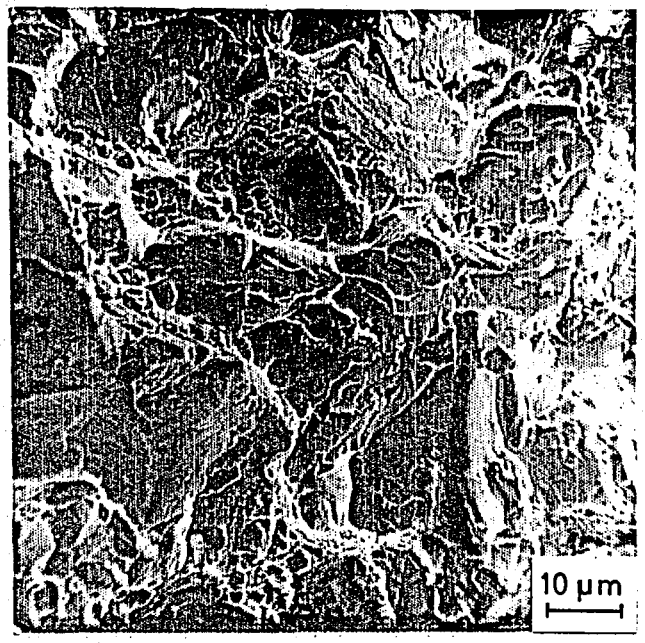

Figure 62 (a) 845°C

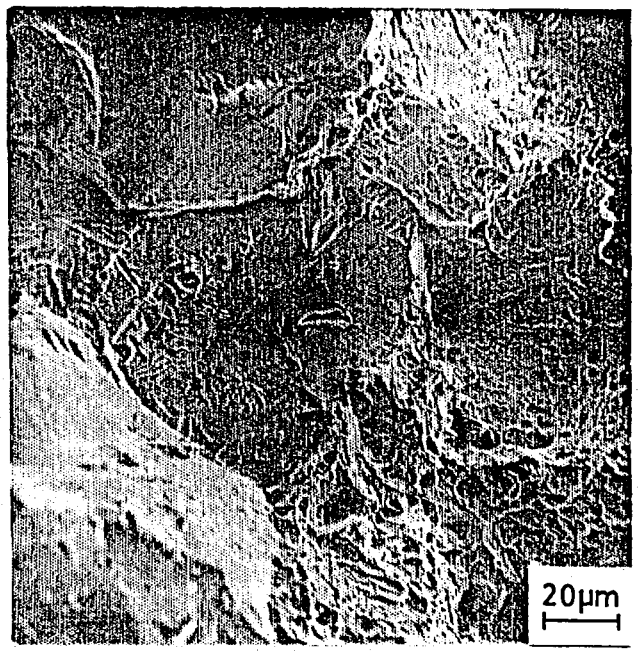

Figure 62 (b) 1000°C

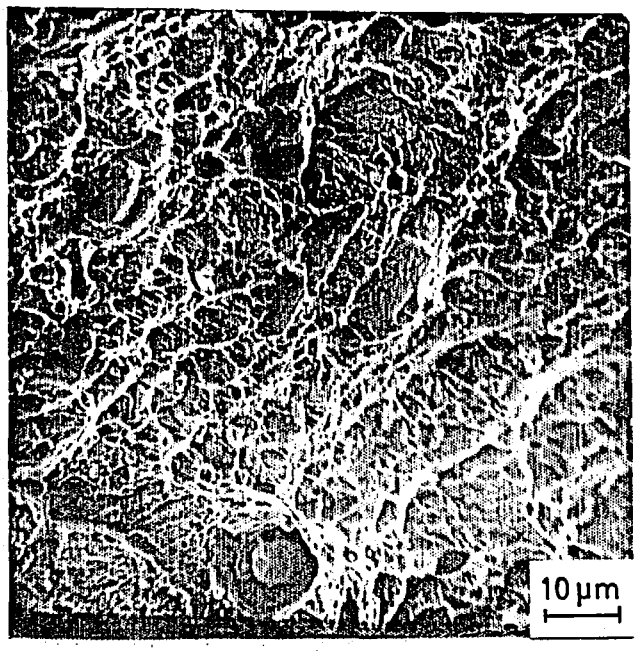

Figure 62 (c) 1100°C

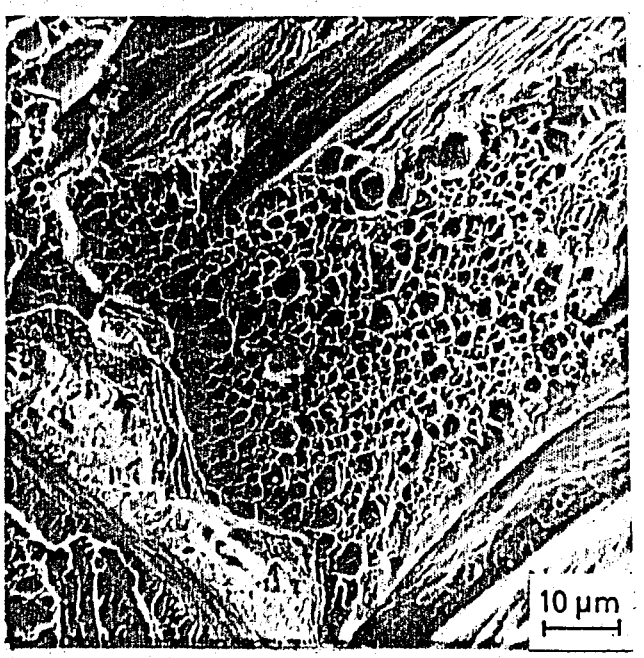

Figure 62 (d) 1200°C

Figure 62. The SEM photomicrographs of the fracture toughness specimens (200°C tempered).

VII. DISCUSSION

The heat treatment of steel and its effects on the resulting microstructure and mechanical properties is an extremely complex phenomenon. Each step in the heat treatment used in this investigation, the austenitization temperature, the quenching medium and the tempering temperature affects the final microstructure of the steel. The microstructure in turn controls all the properties that a particular steel exhibits.

The object of this investigation was to develop a heat treatment and hence microstructure that would result in an improvement in the fracture characteristics of AISI 5140 low alloy steel. For that reason, high austenitization temperatures such as 1000°C, 1100°C and 1200°C as well as the conventional austenitizing temperature, i.e., 845°C have been used.

The results indicated that, for AISI 5140 low alloy steel, increased austenitization temperatures improved the plane strain fracture toughness and Charpy impact energy of lightly tempered (at 200°C) specimens without no loss in strength.

As explained in Section 6.2, the necessary conditions for a valid plane strain fracture toughness testing were met by 200°C tempered specimens. The load-displacement records for plain strain fracture toughness testing of 570°C tempered specimens exhibited non-linearity (Figure 50) and did not obeyed the condition of $P_{max}/P_Q \leq 1.1$ for a valid plane strain fracture toughness testing.

The same type of non-linearity for high temperature tempered structures in the load-displacement diagram of fracture toughness testing was also encountered by Kumar and Seal [14], and it was believed by Wood [9], Parker et al.[11] that the first requirement have been added to ASTM standards because of the discrepancies in fracture toughness testing of titanium alloys. For the alloys which do not contain titanium, the first condition makes no difference, whether it is met or not. But in the case of Wood [9] and Parker et al.[11] the ratio of P_{max}/P_Q was not so large as it happened in our case.

Using either K_{max} calculated from P_{max} or a 1.5 amplification factor applied to K_Q [49], the probable minimum specimen thickness for plane strain behavior in this tempering condition (at 570°C) would be 40-50 mm.

In fact, it is known that the high temperature tempered structures have high toughness, and the aim of this study was to investigate the improvement of fracture toughness of lightly tempered structures (at 200°C by high austenitization temperatures. 570°C tempered structures have been examined for general information only. It has been also known that tempering at 500°C or above, the high temperature austenitization makes no difference in plane strain fracture toughness for some alloys [10,20].

7.1. Effect of High Austenitizing Temperatures on Hardenability

The main reason for heat treating an alloy steel is to obtain better strength and toughness that cannot be gained by other means. The ferrite/pearlite structure is the weakest of all structures discussed up to now, and is thus generally avoided in the heat treatment of alloy steels. One way of avoiding this structure is to apply a high cooling rate. This is feasible when the thickness of the steel being heat treated is relatively small, but becomes progressively more difficult as the thickness is increased

owing to the relatively low thermal conductivity of the steel and the inadvisibility of using faster quench because of the thermal stresses causing quench cracking.

The other way of avoiding ferrite/pearlite is to delay the start of transformation by moving the transformation lines in continuous cooling diagrams to the right, i.e., ensure the transformation at all temperature levels to start later and to go to completion later. This may be achieved by two means, (i) by increasing the alloy content, (ii) by employing higher austenitization temperatures than conventional austenitization temperatures which increases the grain size.

Increased austenitizing temperatures leads to grain growth. The ferrite and carbide formation from the austenite starts at the grain boundary. A fine grained structure offers more grain boundary area per unit volume on which decomposition can be nucleated than does a coarse grained steel [33]. Thus, the effect of increasing the grain size of the austenite is to delay the start of transformation [24,35,36].

It has also been reported that the homogeneity of austenite will affect the transformation rates [24]. Inhomogeneous austenite will speed up the start of transformation. This occurs because the initial transformation will occur in the portions which are leaner in alloy. In addition, undissolved carbides may act as nuclei for transformation, thereby hastening the start of transformation.

The results of Jominy end-quench tests showed that the increased hardenability accompanying high austenitizing temperature is quite visible. Hardenability bars showed an increase not only in the center hardness with increasing austenitization temperatures, but also in the surface hardness, the difference in surface hardness being greater as the diameter of the bar increases.

The micrographs taken from surface, mid-radius and center of 60 mm bars austenitized at either 845°C (Figure 63) or 1200°C (Figure 64) explain the difference

(a) 845°C, surface

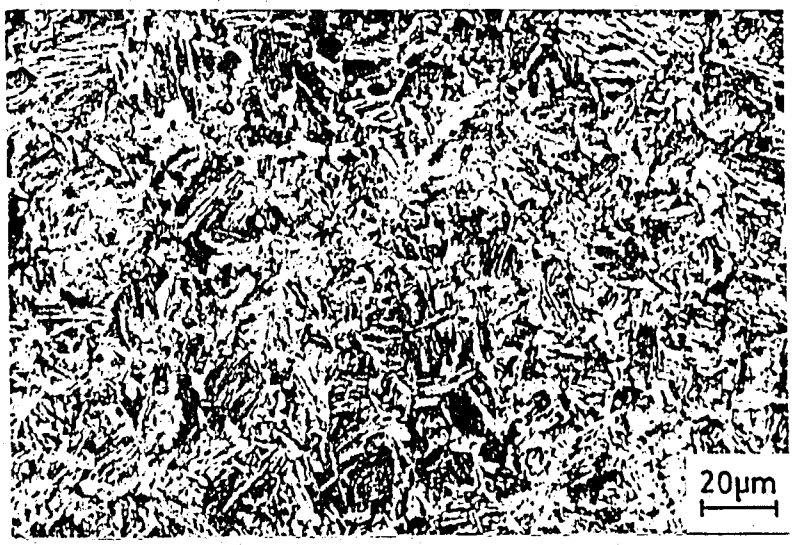

(b) 845°C, mid-radius

(c) 845°C, center

Figure 63. Micrographs taken from surface, mid-radius and center of 60 mm diameter bar, quenched from 845°C.

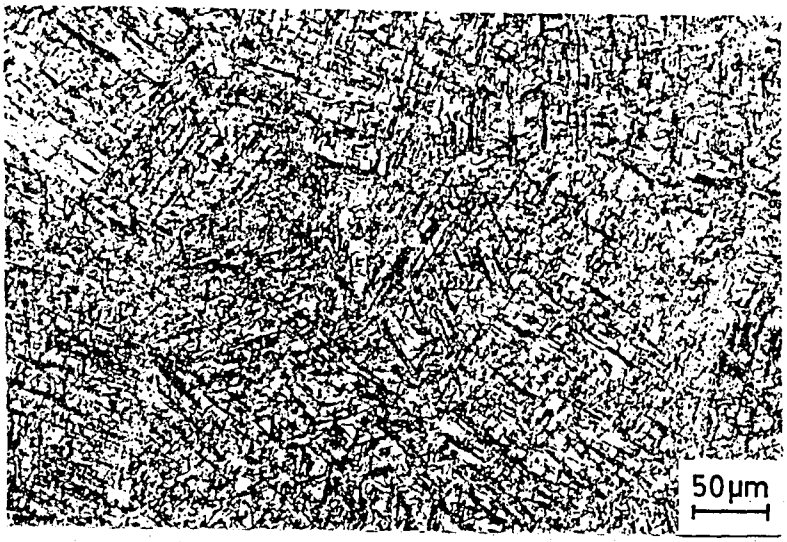

(a) 1200°C, surface

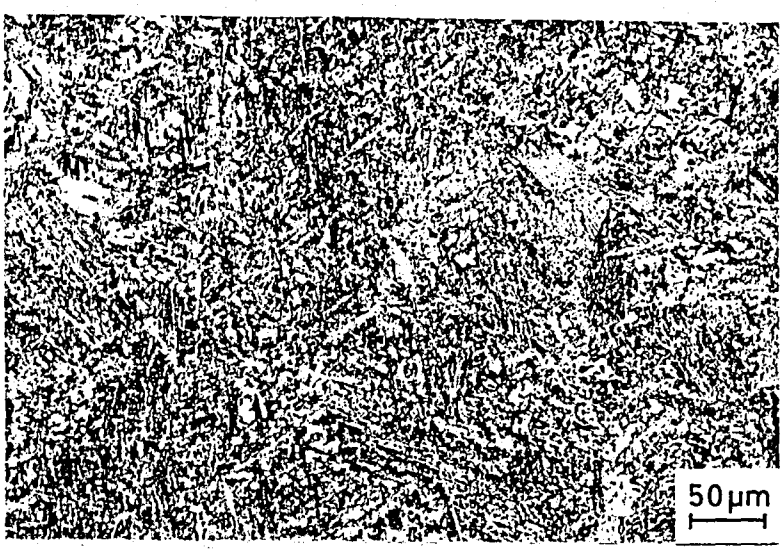

(b) 1200°C, mid-radius

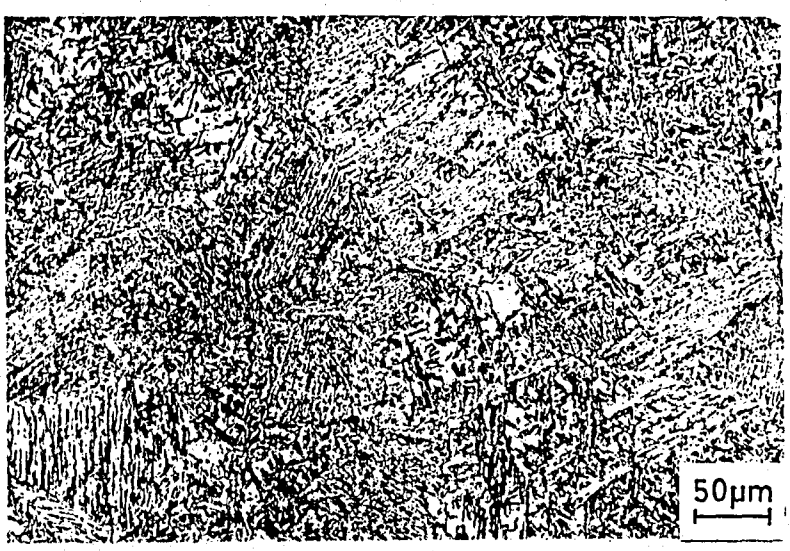

(c) 1200°C, center

Figure 64. Micrographs taken from surface, mid-radius and center of 60 mm diameter bar, quenched from 1200°C.

in hardness. The surface appearance of both specimens consisted of ferrite, upper bainite and martensite. The proportion of ferrite and upper bainite was considerably larger in 845 °C structure. The center microstructures of these two specimens differed too much. 1200 °C structure consisted of primarily upper bainite with some ferrite at the grain boundaries in a martensitic matrix, whereas the 845 °C structure consisted of ferrite/pearlite and upper bainite [9,51]. The proportions of non-martensitic constituents of 845 °C is undoubtfully higher than that of 1200 °C structure in each case.

The change in microstructure between these two structures was reflected in the hardness measurements. Both the center and surface hardness of 1200 °C austenitized specimen were higher than those of 845 °C austenitized specimen.

7.2. Effect of High Austenitizing Temperatures on Toughness

The results of this study have shown that, while the conventionally treated lightly tempered fracture toughness of a low alloy steel, AISI 5140, was very low, large increase in the fracture toughness could be achieved by altering the heat treatment. Examination of the foregoing data have shown that a large improvement in plane strain fracture toughness and Charpy impact strength result when 5140 steel is austenitized at 1200 °C rather than 845 °C. The yield and ultimate tensile strengths are not significantly changed by the higher austenitization temperatures, but the ductility is lowered by the 1200 °C treatment.

For alloys with limited hardenability such as AISI 5140 steel, the conventional austenitization at 845 °C produced a fine microstructure consisting of proeutectoid ferrite, upper bainite and martensite [9]. By employing higher austenitization temperatures, the undesirable constituent, ferrite and upper bainite, have been eliminated and the structure has been changed to a nearly

martensitic one. This is evident when the as-quenched microstructures of 5140 steel resulting from 845°C and 1200°C are compared (Figure 57).

The effect of mixed structures are detrimental to fracture toughness and elimination of these non-martensitic structures are reported to increase the fracture toughness for 4130 and 4140 steels [7-9,11-49,51]. Thus, the increase in both plane strain fracture toughness and Charpy impact energy of AISI 5140 steel is attributed to the prevention of ferrite and upper bainite with increasing austenitization temperature.

The other possible explanations for the improvement in fracture toughness with increasing austenitizing temperatures have been concentrated on:

(i) Increase in the amount of retained austenite,

(ii) Change in submicrostructure,

(iii) Elimination of undissolved carbides.

Larger proportions of austenite films of 100 to 200 °A thick are retained around martensite plates and packets of laths after austenitizing at high temperatures [6,8,12-16]. The presence of retained austenite has been shown by Webster [52] to improve toughness through its crack arresting ability. Cracks propagating through martensite would be stopped upon intersecting a region of tough retained austenite. With further loading, the cracks would branch out and grow around the austenitic area. This sort of crack motion would necessarily involve more energy absorbtion than straight propagation through martensite plates. Thus, the increased austenite content could certainly help explain the greater fracture toughness of specimens austenitized at 1200°C.

Webster's explanation [52] of enhanced toughness was based upon the assumption that the retained austenite was stable with respect to stress and strain. Recent studies by Gerberich et al.[53] and Antolovich et al.[54] suggested that an enhancement of the fracture toughness could also occur if austenite is converted to martensite by strain (or stress) induced transformation. These workers

showed that about five times more energy is absorbed by this type of transformation than for the plastic deformation of a stable matrix.

Another possible explanation for the improved fracture toughness appear to lie in the change of sub-microstructure, i.e., less twinning with higher austenitizing temperature. As described previously, the 845°C austenitization resulted in a fine grain size. According to Lai et al.[13], these grains were often traversed by large lenticular martensite plates. Some of the martensite plates were dislocated, however, others are twinned. The specimens austenitized at 1200°C did not exhibit any twinned plates. Furthermore, none of the dislocated plates were large enough to extend across the larger grains resulting from the higher temperature. Thus, there is possibility that the presence of transformation twins could have been responsible for the lower fracture toughness of 845°C austenitized material. Several previous investigators [8,12,13,15-18] have associated a drop in fracture toughness with the presence of increased amounts of twinned martensite. Kelly and Nutting [30] attribute the loss in toughness to a decrease in the number of available slip system in twinned plates by a factor of four. The decreasing tendency for twinning noted with increasing austenitizing temperature is due to the increase in M_s, which raises the critical resolved shear stress for twinning above that for slip. For the modified heat treatment, tempering at 200°C caused precipitation of epsilon carbides and refinement during subsequent austenitization. This austenite which transforms to martensite is of lower free carbon content, hence M_s is increased and thus an increase in dislocated lath martensite and a decrease in twinned plate martensite may be observed.

The third feature influenced by the austenitizing treatment is the presence of undissolved carbides. The presence of undissolved carbides in the martensite has been observed to lower the fracture toughness [3,8-12,55]. For

Fe/Cr/C steels, CrC exists up to 1020°C [3]. The rapid increase in fracture toughness in this study after 1100°C may be attributed to this effect. The high fracture toughness of double austenitized specimens may also be caused by the homogeneous austenite phase free from alloy carbides.

VIII. CONCLUSION

1. High austenitization treatments improved both the plane strain fracture toughness and Charpy V-notch impact energy of AISI 5140 steel.

2. Yield strength and ultimate tensile strength were not affected by high austenitization temperatures, but ductility (per cent elongation and reduction in area) decreased with increasing austenitizing temperatures.

3. Hardenability increased with increasing austenitization temperatures.

4. The increase in plane strain fracture toughness and Charpy impact energy may be attributed to the prevention of proeutectoid ferrite and upper bainite with increasing hardenability resulted from the high temperature austenitizing.

5. For steels with limited hardenability, such as AISI 5140, the improvement in both Charpy impact energy and plane strain fracture toughness makes no doubt on the employment of high austenitization temperatures is beneficial.

6. For AISI 5140, which an example of low hardenability steel, there is no need for double austenitization - designed to increase the low Charpy impact energy of high temperature austenitized structures for steels with high hardenability -.

BIBLIOGRAPHY

1. Ritchie, R.O., Francis, B. and Server, W.L., "Evaluation of Toughness in AISI 4340 Alloy Steel Austenitizet at Low and High Temperatures," Metallurgical Transactions A, Vol. 7A, No.6, pp.831-838, June 1976.

2. Ritchie, R.O. and Horn, R.M., "Further Considerations on the Inconsistency in Toughness Evaluation of AISI 4340 Steel Austenitized at Increasing Temperatures," Metallurgical Transactions A, Vol. 9A, No:3, pp.331-341, March 1978.

3. Carlson, M.F., Narasimha, B.V. and Thomas, G., "The Effect of Austenitizing Temperature Upon the Microstructure and Mechanical Properties of Experimental Fe/Cr/C steels," Metallurgical Transactions A, Vol. 10A, No.9, pp.1273-1284, September 1979

4. Datta, E.P., "Sharp Crack and Blunt Notch Toughness Behavior of Quenched and Tempered AISI 4340 Steel," Materials Science and Engineering, Vol.51, No.2, pp.241-252, 1981.

5. Firrao, D., Begley, J.A., Silva, G., Roberti, R. and Benedetti, B.D., "The Influence of Notch Root Radius and Austenitizing Temperature on Fracture Appearance of As-quenched Charpy-V Type AISI 4340 Steel Specimens," Metallurgical Transactions A, Vol.13A, No.6, pp.1003-1013, June 1982.

6. Sarıkaya, M., Steinberg, B.G. and Thomas, G., "Optimization of Fe/Cr/C Base Structural Steels for Improved Strength and Toughness," Metallurgical Transactions A, Vol.13A, No.12, pp.2227-2237, December 1982.

7. Zackay, V.F., Parker, E.R., Goolsby, R.D. and Wood, W.E., "Untempered Ultra-high Strength Steels of High Fracture Toughness," Nature Physical Science, Vol.236, No.68, pp.108-109, April 17 1972.

8. Parker, E.R. and Zackay, V.F., "Microstructural Features Affecting Fracture Toughness of High Strength Steels," Engineering Fracture Mechanics, Vol.7, pp.371-375, 1975.

9. Wood, W.E., "Effect of Heat Treatment on the Fracture Toughness of Low alloy Steels," Engineering Fracture Mechanics, Vol.7, pp.219-234, 1975.

10. Youngblood, J.L. and Raghavan, M., "Correlation of Microstructure with Mechanical Properties of 300M Steel," Metallurgical Transactions A, Vol.8A, No.9, pp.1439-1448, September 1977.

11. Wood, W.E., Parker, E.R. and Zackay, V.F., "An Investigation of Metallurgical Factors which Affect the Fracture Toughness of Ultra-High Strength Steels," LBL-1474, Lawrance Berkeley Baloratory, Berkeley, California, May 1973.

12. Lai, G.Y., Wood, W.E., Parker, E.R. and Zackay, V.F., "Influence of Microstructural Features on Fracture Toughness of an Ultra-High Strength Steel," LBL-2236, Lawrance Berkeley Laboratory, Berkeley, California, April 1975.

13. Lai, G.Y., Wood, W.E., Clark, R.A., Zackay, V.F. and Parker, E.R., "The effect of Austenitizing Temperature on the Microstructure and Mechanical Properties of As-quenched 4340 Steel," Metallurgical Transactions, Vol.5, No.7, pp.1663-1670, July 1974.

14. Kumar, A.N. and Seal, A.K., "Fracture Toughness Studies of Low Alloy Steels," Transactions of the Indian Institute of Metals, Vol.36, No.6, pp.452-458, 1983.

15. Padmanabhan, R. and Wood, W.E., "Microstructural Analysis of a Multistage Heat-treated Ultrahigh Strength Low Alloy Steel," Materials Science and Engineering, Vol.66, No.1, pp.125-143, 1984.

16. Parker, E.R., Zackay, V.F., Lai, G.Y. and Horn, R.M., "Untempered Ultra High Strength Steels of High Fracture Toughness," Lawrance Berkeley Laboratory, Berkeley, California, April 1974.

17. Khan, K.H. and Wood, W.E., "The Effect of Step Quenching on the Microstructure and Fracture Toughness of AISI 4340 Steel," Metallurgical Transactions A, Vol.9A, No.7, pp.899-907, July 1978.

18. Sastry, C.N., Padmanabhan, R., Dilipkumar, D. and Wood, W.E., "Achieving Optimum Properties in Ultrahigh-strength Low-alloy Steel," Metals Technology, Vol.8, No.12, pp.454-457, December 1981.

19. Clark, G., Ritchie, R.O., and Knott, J.F., "Segregation Effects and the Toughness of Untempered Low-Alloy Steels," Nature Physical Science, Vol.239, No.94, pp.104-106, October 16 1972.

20. McDarmaid, D.S., "Effects of Different Austenitization Treatments on K_{1c}, K_{1scc}, and other Mechanical Properties of 300M Steel Bar," Metals Technology, Vol.5, No.1, pp.7-16, January 1978.

21. Ferguson, W.G., Clark, N.E. and Watson, B.R., "Effect of Austenitizing Temperature on Toughness of Martensitic Steels," Metals Technology, Vol.3, No.4, pp.208-209, April 1976.

22. Unterweiser, P.M., Bayer, H.E., and Kubbs, J.J. Heat Treater's Guide - Standard Practices and Procedures for Steel. Ohio: American Society for Metals, 1982.

23. Struers Scientific Instruments, Copenhagen, Denmark.

24. McGannon, H.E. The Making, Shaping and Treating of Steel. 8th ed. Pitsburg, Pa.: United States Steel, 1964.

25. Hanson, A., Parr, J.G. The Engineer's Guide to Steel. Michigan: Addison-Wesley Publication Co., 1965.

26. Wilson, R. Metallurgy and Heat Treatment of Tool Steels. London, McGraw Hill Book Co., 1975.

27. Duckworth, W.E., "The Heat-treatment of Low-alloy Steels," Metals and Materials, Vol.2, No.11, pp.145-170, November 1968.

28. Metals Handbook. Vol2, 8th ed. Ohio: American Society for Metals, 1967.

29. Umemoto, M., Yoshitake, E. and Tamura, I., "The Morphology of Martensite in Fe-C, Fe-Ni-C and Fe-Cr-C alloys," Journal of Materials Science, Vol.18, No.10, pp.2893-2904, October 1983.

30. Kelly, P.N. and Nutting, J., "The Morphology of Martensite," Journal of The Iron and Steel Institute, Vol.197, pp.199-211, March 1961.

31. Thelning, Karl-Erik. Steel and Its Treatment, Bofors Handbook. London: Cox and Wyman Ltd., 1978.

32. Metals Handbook, Vol.1, 8th ed. Ohio: American Society for Metals, 1967.

33. Van Vlack, Lowrence H. Elements of Materials Science and Engineering. Michigan: Addison-Wesley Publication Co., 1980.

34. Annual Book of ASTM Standards (American Society for Testing and Materials), ASTM Standards E44-75, Philadelphia, 1976.

35. Bullens, D.K. Steel and Its Heat Treatment. New York: John Wiley and Sons, Inc., 1946.

36. Grossman, M.A., and Bain, E.C. Principles of Heat Treatment, Ohio: American Society for Metals, 1968.

37. Speich, G.R. and Leslie, W.C., "Tempering of Steel," Metallurgical Transactions, Vol.3, No.5, pp.1043-1054, May 1972.

38. Lai, G.Y., "On High Fracture Toughness of Coarse-grained AISI 4340 Steel," Materials Science and Engineering, Vol.19, No.1, pp.153-156, 1975.

39. Yokota, M.J. and Lai, G.Y., "Toughness of Lath vs Plate Martensites," Metallurgical Transactions A, Vol.6A, No.9, pp.1832-1835, September 1975.

40. Thomas, G. and Chen, Y.L., "Structure and Mechanical Properties of Fe-Cr-Mo-C Alloys with and without Boron," Metallurgical Transactions A, Vol.12A, No.6, pp.933-950, June 1981.

41. McDarmaid, D.S., "Effect of Notch-root Radius and High Austenitizing Temperatures on Impact Properties of 300M Steel," Metals Technology, Vol.7, No.9, pp.372-377, September 1980.

42. Wood, W.E., "Discussion of Evaluation of Toughness in AISI 4340 Alloy Steel Austenitized at Low and High Temperatures," Metallurgical Transactions A, Vol.8A, No.7, pp.1195-1196, July 1977.

43. Ritchie, R.O., Francis, B. and Server, W.L., "Authors' Reply," Metallurgical Transactions A, Vol.8A, No.7, July 1977.

44. Annual Book of ASTM Standards (American Society for Testing and Materials), ASTM Standards E23-82, Philadelphia, 1985.

46. Annual Book of ASTM Standards (American Society for Testing and Materials), ASTM Standards E399-83, Philadelphia, 1985.

47. Annual Book of ASTM Standards (American Society for Testing and Materials), ASTM Standards A255-67, Philadelphia, 1976.

48. Annual Book of ASTM Standards (American Society for Testing and Materials), ASTM Standards E112-74, Philadelphia, 1976.

49. Rolfe, S.T. and Barson, J.M. Fracture and Fatigue Control in Structures. New Jersey: Prentice-Hall, Inc., 1977.

50. Petty, E.R. Physical Metallurgy of Engineering Materials. New York, American Elsevier Publishing Co. Inc., 1968.

51. Liebowitz, H. Fracture, an Advanced Tritise, V.1. New York: Academic Press, 1971.

52. Webster, D., "Development of a High Strength Stainless Steel with Improved Toughness and Ductility," Metallurgical Transactions, Vol.2, No.8, pp.2097-2105-August 1971.

53. Gerberich, W.W. and Birat, J.P., "A Metastable Austenite With Plane Stress Fracture Toughness near 500,000 lb/in^2 $-(in)^{1/2}$," International Journal of Fracture Mechanics, Vol.7, pp.108-110, 1971.

54. Antolovich, S.D. and Singh, B., "on the Toughness Increment Associated with the Austenite to Martensite Phase Transformation in TRIP Steels," Metallurgical Transactions, Vol.2, No.8, pp.2135-2141.

55. Lee, S., Majno, L. and Asaro, R.J., "Correlation of Fracture Toughness in Two 4340 Steels," Metallurgical Transactions A, Vol.16A, No.9, pp.1633-1648, September 1985.